



Title	Development of CuNWs based conductors with high reliability and stretchability for wearable electronics
Author(s)	張, 博雯
Citation	大阪大学, 2020, 博士論文
Version Type	VoR
URL	https://doi.org/10.18910/76533
rights	
Note	

The University of Osaka Institutional Knowledge Archive : OUKA

<https://ir.library.osaka-u.ac.jp/>

The University of Osaka

Doctoral Dissertation

**Development of CuNWs based conductors with
high reliability and stretchability for wearable
electronics**

Bowen Zhang

January 2020

Department of Adaptive Machine Systems,

Graduate school of Engineering,

Osaka University

Abstract

Copper nanowires (CuNWs) have become an irreplaceable conductive material in the field of flexible electronics due to their cost-effective as well as high conductivity and transparency. However, the fast degradation of CuNWs in ambient conditions largely overshadows their practical applications. Therefore, three strategies have been provided in this dissertation to enable CuNWs based conductors with outstanding conductivity, oxidation resistance, as well as flexibility: encapsulating or embedding CuNWs into a plastic substrate to achieve a composite structure; formation of the core-shell structure that encapsulates Cu with an inert shell; the combination of embedded structures and core-shell structures.

At first, CuNWs are fully embedded into the surface layer of poly(dimethylsiloxane) (PDMS) and followed with a high-intensity pulsed light technique. The light energy absorbed by the film not only removes the oxides on the surface of nanowires but also enhances the inter-nanowire connection to achieve high conductivity. Due to the outstanding stretchability of PDMS matrix and the strong adhesion between CuNWs and PDMS substrates, CuNWs/PDMS conductors could maintain high conductivity after 1000 stretching cycle tests. Compared with traditional semi-embedded conductors, the fully embedded CuNWs/PDMS conductors could maintain their high conductivity unchanged even at a high temperature of 85 °C and high humidity of 85 % for 12 h.

After that, a facile adsorption and decomposition process is developed for galvanic replacement free and large-scale synthesis of highly stable Cu@Ag core-shell nanowires. The introduced Ag-ammonia complex ($\text{Ag}[(\text{NH}_2\text{R})_2]^+$) as silver source adsorbs on the surface of CuNWs to form Cu@Ag-ammonia core-shell structure and block the traditional galvanic replacement between Ag^+ and CuNWs. Through a simple thermal annealing process under air, the Ag-ammonia complex shell can easily decompose into pure Ag shell, and form Cu@Ag core-shell nanowires. The thickness of the Ag shell can easily be controlled by adjusting the concentration of Ag-ammonia. The obtained core-shell nanowires exhibit high stability for at least 500 h at high temperature (140 °C) and high humidity (85 °C, 85% RH) due to the protection of Ag shell.

Finally, CuNWs-core/Ag-shell nanowires are fabricated first and then transformed into Cu@Ag alloy nanowires with dense surfaces and strong interfaces between CuNWs-core and Ag-shell by using high-intensity pulsed light (HIPL) technique. The HIPL also selectively softens the surface layer of the stretchable substrate and results in fully embedded structures of Cu@Ag alloy nanowires. The combination of alloy nanowires and embedded structures greatly improve the thermal stability of the transparent electrodes that keep high conductivity unchanged in both high temperature (140 °C) and high humidity (85 °C, 85% RH) for at least 500 h, which is much better than previous reports. The transparent electrodes also exhibit high electro-mechanical stability due to the strong adhesion between alloy nanowires and substrates, which remain stable after 1000 stretching-relaxation cycles at 30% strain.

To sum up, this dissertation proposes feasible and effective strategies to greatly improve the stability, conductivity, and flexibility of CuNWs-based transparent conductors, which is promising for the application in next-generation wearable electronics.

Table of contents

Abstract	I
Table of contents	III
List of figures	V
Chapter 1	1
Research background	1
1.1 Flexible electronics	1
1.1.1 Definition and advantages of flexible electronics	1
1.1.2 Strategies to enable stretchability of electronics	2
1.1.3 Application of flexible electronics	6
1.2 Next-generation stretchable electronics	10
1.2.1 Carbon based conductors	11
1.2.2 Conductive polymers based conductors	14
1.2.3 Metallic nanomaterials	17
1.3 Motivation of present research	21
1.3.1 Synthesis and film formation of CuNWs	21
1.3.2 Strategies to improve the performance of CuNWs films	24
1.4 Purpose and scope of this study	29
References.....	31
Chapter 2	44
Fabrication of fully embedded CuNWs/PDMS conductors	44
2.1 Introduction.....	44
2.2 Experimental.....	45
2.2.1 Synthesis of CuNWs	45
2.2.2 Fabrication of fully embedded CuNWs conductors	45
2.2.3 Characterization	46
2.3 Results and discussion	47
2.3.1 Comparison of microstructure and electrical resistivity.....	47
2.3.2 Comparison of stretchability and stability.....	53
2.3.3 Applications of fully embedded CuNWs/PDMS conductors	56
2.4 Conclusions.....	58

References.....	59
Chapter 3	63
Galvanic replacement free synthesis of Cu@Ag core-shell nanowires	63
3.1 Introduction.....	63
3.2 Experiment section	65
3.2.1 Synthesis of CuNWs	65
3.2.2 Fabrication of Cu@Ag core-shell nanowire networks.....	66
3.2.3 Characterization.	66
3.3 Results and discussion	67
3.3.1 Characterization of Cu@Ag core-shell nanowires.....	67
3.3.2 Formation mechanism of core-shell structure.....	72
3.3.3 Stability and applications of core-shell nanowires based conductors	72
3.4 Conclusions.....	79
References.....	79
Chapter 4	84
Alloying and embedding of Cu-core/Ag-shell nanowires	84
4.1 Introduction.....	84
4.2 Experiment section	85
4.2.1 Fabrication of TAE electrodes	85
4.2.2 Characterization	86
4.3 Result and discussion.....	86
4.3.1 Resistance and transparent evolution	86
4.3.2 Surface morphology and crystal structure evolution.....	90
4.3.3 Thermal stability and application of TAE electrodes.....	93
4.4 Conclusions.....	98
References.....	99
Chapter 5	103
Conclusions	103
List of publications	105
Acknowledgements	107

List of figures

Figure 1.1 (a) A schematic showing the fabrication process of the composite AgNW/PDMS stretchable conductors. (b) SEM image of the AgNW film on Si substrate. (c) SEM image of the AgNW film after transferred to PDMS substrate.

Figure 1.2 Schematic illustrations of the mechanical buckling processes: a) Prestrain–release–buckling and b) stretching–release–buckling along the longitudinal direction.

Figure 1.3 a) Schematic illustration of the hyper-stretchable and deformable nanocomposite generator. (b) SEM images show the loop structure of the CNT in corresponding places.

Figure 1.4 (a) Demonstration of the touch-screen panel fabricated with a laser-nanowelded CuNWs transparent conductor. (b) Schematic illustration the fabrication process of semitransparent small molecular weight organic photovoltaic cells.

Figure 1.5 (a) Optical photographs of a PLED using GO-AgNW/PUA composite electrode as both anode and cathode being driven at 14 V and stretched to specified strains. (b) Motion detection of index and middle fingers, and control of avatar fingers in the virtual environment using wireless AgNWs/PDMS nanocomposite strain sensors.

Figure 1.6 (a) Infrared camera images of ligand exchange AgNW/SBS meshes at applied strains of 0, 20, 40, and 60% and applied voltage of 0.75 V. (b) Schematic of an electrochromic device in an electrolyte solution. (c) Optical transmittance spectra of colored and bleached states of prussian blue films deposited on a RG-O/CuNW transparent electrode. (d) As-prepared mixed transparent electrode composed of pure CuNW films and RG-O/CuNW films.

Figure 1.7 Optical image (a) and SEM (b) of aligned arrays of SWNTs transferred from a quartz growth substrate to the surface of a glass cylinder. The inset in (b) provides a high-magnification view. Optical image (c) and SEM (d) of aligned arrays of SWNTs transferred from a quartz growth substrate to a thin sheet of polyimide (Kapton).

Figure 1.8 SEM images of the sample after the transfer process. (a) Top view. Inset is a high-resolution image. (b) Image of the sample viewed from the tilted angle. The inset image shows

that the linewidth is around 5 μm . (c) Schematic diagram of graphene/EVA/PET-based triboelectric nanogenerator. (d) Working mechanism of the triboelectric nanogenerator.

Figure 1.9 (a) Schematic Illustration of the formation of PANI Nanobelts and nanospheres. (b) SEM images of PANI nanobelts. (c) SEM image of PANI nanospheres.

Figure 1.10 (a) Schematic illustration of the procedure for fabricating highly stretchable, conductive lines. (b) SEM image showing the composites in the trenches. The inset is a magnified image. (c) TEM image of the composite structures, showing an interpenetrating network between the gel and AgNPs.

Figure 1.11 (a) The fabrication process of stretchable and conductive self-assembled AuNWs electrode. (b) SEM image of monolayer AuNWs film on PDMS substrate (Scale bar: 1 mm). (c) Atomic force microscopy image of monolayer AuNWs film on mica substrate (Scale bar: 50 nm). (d) UV-Vis-NIR transmission spectra of monolayer and multilayers AuNWs mesh films on PDMS substrates. (e) Transmittance as a function of sheet resistance.

Figure 1.12 Pictures of the reaction flask (a) before the synthesis and (b) after growth of CuNWs at 80 $^{\circ}\text{C}$ for 1 hr. (c) SEM image of CuNW product. The nanowires are 90 ± 10 nm in diameter and 10 ± 3 μm in length. (d) SEM and (e) TEM of CuNW products of a 24 h synthesis.

Figure 1.13 Schematic illustration of the fabrication process of a CuNW–PU composite electrode.

Figure 1.14 SEM images of (b) Cu–Ag core–shell NWs, and (c) Cu–Au core–shell NWs. Average diameters were calculated from 50 distinct nanowires. (d) TEM–EDS images of Cu–Ag and Cu–Au NWs.

Figure 1.15 (a) SEM image of the drop-casted AgNWs. (b) SEM image of the sprayed AgNWs. Inset: annealed AgNWs at 230 $^{\circ}\text{C}$ for 20 min. (c) Schematics of drop-casted and sprayed AgNWs and TEM images of PVP layers after 1-time and 5-time solvent washing process.

Figure 2.1 The cross-sectional and over view showing the fabrication process of fully embedded CuNWs/PDMS conductors.

Figure 2.2 (a) SEM image of as prepared CuNWs, inset is the cross-section of a CuNW. (b) High-resolution TEM images of the CuNWs. (c) and (d) The SEM images of the cross section for fully embedded conductor. SEM image of (e) fully embedded and (f) semi-embedded conductor.

Figure 2.3 (a) Resistivity change of CuNWs/PDMS conductors during the stretching/releasing process. (b) XRD images of the CuNWs/PDMS conductor before and after high-intensity pulsed light treatment. (c) The surface microstructure changes of the fully embedded structure and semi-embedded structure after the light treatment. (d) SEM image of the CuNWs after the light treatment.

Figure 2.4 The SEM images of the embedded and semi-embedded conductors before and after the light treatment.

Figure 2.5 (a) Relative resistance (R/R_0) of fully embedded and semi-embedded CuNWs/PDMS conductors with strain up to 70% at a constant stretching speed of 1 mm/min. (b) SEM image of the CuNWs/PDMS conductor after stretching.

Figure 2.6 Performance comparison between semi-embedded and fully embedded CuNWs/PDMS structures. (a) and (b), relative resistance of the conductors during the stretching-releasing process with the peak value of 10%, 20%, 30% strain. (c) The change of relative resistance in harsh environment (85 °C/85% RH). (d) After 85 °C/85% RH test, the relative resistance of conductors during the stretching-releasing process with the peak value of 20% strain.

Figure 2.7 Applications of fabricated CuNWs/PDMS conductors for wearable electronics. (a) Optical images during the stretching process of CuNWs/PDMS antenna and (b) its return loss before and after the 500-cycles stretching test. The time-dependent average temperature of the (c) semi-embedded and (d) fully embedded conductors at on/off responses over 10 cycles under an applied voltage of 4 V. The insets present infrared images of the conductor during repeated heating tests.

Figure 3.1 Schematic diagram of the galvanic replacement free formation of Cu@Ag core-shell nanowires.

Figure 3.2 SEM images of (a) CuNWs, (b) Cu@Ag-ammonia core-shell structure and (c) Cu@Ag core-shell nanowires. TEM image of the cross-section for Cu@Ag core-shell nanowires (d), and the corresponding elemental mapping images (e-g). The samples all with 20 wt% of silver.

Figure 3.3 The SEM images of core-shell precursors with (a) 5 wt%, (b) 20 wt%, (c) 30 wt% of Ag and Cu@Ag core-shell nanowires with (d) 5 wt%, (e) 20 wt%, (f) 30 wt% of Ag.

Figure 3.4 The growth process for the Cu@Ag-ammonia core-shell precursors. The SEM image

of (a) pure CuNWs, the Cu@Ag-ammonia core-shell structure obtained with different stirring times: (b) 1 min, (c) 5 min and (d) 10 min. TEM image of the cross-section for (e) Cu@Ag nanowire, (f-h) the corresponding elemental mapping images, which obtained from the solution that mixed for 5 min. The silver is 20 wt% in complex inks.

Figure 3.5 The adsorption process of (a) $\text{Ag}[(\text{NH}_2\text{CH}_2\text{CH}(\text{CH}_2\text{CH}_3)(\text{CH}_2)_3\text{CH}_3)_2]^+$ by atomistic molecular dynamics simulation. Time evolution of (b) electrostatic energy and van der waals energy, (c) total valence energy and total potential energy of CuNWs and Ag-ammonia mixed solution. (d) The adsorption process of $\text{Ag}[(\text{NH}_3)_2]^+$ on the surface of CuNWs by atomistic molecular dynamics simulation.

Figure 3.6 The appearance change of Ag (I) β -ketocarboxylate and 2-ethylhexylamine mixed solution at room temperature.

Figure 3.7 (a) XRD patterns of Ag-ammonia complex at different decomposition temperatures. (b) XRD patterns of the Cu@Ag core-shell nanowires with different amount of silver.

Figure 3.8 (a) Transmittance versus the sheet resistance of transparent conductors made from CuNWs, Cu-5Ag, Cu-20Ag and Cu-30Ag. Stability of transparent conductors ($T = 80\%$) in (b) standard harsh condition ($85\text{ }^\circ\text{C}$, 85% RH) and (c) high temperature environment ($140\text{ }^\circ\text{C}$). (d) On/off responses of transparent conductive heater (Cu-20Ag, $T = 80\%$) with the applied voltage of 6 V. (e) The temperature changes of the heater with the applied voltage changed from 1V to 8V, as well as the corresponding infrared images.

Figure 4.1 (a) Schematic of the fabrication process of TAE electrodes and corresponding SEM images of the products for each step: Cu@Ag-amine core-shell structures, Cu@Ag core-shell nanowires, and TAE electrodes. Optical images of the large-size TAE electrode before (b) and during (c) the stretching. (d) Typical force-strain curves of pure PU substrates and TAE electrodes.

Figure 4.2 Resistance evolution and top-view images of Cu@Ag nanowires/PU electrodes as a function of supplied energies for HIPL process. (a) Resistance and transparent changes of Cu@Ag nanowires/PU electrodes treated with different light energy. SEM images of Cu@Ag networks on PU substrates treated with light energy of (b) 0.8 J/cm^2 , (c) 2.4 J/cm^2 , and (d) 3.2 J/cm^2 .

Figure 4.3 (a) The evolution of transmittance of the samples under different strain. (b)The surface

roughness evolution of the Cu@Ag core-shell nanowires/PU electrodes ($T = 89\%$) that treated with the light energy of 0, 0.8, 2.4 to 3.2 J/cm^2 .

Figure 4.4 The evolutions of surface morphology and crystal structure of Cu@Ag nanowire electrodes treated with different light energies. SEM images of the surface transformation for Cu@Ag nanowires treated with energies of (a) 0 J/cm^2 , (b) 1.6 J/cm^2 , (c) 3.2 J/cm^2 . (d-f) The EDS mapping images of Cu@Ag alloy nanowires. (g) XRD patterns of Cu@Ag nanowires after HIPL process with different energies. (h) The solid solubility changes of Cu in Ag and Ag in Cu.

Figure 4.5 (a) The shift tendency of 2θ positions of Ag(111) and Cu(111) diffraction peaks as the input light energy increases. XRD patterns of (b) pure Ag electrode and (c) pure Cu electrode after HIPL process using the light energy of 4.1 J/cm^2 . (d) Spacing changes of Ag (111) and Cu (111) diffraction directions with different input energy.

Figure 4.6 Thermal stability and electro-mechanical stability of TAE electrodes ($T = 85\%$, $\text{SR} = 23 \text{ } \Omega/\text{sq}$). (a) Evolution of the R/R_0 of CuNW electrodes, Cu@Ag core-shell NW electrodes, TAE electrodes, and previously reported electrodes during the high temperature and high humidity aging test. (b) Evolution of the R/R_0 of the CuNW, Cu@Ag core-shell NW and TAE electrodes under high temperature of $140 \text{ }^\circ\text{C}$. (c) Evolution of the R/R_0 of electrodes under a strain of up to 80% . (d) Evolution of the R/R_0 of electrodes during the cyclic test at 30% strain (12 s for one cycle).

Figure 4.7 SEM images of the structure changes for (a, b) CuNW conductor and (c, d) AE conductor exposed at standard harsh environment ($85 \text{ }^\circ\text{C}$, $85\% \text{ RH}$) for (a, c) 10 h and (b, d) 50 h .

Figure 4.8 Characterization of stretchable transparent heaters based on TAE electrodes. (a) The temperature evolution of the heater for stepwise increases in voltage from 1 to 6 V . (b) The cyclic thermal stability test of the heater with the applied voltage of 5 V . (c) Temperature as a function of time for different applied voltages and for different initial SR. (d) Relative temperature change and the corresponding IR images of the heater ($T = 80\%$, $\text{SR} = 11 \text{ } \Omega/\text{sq}$) as a function of applied tensile strain. The applied voltage is 4 V .

Chapter 1

Research background

1.1 Flexible electronics

1.1.1 Definition and advantages of flexible electronics

Researchers listed flexible electronic technology as one of the world's top ten scientific and technological achievements in 2000, juxtaposed with major discoveries such as human genome sketches and biocloning techniques [1, 2]. Flexible electronics are of fundamental importance in the development of conductive devices due to their high flexibility and low manufacturing costs [3]. The flexible conductors, generally consisting of electronic circuits and flexible elastomers, which could maintain intimate contact with curvilinear surfaces during the large deformation process [4, 5]. Compared with traditional conductors, flexible conductors have greater flexibility, can adapt to different working environments to a certain extent, and meet the deformation requirements of the equipment. However, the corresponding technical requirements also restrict the development of flexible conductors. First of all, the tensile strength and flexibility of the stretchable conductor on the basis of not damaging its own electronic properties pose new challenges and requirements for the fabrication of the circuits. Secondly, the preparation conditions of flexible conductors and the performance of electronic devices constituting the circuit are still insufficient compared with the conventional electronic devices, which is the major problem for its development [6, 7].

Flexible electronics cover organic electronics [8], plastic electronics [9], bioelectronics [10, 11], nanoelectronics [12], printed electronics [13], etc., which including a variety of applications such as RFID, flexible displays, organic electroluminescence illumination, chemical and biosensors, flexible photovoltaics, flexible logic and storage, flexible batteries, and other wearable devices [14-16]. With its rapid development, the fields involved have been further expanded, and it has become one of the research hotspots in interdisciplinary fields. In 2012, Rogers et al. published a review article describing the development of flexible electronics in the biomedical

field [17]. Bao et al. elaborated on the research progress of flexible electronic applications in electronic skin in the 25th anniversary of Advanced Materials [18]. Chiolerio et al. published a classic review in 2014 to further discuss the research progress and development trend of flexible electronic devices for the manufacture of wearable devices [19]. At present, artificial intelligence has been rapidly developed, and various human-like intelligent robots emerge in an endless stream. Tactile perception is one of the basic functions of human and future intelligent machines to explore the physical world. Therefore, the development of tactile-like bionic electronic skin flexible devices and implementation of devices mechanical matching with soft tissue has important scientific significance and application value. Flexible wearable electronics, refer to electronic devices or devices that are mechanically flexible and that can be directly or indirectly attached to the skin [20, 21]. Wearable electronics can be a set of various functional devices, such as displays, sensors, batteries, etc., that work on the surface of the human body or in the human body. The research and application of wearable electronics is embodied in many aspects of human life, such as electronic skin, wearable physiological monitoring and treatment devices, flexible conductive fabrics, thin film transistors and transparent film flexible gate circuits [22-24]. Recently, the research on flexible electronics has entered a stage of substantive development from the initial stage.

1.1.2 Strategies to enable stretchability of electronics

The straightforward strategy for obtaining stretchable electronics is to build electronic circuits on top of the stretchable substrate or embed them in elastomers to form composite structures [25, 26]. During the stretching process, the electronic circuits offer good electrical conductivity, and the elastomers provide mechanical deformability and protect the conductive pathways from fracture. In addition to the formation of composite structures, tensile structures such as grid, wavy, spring-like, and coiled structures are often introduced to cope with the large deformations [27, 28].

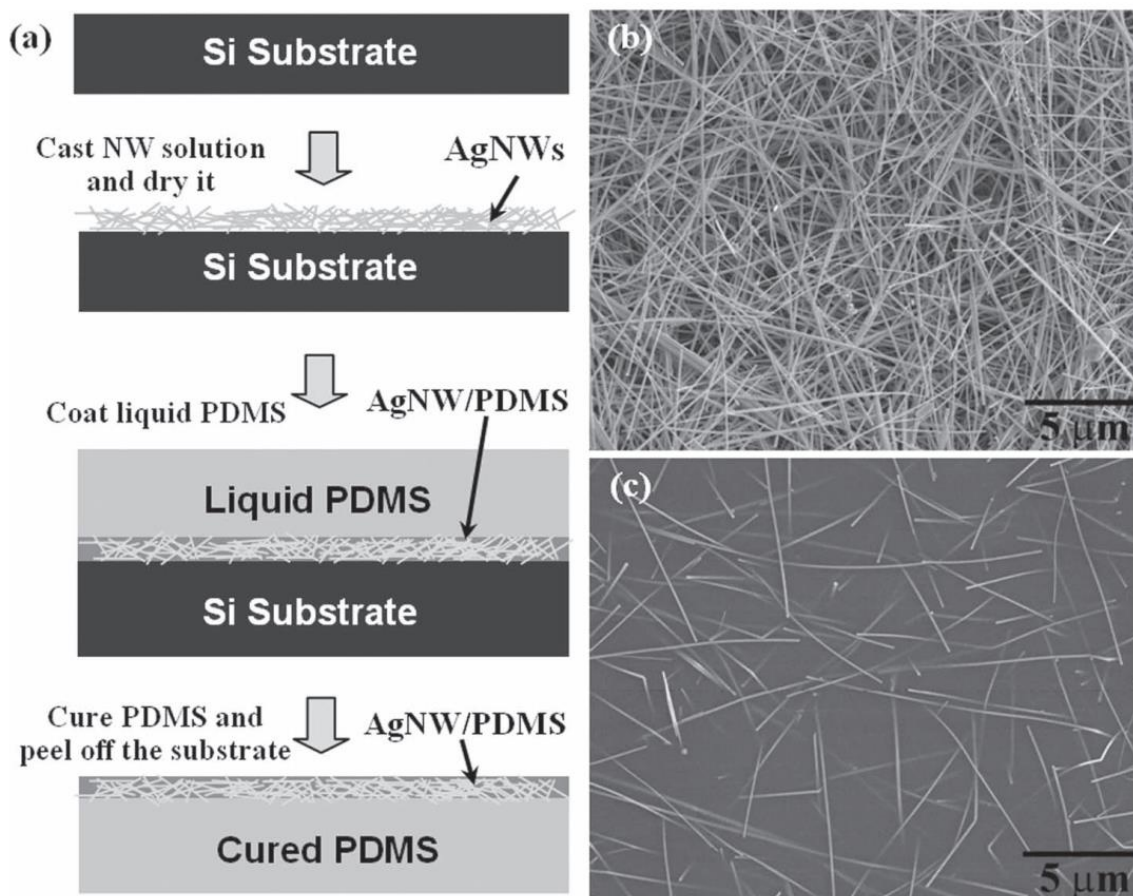


Figure 1.1 (a) A schematic showing the fabrication process of the composite AgNW/PDMS stretchable conductors. (b) SEM image of the AgNW film on Si substrate. (c) SEM image of the AgNW film after transferred to PDMS substrate [29].

Dispersing conductive nanomaterials into elastomeric substrates to form composite structure is one method to increase the stretchability, as shown in Figure 1.1 [29]. Highly stretchable and electrically conductive composites can be obtained by balancing the electrical conductivity of the rigid filler nanomaterials (silver nanowire, AgNW) with the mechanical deformability of the soft matrix (poly(dimethylsiloxane), PDMS). The aspect ratio and purity of conductive nanomaterials, the choice of processing methods, and the addition of surfactants are important for the performance of stretchable composite electronic devices. Therefore, dispersion techniques such as jet milling and ultrasonic treatment are used to ensure uniformity and density of the conductive nanomaterial in the surrounding polymer matrix [30]. Generally, such composites electronics composed of conductive nanomaterial fillers and polymer matrixes exhibit reasonable electrical conductivity

during the stretching process. However, the sliding of the conductive circuits during the stretching process reduces the contact area between the nanomaterials, and the electrical conductivity gradually decreases as the applied strain increases. Therefore, the stretchable conductor with stable conductivity can be realized only by further introduce net-shaped or wavy structured conductive pathways [31, 32].

Pre-strain is another effective method to achieve electronics with high stretchability on an elastomeric matrix. With this method, the weak conductive pathways formed by inorganic nanomaterials during stretching process can maintain their high conductivity. Figure 1.2a schematically illustrates the pre-strain process [25]. The first step is to pre-stretch the elastomeric matrix and increase its original length. After that, transfer or embed conductive nanomaterial onto the pre-stretch elastomeric matrix. Finally, release the pre-stretch matrix to restore its original length. After pre-strain treatment, a periodic wavy structure is formed on the elastomeric matrix, which can cope with various deformations such as stretching, compression, and bending. During the stretching process, the presence of wavy structures greatly reduces strain experienced inside of the material, which results in constant conductivity. The interface property between conductive nanomaterial and elastomeric matrix is crucial to enhance the stretchability and electrical properties of samples [33, 34].

In the case of pre-strain method, the pre-stretch of the elastomer matrix largely limits the large-scale productions like a roll-to-roll process. Therefore, another method is demonstrated without pre-strain treatment as shown in Figure 1.2b [25]. In this strategy, the pre-stretch process is conducted after the transferring or embedding of conductive nanomaterial onto the elastomeric matrix. During the stretching process, the electrical resistance is typically heavily dependent on the strain history and is stabilized after the release of elastomeric matrix. The sample can be bent in the direction of the tensile strain or in the vertical direction. According to the Poisson effect, when longitudinal stretching is performed, the stress in the vertical direction is at a relatively lower stage. When the strain is released, the vertical direction quickly returns to the initial state, which particularly suitable for the application of one-dimensional nanomaterials [35]. However, this

method also exhibits some disadvantages, which are not suitable for vertical direction stretching and are only suitable for tensile strain direction stretching.

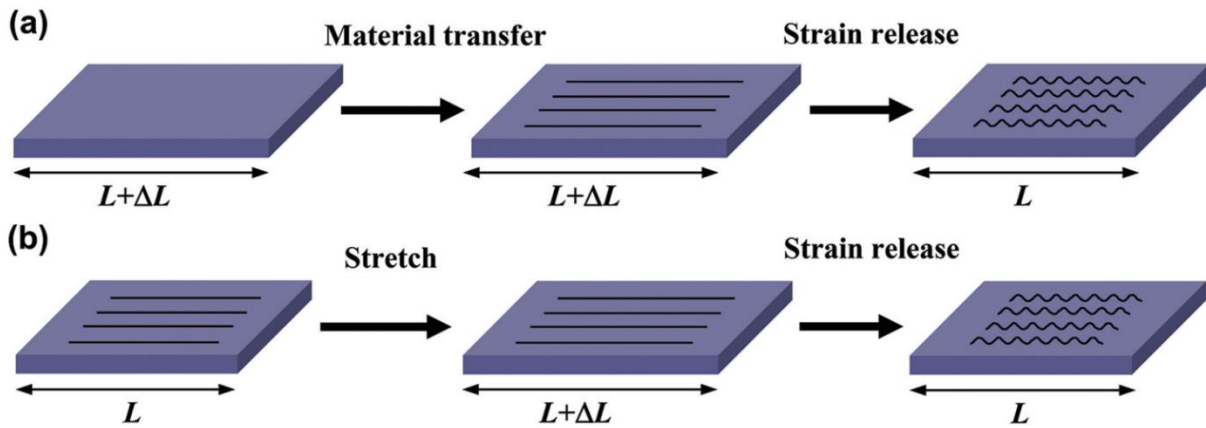


Figure 1.2 Schematic illustrations of the mechanical buckling processes: a) Prestrain–release–buckling and b) stretching–release–buckling along the longitudinal direction [25].

Besides the above methods, other methods like conductive networks and spiral structures are used to enhance the stretchability of the devices as shown in Figure 1.3 [36, 37]. Recently, electrospinning, spring coating, and cross stacking method are usually used to form the conductive networks. Carbon nanotubes (CNTs) and metal nanowires are the most commonly used materials to fabricate conductive networks. When a tensile force is applied, the nanomaterial in the network structure will adapt to most of the strain by shape changes such as mutual rotation and sliding, thereby maintaining high electrical conductivity during the stretching process. In addition, high intense plus light or laser sintering method are introduced to form strong connections between the nanowires to further improve the electrical conductivity. The spiral structures are always formed by the twisting of substrates, which could absorb the strain by straightening the loops [38].

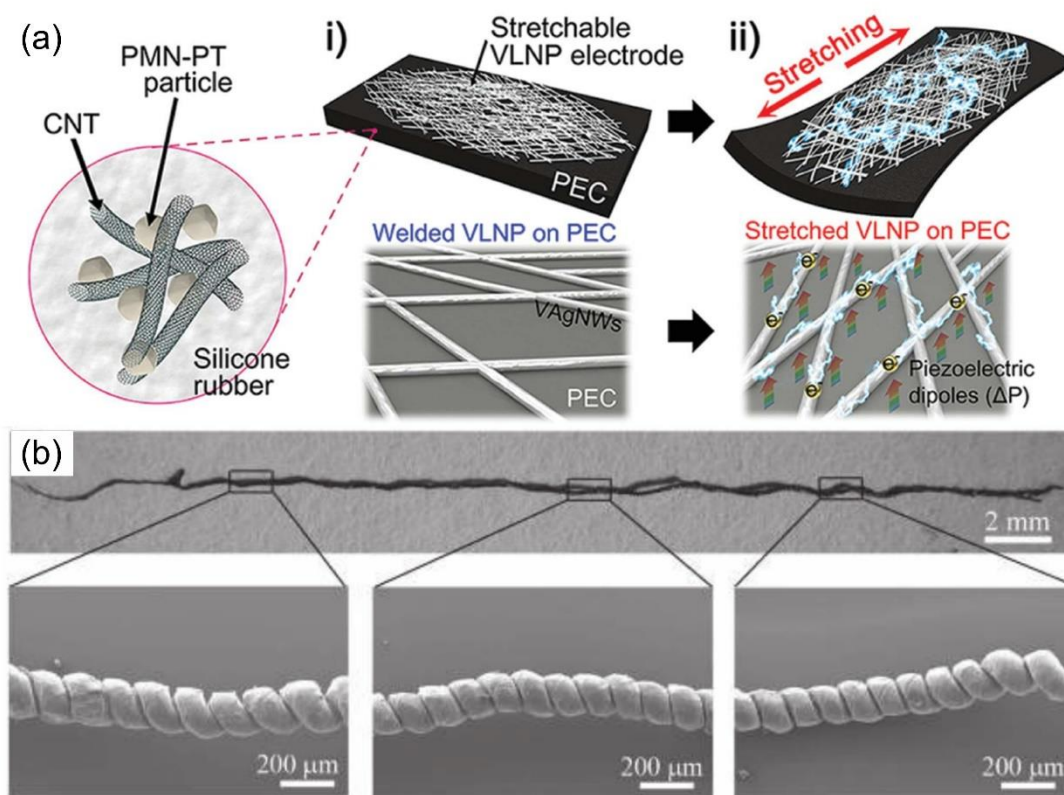


Figure 1.3 a) Schematic illustration of the hyper-stretchable and deformable nanocomposite generator. (b) SEM images show the loop structure of the CNTs in corresponding places [36, 37].

1.1.3 Application of flexible electronics

The emerging flexible electronics have foreseen the revolution of future electronics, ranging from design, shape, functions, applications and even user experience. For example, touch screens are now widely used in electronic devices, which consists of two transparent layers. However, the high price and non-renewable nature limit the commercial application of traditional Indium tin oxide (ITO) materials in touch screens. Therefore, the search for low-cost alternative materials has become a hot research topic. Transparent stretchable films made from AgNWs and copper nanowires (CuNWs) have been proven to be used in touch screens. Han et. al used flexible CuNWs films as conductive layers for writing on a touch screen, as seen from Figure 1.4a [39]. Herein, metal nanowire based flexible conductors are expected to be widely used to fabricate touch screens while ensuring low cost and excellent performance.

Organic photovoltaic cells (OPV) have been proven to effectively absorb the energy of sunlight, and with a low price, which become one of the promising electronic devices. The cost of existing solar energy conversion system is about ten times than that of OPV, and the expensive cost makes it less competitive when faced with fossil fuels. However, the use of ITO in OPV greatly increases manufacturing costs. Around 2010, researchers began to replace ITO with AgNWs films, but their energy conversion efficiency was only around 0.63 % to 2.8 % (Figure 1.4b) [40]. The low conversion efficiency is due to the fact that the surface roughness of the nanowire networks is too large, which is comparable to the dimensions of the polymer active layer. In order to reduce surface roughness, Wiley et al. prepared OPV by coating PEDOT:PSS on the pressurized AgNWs and CuNWs networks [41]. The conversion efficiency can be increased to 5 %, which is higher than the industrialized ITO.

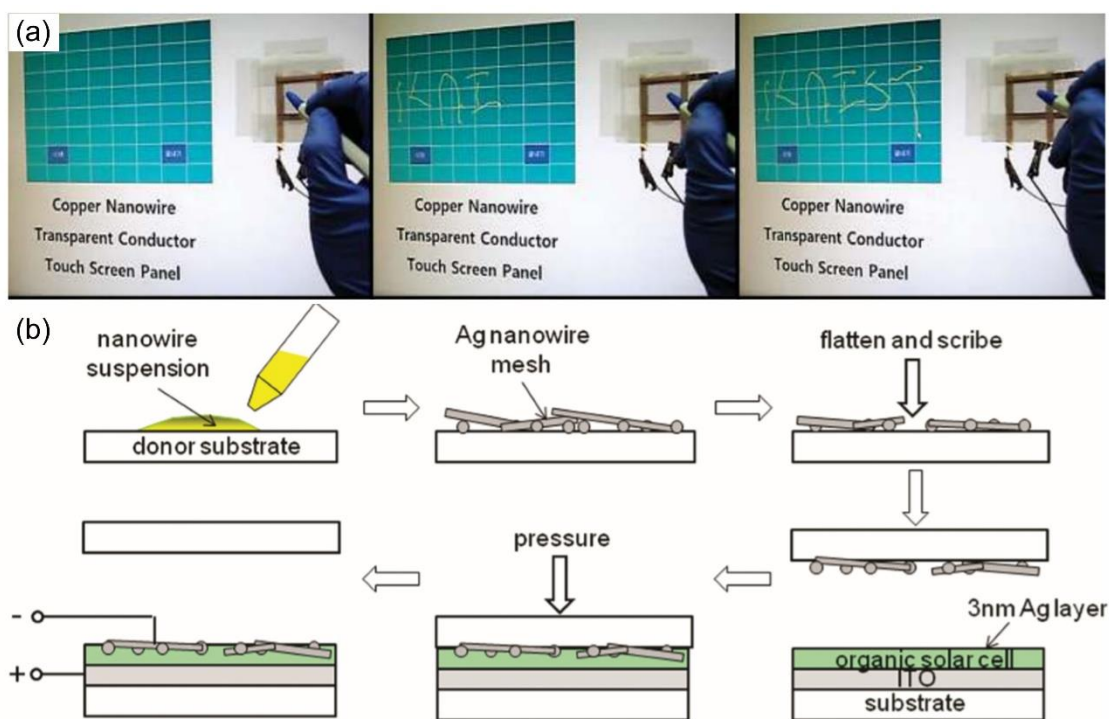


Figure 1.4 (a) Demonstration of the touch-screen panel fabricated with a laser-nanowelded CuNWs transparent conductor. (b) Schematic illustration the fabrication process of semitransparent small molecular weight organic photovoltaic cells [39, 40].

High-performance and low-cost flexible conductors are also an important component for the fabrication of organic light-emitting diodes (OLED). The larger resistance of conductors will increase operating voltage of a device and cause the uneven illumination and aging of LED [42]. In addition, a conductor should exhibit excellent flexibility in order to cope with the roll-to-roll process of OLED. Pei et al. transferring AgNWs to composite films by curing composite films (polyurethane acrylate, PUA) on the surface of AgNWs networks [43]. The obtained polymer light-emitting diodes (PLED) has high efficiency of 14.0 cd/A. In 2014, they further covered the surface of the AgNWs networks with the sheet-like graphene oxide (GO) to obtain high-performance composite films (Figure 1.5a) [44]. The stretchable white OLED was successfully prepared with the obtained composite films as anode and cathode, which could work normally after 130 % tensile deformation.

Sensors respond to mechanical deformation through changes in electrical signals such as resistors and capacitors. Sensor performance includes sensitivity, stretchability, reaction speed, and stability. In order to facilitate a wide range of uses, processing costs and operation easiness are also issues that must be considered. However, sensors currently used cannot be stretched and have low sensitivity, it is necessary to develop novel stretchable conductors to fabricate sensors. The stretchable sensors can be used in many areas such as personal health monitoring, human motion capture, and etc [45]. As shown in Figure 1.5b, Amjadi et al. used AgNWs to make sensors that could be attached to the glove or applied directly to the skin [46]. The sensor uses a sandwich structure of PDMS-AgNWs-PDMS to ensure the stability of the sensor during stretching process. When the finger is bent, the resistance of AgNWs sensor rises under tensile strain, and when the finger returns to straight, the stress applied to the sensor disappears and the resistance returns to the original value. This sensor could maintain high sensitivity at 70 % stretch, which is superior to the traditional stress sensors.

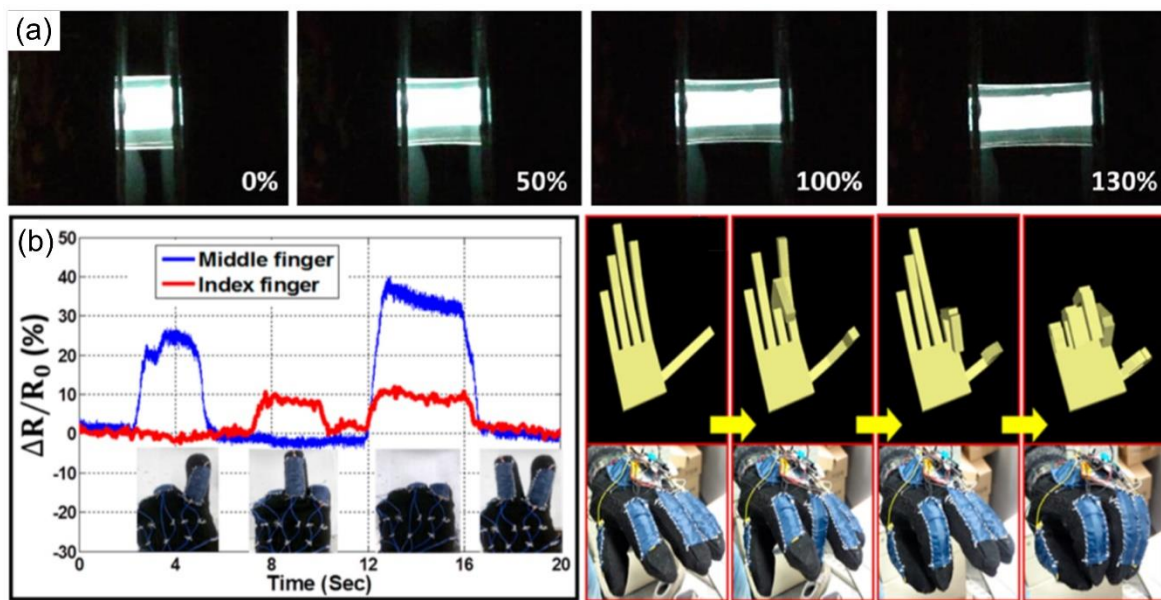


Figure 1.5 (a) Optical photographs of a PLED using GO-AgNW/PUA composite electrode as both anode and cathode being driven at 14 V and stretched to specified strains. (b) Motion detection of index and middle fingers, and control of avatar fingers in the virtual environment using wireless AgNWs/PDMS nanocomposite strain sensors [44, 46].

Due to obesity, occupational habits and aging, human joints are more vulnerable to injury, resulting in a series of joint diseases. Heater therapy is one of the common treatments for these diseases, which accelerates blood flow and collagen swelling to relieve pain and muscle stiffness. The commonly used heating methods are infrared radiation or electrotherapy. Instruments used in these methods are cumbersome and the temperature is difficult to control. Therefore, people hope to find a wearable lightweight heating device. Nian et al. successfully fabricate a soft, lightweight, stretchable heater by the introduction of AgNWs on styrene butadiene styrene (SBS) thermoplastic elastomer, as seen from Figure 1.6a [47]. The prepared heater can be worn on wrist and controlled generated temperature by adjusting applied voltage. When the input voltage of the AgNWs film is 5 V, the temperature of the heater can reach 50 °C.

In addition to the above applications, flexible conductors are also used to achieve normal operation of the functional device under stretching process. Pyo et al. have used AgNWs conductors as conductive layers for electrostrictive devices due to their high conductivity under

stretching conditions [48]. When the voltage is applied, the AgNWs conductor is stretched in plane as the device expands. Although the area of conductor has expanded 1.8 times, it still maintains ultra-high conductivity. As depicted in Figure 1.6b, Kholmanov et al. used reduced graphene oxide (RG-O)/CuNWs conductors instead of ITO mounted on the blue electrochromic devices [49]. When energized, blue color is bleached to transparent, and the transmittance of the conductive film is significantly improved. Due to the protection of CuNWs by reduced graphene, the reaction can be repeated without damaging the conductivity of the conductive film.

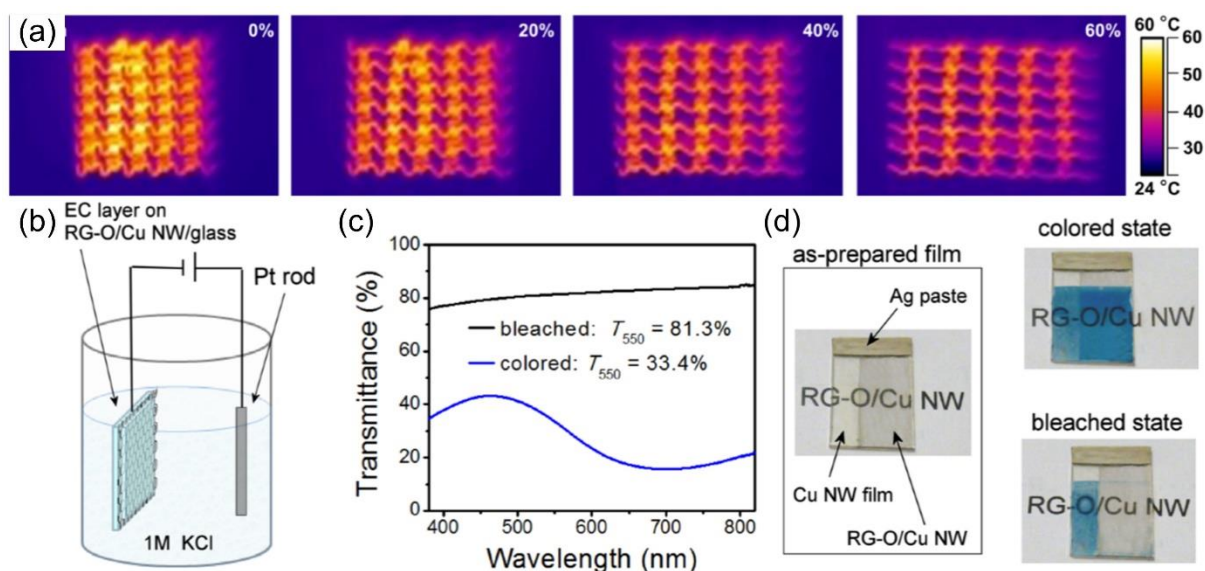


Figure 1.6 (a) Infrared camera images of ligand exchange AgNW/SBS meshes at applied strains of 0, 20, 40, and 60% and applied voltage of 0.75 V. (b) Schematic of an electrochromic device in an electrolyte solution. (c) Optical transmittance spectra of colored and bleached states of prussian blue films deposited on a RG-O/CuNW transparent electrode. (d) As-prepared mixed transparent electrode composed of pure CuNW films and RG-O/CuNW films [47, 49].

1.2 Next-generation stretchable electronics

As mentioned in the foregoing section, ITO is the commercially used conductive material in flexible electronics. However, it is not suitable for deposition on flexible substrates to prepare conductive films due to high deposition temperatures. In addition, the friability of ITO makes the conductive film have poor mechanical properties, which is prone to cracking during bending and stretching. Therefore, there is an urgent need to find a conductive material to replace ITO [50].

Exciting progress has been made in the field of stretchable electronics, mainly through the exploration of conductive materials used to form electronic circuits. The newly developed conductive materials can be divided into three categories: carbon-based materials, conductive polymers, and metallic nano/micro particles and nanowires.

1.2.1 Carbon based conductors

In recent years, carbon based materials represented by CNTs and graphene have received extensive attention in the field of conductive materials due to its excellent electrical and thermal conductivity, outstanding physical and chemical stability as well as excellent mechanical properties [51, 52]. Due to the excellent aspect ratio and easy regulation of structure and properties, CNTs are an ideal conductive material for stretchable electronics [53]. CNTs can be prepared by arc discharge method, laser ablation method and chemical vapor deposition method (CVD) [54]. Among them, the requirement of strong controllability, low cost, and easy realization of mass production of CNTs make the CVD method widely used both in basic scientific research and in industrial production applications. CNTs with various morphologies were prepared by CVD method, such as the horizontal array of CNTs, the vertical array of CNTs, and CNTs film, etc., which can be used for preparing wearable devices, conductive materials, and stretchable sensors [55].

CNTs array refers to CNTs samples aligned in same direction, which is usually carried by stretchable substrates. The sample in which CNTs are axially parallel to the substrate is called as horizontal array of CNTs, and the sample in which CNTs are axially perpendicular to the substrate is named as the vertical array of CNTs [56]. Both of them can be directly prepared by a CVD method. The horizontal array of CNTs have good application prospects in the field of stretchable electronic devices due to their strong controllability, good orientation, and low defect content. Liu et. al first proposed a gas-directed CVD method [57]. By using different heating rates for substrate and gas carbon source precursor, the temperature difference between gas and substrate causes CNTs to float growth in a horizontal direction. In addition, the orientation of CNTs can be induced

by the application of an electric field or a magnetic field. Rogers et. al conducted a study on the horizontal array of single-walled carbon nanotubes (SWNTs) in flexible electronic materials as shown in Figure 1.7 [58]. Firstly, high-density horizontal arrayed CNTs are grown on the surface of quartz substrates. After that, PDMS-assisted transfer method was used to transfer the horizontal arrayed CNTs to Si wafers, glass, and some curved structures to design as stretchable conductors.

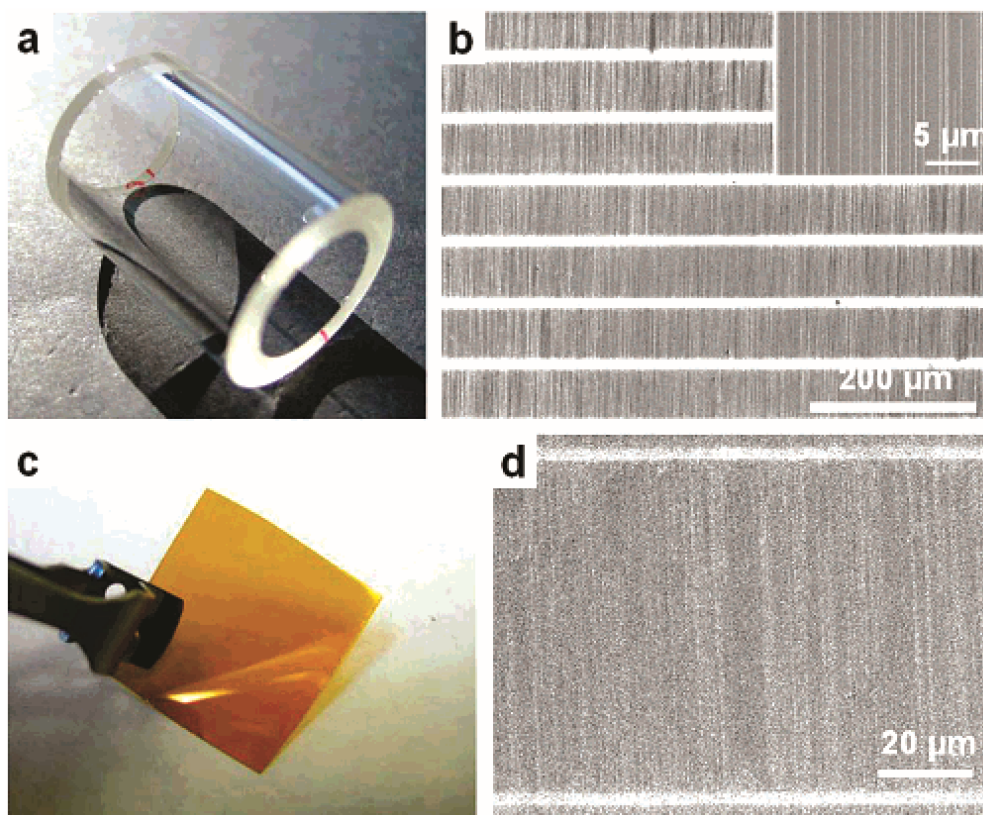


Figure 1.7 Optical image (a) and SEM (b) of aligned arrays of SWNTs transferred from a quartz growth substrate to the surface of a glass cylinder. The inset in (b) provides a high-magnification view. Optical image (c) and SEM (d) of aligned arrays of SWNTs transferred from a quartz growth substrate to a thin sheet of polyimide [58].

The vertical array of CNTs is a macroscopic body of CNTs grown perpendicular to a catalyst substrate and arranged nearly parallel to each other. At present, the mainstream method for preparing vertical arrayed CNTs is the catalyst thin film assist method, which uses substrates pre-deposited with a high bulk density nanoscale catalyst film to grow the vertical arrayed CNTs [59]. As depicted in Figure 1.8a and b, the obtained vertical array of CNTs has a high orientation of

CNTs and excellent electrical conductivity, which is considered to be one of the ideal electrode materials [60]. By partially embedding vertical arrays, fully embedding vertical arrays and tiling with vertical array sheets, the vertical arrayed CNTs can be used in stretchable conductors. In addition, sensitivity coefficient and stretching range of vertical arrayed CNTs based sensors are generally higher than those obtained by other materials.

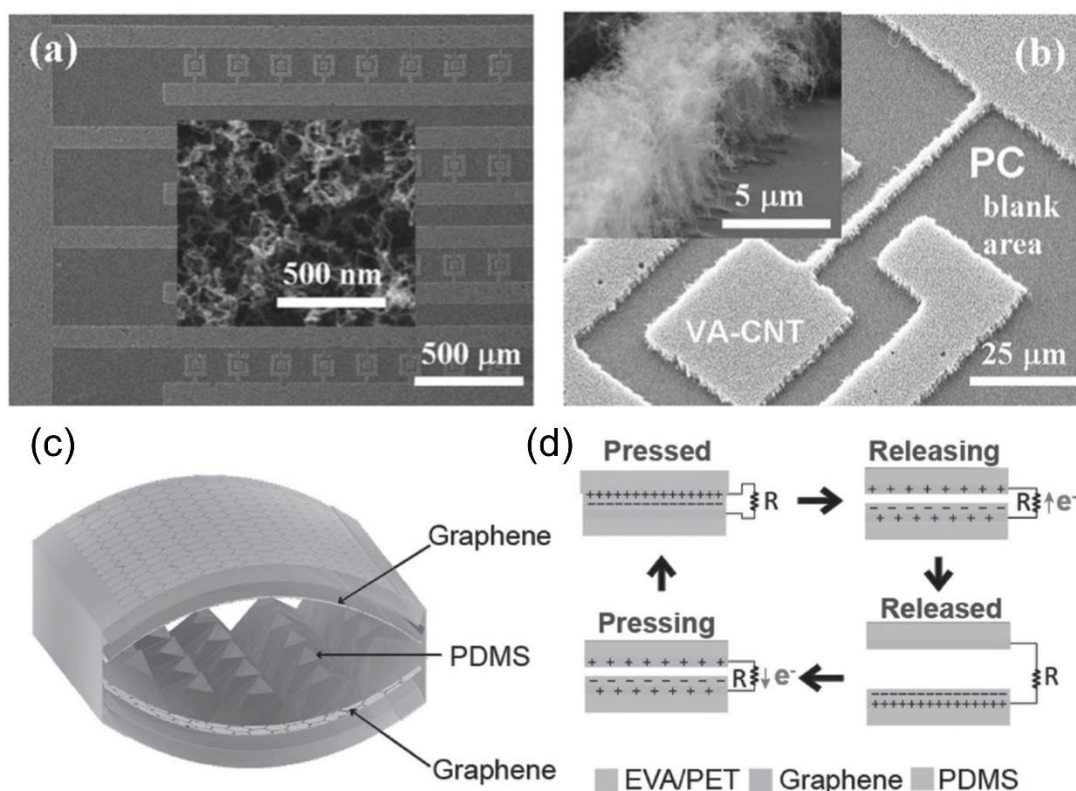


Figure 1.8 SEM images of the sample after the transfer process. (a) Top view. Inset is a high-resolution image. (b) Image of the sample viewed from the tilted angle. The inset image shows that the linewidth is around 5 μm . (c) Schematic diagram of graphene/EVA/PET-based triboelectric nanogenerator. (d) Working mechanism of the triboelectric nanogenerator [60, 61].

Graphene is another hot spot in the field of carbon based materials. Graphene is a honeycomb structure composed of sp^2 hybridized carbon atoms. The thickness of single-layer graphene is only 0.335 nm, with a high transmittance of 97.7 %, which is considered to be an ideal material for the preparation of flexible conductive materials onto ethylene vinyl acetate/poly(ethylene terephthalate) (EVA/PET) substrate (Figure 1.8c and d) [61]. At present, the preparation of

graphene based electronics is mainly divided into two categories according to the source of graphene. One of the methods is the introduction of mechanically stripped oligo-graphene solution or chemically stripped graphene oxide (GO) solution. The other method is to obtain high quality single or small layer graphene by a CVD method and then transfer it to the surface of elastomeric substrates. Among them, GO can be prepared by a simple, low-cost, and mass-produced method. More importantly, reduced graphene oxide (rGO) can be obtained by the subsequent chemical reduction, thermal reduction or photoreduction processed to improve its conductivity, which is advantageous for large-scale production [62, 63]. In contrast, CVD method can obtain graphene films with a large area and less defects, and thus excellent performance. However, this method is costly and severely limited by CVD equipment, and are often introduced defects and impurities in transferring graphene films to a flexible substrate. The combination of CNTs and graphene and their combination with other conductive nanomaterials can produce carbon nanomaterial composites with excellent properties, obtaining higher conductivity on the basis of ensuring flexibility and transparency, which is an important development direction for carbon nanomaterials based stretchable electronics.

1.2.2 Conductive polymers based conductors

Many kinds of polymers have been considered to be excellent electrical insulator for a long time. Since the first conductive polymer (Iodine or arsenic pentafluoride doped polyethylene film) was reported in 1977, conductive polymers as novel intrinsic flexible conductors have received increasing attention due to their easy processing, excellent mechanical properties, dimensional stability, and electrical conductivity [64]. In 1984, MacDiarmid first obtained conductive polyaniline under acidic conditions. They believed that conductive polymer is a kind of polymer material which is formed by chemical or electrochemical doping of a polymer having a conjugated bond, and the conductivity extends from insulator to conductor [65]. Conductive polymer consists of a polymer chain and a chain non-bonded monovalent pair of anions (p-type doping) or a pair of cations (n-type doping), which can be divided into two types, one is the coordination of polymer

conductive materials, and the other is conjugated conductive polymer materials. The conjugated conductive polymers are more common [66, 67].

Currently, various conjugated conductive polymers have been synthesized such as polypyrrole (PPy), polyacetylene (PA), polyaniline (PANI), poly(3,4-ethylenedioxythiophene) (PEDOT), polythiophene (PTH), and poly(3-hexylthiophene) (P3HT) [68-71]. These conductive polymers all exhibit metallic or semiconducting properties and have very low thermal conductivity. Conductive polymers have broad application prospects in solar cells, supercapacitors and biological fields due to their diversified structure, adjustable conductivity, lightweight, and easy processing. The size and morphology of the conductive polymers can be controlled by emulsion polymerization, interfacial polymerization, templating, and self-assembly method [72, 73]. In recent years, research on electrochemical polymerization of nano-scale conductive polymers and their composites has attracted extensive attention, including nanowires, nanofibers, nanotubes, nanobelts, and etc [74, 75].

Electrochemical polymerization method refers to oxidative polymerization of monomers in an electrolyte on the surface of an inert electrode by adjusting electrochemical parameters such as voltage, current, and electrolyte concentration under the action of an electric field to obtain a conjugated polymer film on the surface of electrodes [76]. This method has the advantages of low cost, simple process flow, controllable polymer film thickness, and simultaneous polymerization and doping. Conductive polymers with specific morphology and structure can be synthesized by typical electrochemical polymerization techniques such as potentiostats, constant current, potentiodynamic scanning, and pulsed methods. Tong et al. used polycurrent methods to prepare polyaniline(PANI) nanomaterials, as shown in Figure 1.9 [77]. By discussing the influence of current density on morphology of PANI, it is concluded that current density can significantly affect the polymerization and elongation of PANI, which in turn affects the morphology of PANI. PANI nanobelts have greater specific surface area and electrochemical performance than PANI nanospheres.

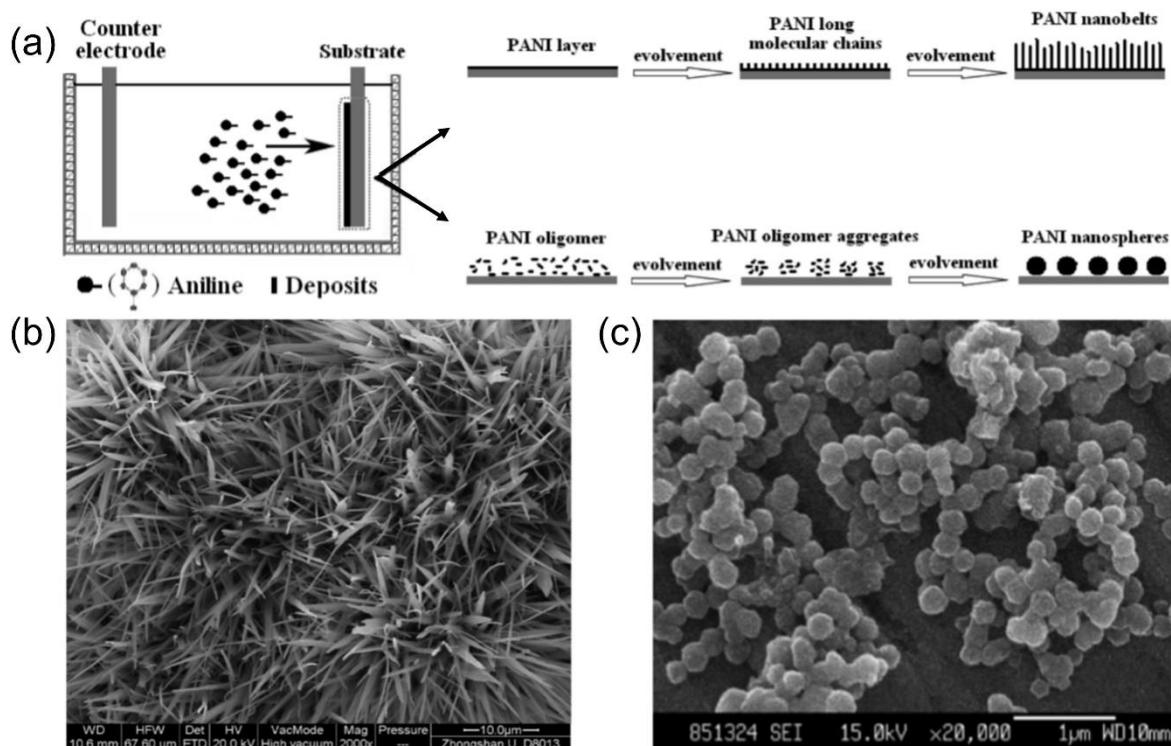


Figure 1.9 (a) Schematic illustration of the formation of PANI nanobelts and nanospheres. (b) SEM images of PANI nanobelts. (c) SEM image of PANI nanospheres [77].

The potentiostatic method is also often used to prepare conductive polymers. Li et al. used a potentiostatic method to assemble single-walled carbon nanotubes (SWNTs), graphene, gold and other nanomaterials and conductive polymers together to form layered conductive nano-surfaces [78]. SWNTs, gold nanoparticles have a high porosity of discontinuous phase, which makes pyrrole easily diffuse near the surface of silicon electrode, and the obtained composite films have unique layered structures due to the unique electrochemical synthesis process. The results show that this method can accurately design and control the type and morphology of conductive polymers, and complete the combination of different functional materials and their physical and chemical properties. Lakard et al. also used the potentiostatic method to deposit polypyrrole films in different electrolytes [79]. This study found that the potential of polypyrrole has a very significant effect on the chemical structure and conductivity of polypyrrole film.

Conductive polymers are widely used in flexible devices like supercapacitors, solar cell, and lithium-ion battery due to their high energy density, low dimensional structure, good electrical conductivity and stability. Cong et al. prepared uniform graphene-polyaniline composite nanopaper electrodes using an in-situ electrochemical method [80]. Electrochemical tests show that the specific capacitance of this composite electrode is as high as 763 F/g when discharge current is 1 A/g. When number of cycles reaches 1000 laps, specific capacitance remains at 85 % of the initial value, showing excellent cycle stability. Tai et al. prepared highly uniform transparent polyaniline electrodes for new dye-sensitized solar cells, which showing high power display efficiency of 6.54 % [81]. Yang et al. successfully synthesized layered MoS₂/polyaniline nanowires [82]. The unique structure of composite material greatly improves storage performance of lithium-ion batteries. When the current density is 100 mA/g, charging capacity reaches 1063 mAh/g, and remains at 90.2 % of the initial capacity after 50 cycles.

1.2.3 Metallic nanomaterials

Metallic nanomaterials have excellent photoelectric properties, which have broad application prospects in stretchable electronics. At present, there are many metallic nanomaterials based structures such as metal thin films, metal grids, and metal nanowire networks. Among them, silver and gold nanomaterials have received special attention due to their excellent catalytic and optical properties.

Silver nanowires (AgNWs) refer to one-dimensional line structures whose lateral dimensions are limited to nanometer scale (generally below 100 nm) and have no limitation in the longitudinal direction [83, 84]. At present, the preparation of AgNWs can be divided into two major categories: physical methods and chemical methods. Physical methods include ultrasonic pulverization, magnetron sputtering and mechanical pulverization methods [85, 86]. Chemical methods include hydrothermal method, electrochemical methods, template methods, photochemical reduction methods, ultrasonic reduction methods, and polyol methods [87, 88]. The synthesis process of physical methods is complicated, energy consumption is large, technical requirements are high,

and form uniformity of obtained product is poor. Relatively speaking, the chemical method has become one of the most suitable methods for industrial production of AgNWs due to its simple process, low cost and easy control of morphology. Among these methods, a polyol method has been widely used in terms of high yield, simple operation, and short reaction time. Jiu et. al used ethylene glycol as solvent and reducing agent, and polyvinylpyrrolidone as protective agent [89]. After adding a ferric chloride solution, the mixture was transferred to a constant temperature reaction vessel at 130 °C for 5 h. AgNWs with high aspect ratio can be obtained by the subsequent centrifugal washing process.

The resulting AgNWs are used to make a wide variety of devices. Kang et. al embedded AgNWs into resin and followed by a photocuring process to prepare AgNWs conductors with a surface roughness of 4.7 nm [90]. OLED devices are fabricated by the obtained conductors, which maintain high luminous efficiency unchanged after 5000 times bending cycles and under stretching process. Yang et. al used AgNWs conductive films as electrodes to prepare solar cells using a full liquid phase method [91]. The photoelectric conversion efficiency of the obtained solar cells on glass and PET substrates was 2.8 % and 2.5 %, respectively. When the bending angle of PET substrate reached 120°, the sample still keep a high photoelectric conversion efficiency of 2.5 %. Gaynor et. al prepared composite transparent electrodes for high-efficiency white LEDs by a full liquid phase method to immerse AgNWs in polymethyl methacrylate films [92]. The fabricated LEDs have a high luminous efficiency exceeds 30 lm/W. Low resistance and low light scattering properties of AgNWs transparent electrodes make them have an extremely high luminous efficiency in LEDs.

In addition to one-dimensional AgNWs, silver nanoparticles (AgNPs) are also used to fabricate stretchable electronics. The size of AgNPs is between clusters and macroscopic particles, which combines the advantages of nanomaterials and Ag elemental, and can be used to fabricate conductors by low-cost inkjet printing techniques. AgNPs can be obtained by simple physical methods such as light/laser irradiation, evaporation and condensation [93, 94]. However, such physical methods have high instrument requirements and high production cost, which is rather

suitable for industrial preparation with low requirements on the size and shape of the nanoparticles. In contrast, chemically synthesized AgNPs have been used in the fields of optics, electricity and biomedicine, which require relatively high performance of nanoparticles. Hyun et al. have fabricated a stretchable conductor with high stretchability and high electrical conductivity by the combination of AgNPs with a wavy structure [95]. As shown in Figure 1.10, the method employs a spin coating technique to cover the polystyrene on polydimethylsiloxane (PDMS) substrates, and then generates wavy structures by heating PDMS substrates. The resulting electrode exhibits excellent stretchability due to the interpenetrating structure of AgNPs into a stretchable substrate and the presence of ordered wave structures.

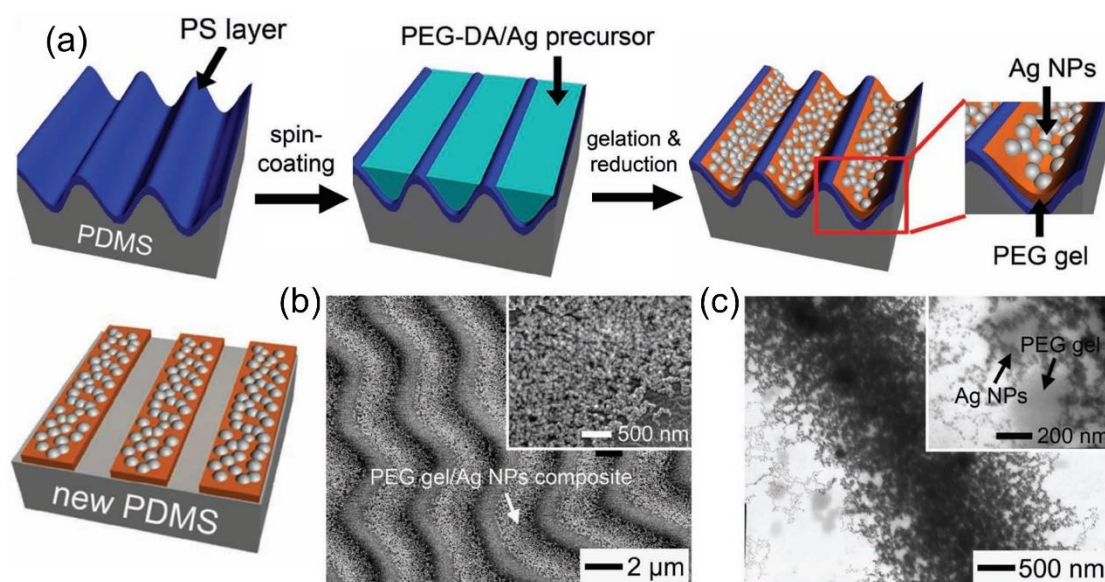


Figure 1.10 (a) Schematic illustration of the procedure for fabricating highly stretchable, conductive lines. (b) SEM image showing the composites in the trenches. The inset is a magnified image. (c) TEM image of the composite structures, showing an interpenetrating network between the gel and AgNPs [95].

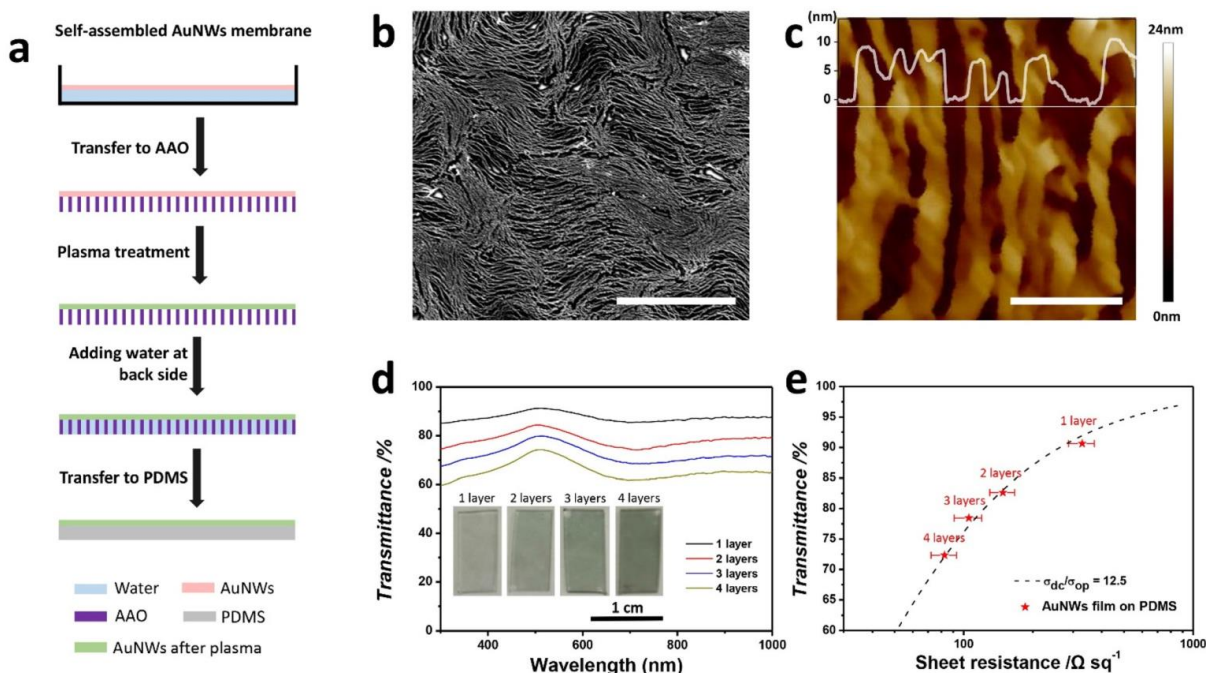


Figure 1.11 (a) The fabrication process of stretchable and conductive self-assembled AuNWs electrode. (b) SEM image of monolayer AuNWs film on PDMS substrate (Scale bar: 1 mm). (c) Atomic force microscopy image of monolayer AuNWs film on mica substrate (Scale bar: 50 nm). (d) UV-Vis-NIR transmission spectra of monolayer and multilayers AuNWs mesh films on PDMS substrates. (e) Transmittance as a function of sheet resistance [97].

Gold nanomaterials especially gold nanowires (AuNWs) have good stability and ductility, which can be preserved for a long time, so they are also regarded as a reliable material for preparing flexible conductors. Xu et al. using chloroauric acid (HAuCl_4) as precursors, introducing oleylamine as solvents, surface stabilizers and reducing agents to synthesize ultrafine AuNWs by a simple one-step wet chemical method [96]. The prepared ultrafine AuNWs not only have a high yield, high purity but also have a large aspect ratio, which has an average diameter of about 2 nm and a length of several tens of micrometers. If another reducing agent oleic acid is added and the volume ratio of oleylamine to oleic acid is adjusted to 1:1, AuNWs will be generated with a diameter of ~ 9 nm. The growth mechanism of ultrafine AuNWs is illustrated by changing reaction temperature and amount of reducing agent: using oleylamine as a template, under the action of a one-dimensional polymeric chain formed by the affinity binding of oleylamine and monovalent gold halide (AuCl), reduced Au atoms adhere to the surface of nucleated particles and grow into ultrafine gold one-dimensionally nanowires. The obtained AuNWs are usually used to fabricate

stretchable devices like stretchable supercapacitors. Gong et. al show a simple and effective method for making AuNWs based supercapacitors with highly stretchable and transparent, as shown in Figure 1.11 [97]. Due to the unique tensile structure and excellent flexibility of AuNWs, the prepared supercapacitor does not degrade after stretching for 80 cycles, exhibiting outstanding stretchability and electrical reversibility. In addition, gold nanoparticles (AuNPs) are also used to fabricate stretchable devices by combining with PU substrates by the layer-by-layer deposition and vacuum-assisted flocculation methods.

1.3 Motivation of present research

Although many researchers have focused on conductive materials like carbon nanomaterials, conductive polymers and metallic nanomaterials in recent years, poor photoelectric properties of carbon nanomaterials, complex manufacturing process of conductive polymers, and high cost of Ag and Au nanomaterials make them lose their competitiveness in the field of flexible electronics [98]. Recently, copper nanowires (CuNWs) have gained more and more attention and become an irreplaceable material in the field of flexible electronics. Firstly, Cu has excellent electrical conductivity, only 6 % lower than Ag. Secondly, the price of Cu is about 100 times cheaper than Ag and ITO, while the resource amount is 1000 times than them. Finally, the flexible conductors prepared by CuNWs exhibit superior performance in terms of conductivity and light transmittance [99].

1.3.1 Synthesis and film formation of CuNWs

At present, many methods have been proposed to synthesis nanomaterials. The template method is one of the most convenient methods to directly synthesis one-dimensional nanomaterial, which can be further divided into hard template method and soft template method. The commonly used hard templates are alumina, porous silicon, molecular sieves, and carbon nanotubes [100, 101]. The soft template method mainly uses a surfactant to form chain structures in the solution, which selectively adsorbs on a specific crystal plane of the element to grow into the one-dimensional nanowires. Wiley et. al prepared CuNWs having a diameter of about 90 nm and a length of about 10 μm in an aqueous alkali solution using ethylenediamine as a surfactant [102].

After reacted at 80 °C for one hour, a large amount of reddish-brown CuNWs precipitate was produced in the solution. During this reaction, ethylenediamine coating on the (100) plane of the Cu element and induce the one-dimensional growth of the CuNWs. At the same time, Cu^{2+} is continuously reduced by hydrazine hydrate to form Cu atoms and deposited at the ends of the nanowires. The washed CuNWs are prepared into CuNWs inks by uniformly dispersing in a suitable organic solvent or aqueous solution. The choice of the solution has a great influence on the uniformity of CuNWs films. The better the dispersibility of the CuNWs always accompany with the better uniformity of the resulting CuNWs films. Since most of the surfactants are chain organic substances, organic solvents are usually selected to obtain CuNWs inks with better dispersibility.

The hydrothermal method is another effective method for the synthesis of CuNWs, which uses an aqueous solution as a reaction medium to produce a high-pressure by the heating and boiling of the reaction system to prepare a nano-material. The basic mechanism of the hydrothermal method is that some of the extremely low solubility oxides are dissolved in an aqueous solution under high temperature and high pressure, which further hydrolyzed to form a highly soluble hydrate or hydroxide, and then the target nanomaterial is precipitated. Shi et. al uses hydrothermally method to reduce copper chloride at 120-180 °C to synthesize CuNWs with length of the several microns (Figure 1.12a-c) [102]. In this reaction, octadecylamine acts both as reducing agent and surfactant to induce the one-dimensional growth of Cu. As shown in Figure 1.12d and e, Konya et. al reduced the reaction temperature to 120 °C by introducing glucose as a reducing agent in the hydrothermal reaction [103]. Although the reaction temperature of this hydrothermal method is higher than that of the template method and the reaction time is longer, the use of amines as surfactants avoid the introduction of highly toxic hydrazine hydrates, and thus guarantee the environmentally friendly synthesis. In order to achieve large-scale production of CuNWs, Xia et. al keep the reaction in a sealed flask to create a high-temperature and high-pressure environment similar to the hydrothermal method, which results in CuNWs with a diameter of about 24 nm and a length from a dozen to several micros [104].

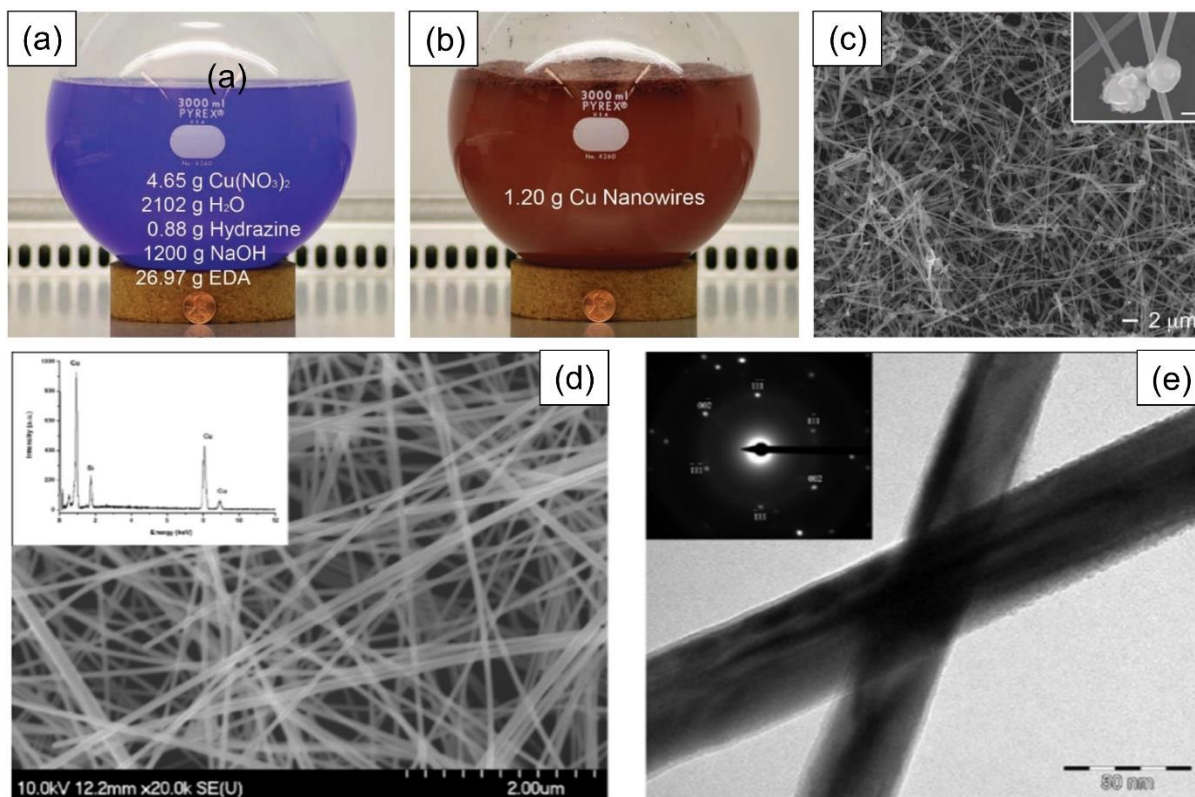


Figure 1.12 Pictures of the reaction flask (a) before the synthesis and (b) after growth of CuNWs at 80 °C for 1 hr. (c) SEM image of CuNW product. The nanowires are 90 ± 10 nm in diameter and 10 ± 3 μm in length. (d) SEM and (e) TEM of CuNW products of a 24 h synthesis [102, 103].

The surfactants play an important role in the synthesis of CuNWs. After the nucleation, the Cu particles are selected to grow along the outer surface that has low energy to form a five-fold symmetric seed crystal [105]. Since the surfactant is selectively adsorbed on the specific 100 crystal plane, newly precipitated copper atoms are continuously deposited on the 111 plane to grow along the 100 direction and form CuNWs. At the same time, due to the presence of surfactants, the obtained CuNWs can be uniformly dispersed in solution to form CuNWs inks. After the preparation of CuNWs by a suitable method, pure nanowires can be obtained by the repeat centrifugation. The CuNWs are typically dispersed in a suitable solvent using mechanical vibration or ultrasonic vibration to obtain uniform inks with different concentrations. The concentration of inks will further affect the subsequent spray process. Therefore, in addition to preparing high quality CuNWs, it is also important to configure a uniform ink with a suitable concentration.

The common film-forming methods can be divided into the following types: drip coating, vacuum suction filtration, spin coating, spray coating, and Mayer rod method. The drop coating method involves two steps of lowering and drying the nanoinks on the substrate. After the solution is dried, a randomly distributed CuNWs networks can be obtained. This method is simple and convenient, but the uniformity of coating is relatively poor [106]. The spin coating method is the application of excess nanowires to the substrate by centrifugal force at high speed [107]. This method controls the deposition thickness of nanowires on the film by the amount of nanoinks and the rotation speed, which is not suitable for mass production. The vacuum filtration method is used to deposit nanoinks on the filter membrane by suction filtration to form a network structure [108]. After that, the nanowire networks are transferred to the target substrate by applying uniform pressure. This method can control the density of the coating by adjusting the concentration of the filtered solution, but still faces the problem of incomplete transfer. The spraying method uses electric power or compressed air as a driving force to break up the nanoinks into tiny droplets and apply it to the substrate [109]. The spraying method is simple and fast, can realize automatic production, and is suitable for the application in substrates with various forms, which is more advantageous than other methods.

1.3.2 Strategies to improve the performance of CuNWs films

Compared with Ag and Au, CuNWs are more easily oxidized in an air atmosphere to form oxide films on the surface of nanowires. The presence of oxide films hinders the electron transfer when a voltage is applied, which results in high resistivity. Therefore, researchers have been devoted to improving the oxidation resistance and conductivity of CuNWs. Encapsulation or embedding CuNWs into flexible substrates to achieve a composite structure is one of the approaches to improve the thermal stability of CuNWs [110]. Won et al. prepared a stretchable conductor by applying pressure to transfer acid-treated CuNWs onto the polydimethylsiloxane (PDMS) substrates [111]. However, the pickling process easily causes Cu crystal defects while causing a new oxide layer on the surface of the nanowires. Cheng et al. partly embedded CuNW into the poly(acrylate) substrate by transferring the CuNW network from a glass substrate to an

elastic poly(acrylate) matrix through in situ photo polymerization [112]. As seen from Figure 1.13, Hu et al. reported the fabrication of CuNW/polyurethane (PU) composite electrode by overcoating the liquid polyurethane precursor on the surface of CuNW network [113]. However, the high-temperature annealing process and the complex and time-consuming transfer step greatly increase the cost.

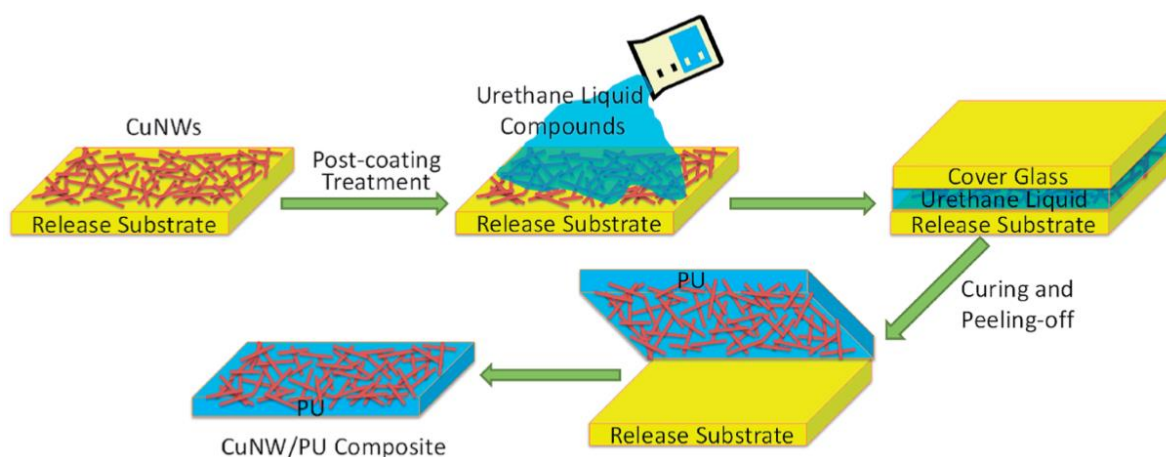


Figure 1.13 Schematic illustration of the fabrication process of a CuNW–PU composite electrode [113].

Another approach that has recently been suggested for enhancing the oxidation stability of CuNWs is to form core-shell structure that encapsulates copper with an inert shell. Cui et. al used atomic layer deposition techniques to coat the surface of CuNWs with an aluminum-doped zinc oxide and zinc oxide passivation layer [114]. After the surface passivation process, the electrical resistance of the CuNWs film increased by only 10% after heating at 160 °C for 8 h. The untreated CuNWs film loses its conductivity after only 40 min at high temperature. However, the atomic deposition techniques are expensive, and the presence of zinc oxide layers reduces the conductivity and transmittance of the films. Therefore, researchers began to choose well-conducted metals or carbon nanomaterials to cover the surface of CuNWs. As depicted in Figure 1.14a, Mehta et. al used a low-temperature plasma-enhanced CVD method to uniformly deposit a graphene layer on the surface of CuNWs, which resulting in nanowires with different widths (180, 280 nm) and lengths (10, 20 μm) [115]. The deposition reaction of graphene is carried out under a high

temperature of 650 °C, with methane and hydrogen as process gases and argon as the carrier gas. The surface passivation of CuNWs caused by the low-density properties of graphene produces partially elastic surface scattering, which enhances the conductivity and stability of the nanowires. As seen from Figure 1.14b-d, Stewart et. al successfully deposit a thin Ag shell and Au shell on the surface of CuNWs by a galvanic replacement process [116]. The approach greatly improves the oxidation resistance of the produced CuNWs without the post-treatment. During the reaction process, the Ag is reduced by adjusting the concentration of the reducing agent in the solution and then deposit on the surface of CuNWs to form core-shell structures, thereby avoiding the generation of porous nanowires to the utmost extent.

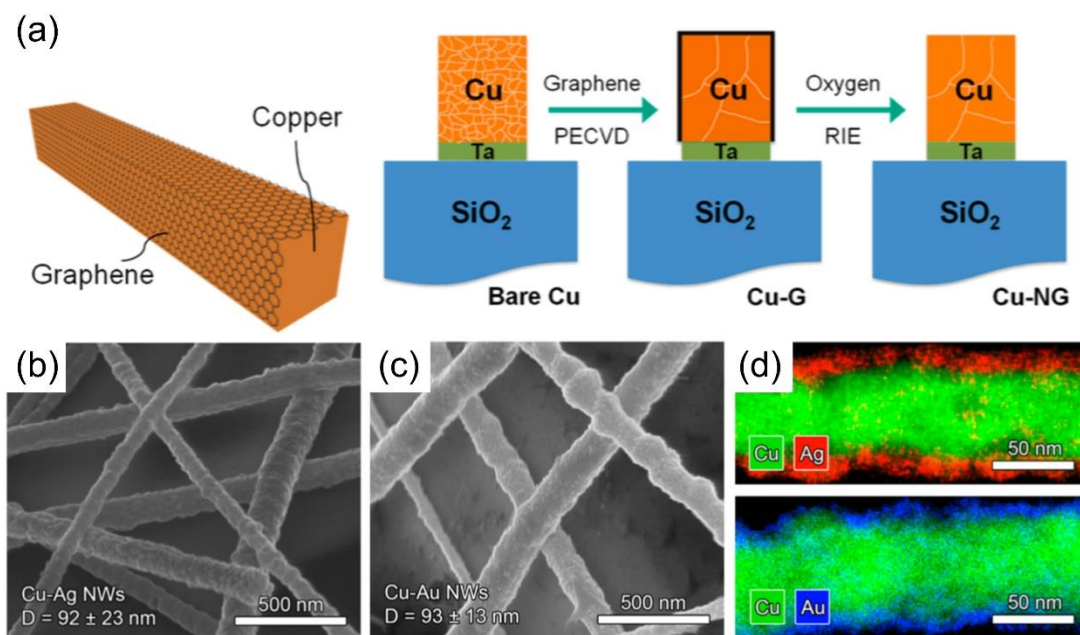


Figure 1.14. SEM images of (b) Cu–Ag core–shell NWs, and (c) Cu–Au core–shell NWs. Average diameters were calculated from 50 distinct nanowires. (d) TEM–EDS images of Cu–Ag and Cu–Au NWs [115, 116].

After the coating process, randomly distributed CuNWs networks were formed on the surface of stretchable substrates, and electrons are transferred through the overlap between the nanowires to form conductive films. The presence of organic species or oxides on the surface of CuNWs, the small contact surface and the large contact resistance between the nanowires reduce the

conductivity of the entire films. Meanwhile, the CuNWs films obtained by simple physical coating process exhibit low smoothness on the substrate compared with ITO and can be detached from the substrate by simple wiping. In addition, the obtained conductive CuNWs film is susceptible to deterioration in performance due to the changes in temperature, humidity, and illumination. Therefore, it is necessary to further process the physically coated CuNWs films to improve the conductivity, flatness, mechanical robustness and long-term stability of the films [110].

The square resistance of the conductive films refers to the resistance of unit area, which mainly, pressurization, photo-sintering, organic solvent or organic acid cleaning [117]. Cui et. al used a thermal sintering method to heat the nanowire networks at 200 °C for 20 min to reduce the square resistance (Figure 1.15) [117]. On the one hand, the polyvinyl pyrrolidone (PVP) on the surface of the nanowire decomposes at high depends on the contact resistance between the nanowires. Therefore, reducing the contact resistance between the wires and wires is essential for improving the conductivity of the film. In order to reduce the contact resistance, it is necessary to increase the contact area between the CuNWs or to remove the insulating layer on the surface of the nanowires, thereby improving the electron transfer efficiency between the nanowires. The methods for reducing the contact resistance between nanowires have been reported mainly includes heating temperatures, which promotes the connection between the nanowires. On the other hand, the heating process promotes fusion of the nanowire contact points to increase the contact area. However, the high sintering temperatures and excessive heating times lead to the melting of the nanowires, so it is necessary to control the heating parameters to obtain highly conductive films.

The electrical conductivity of the nanowire networks can also be improved by a mechanical pressurization method. Suganuma et. al apply pressures to the nanowire networks through two rigid substrates [38]. The pressurization process increases the contact area between the nanowires, thereby improving the conductivity of the nanowire films. This method is suitable for the heat sensitive substrates. Garnett et. al used a halogen lamp to illuminate the nanowire networks for one minute, and the resistance of the sample dropped by three orders of magnitude, which successfully avoids the damage to the substrate [118]. Jiu et. al studied a high-intensity pulse light

method for sintering nanowires, which can rapidly reduce the resistance of nanowire networks within 50 μs [119]. At the same time, this method greatly improves the connectivity between the nanowires and the flexible substrates.

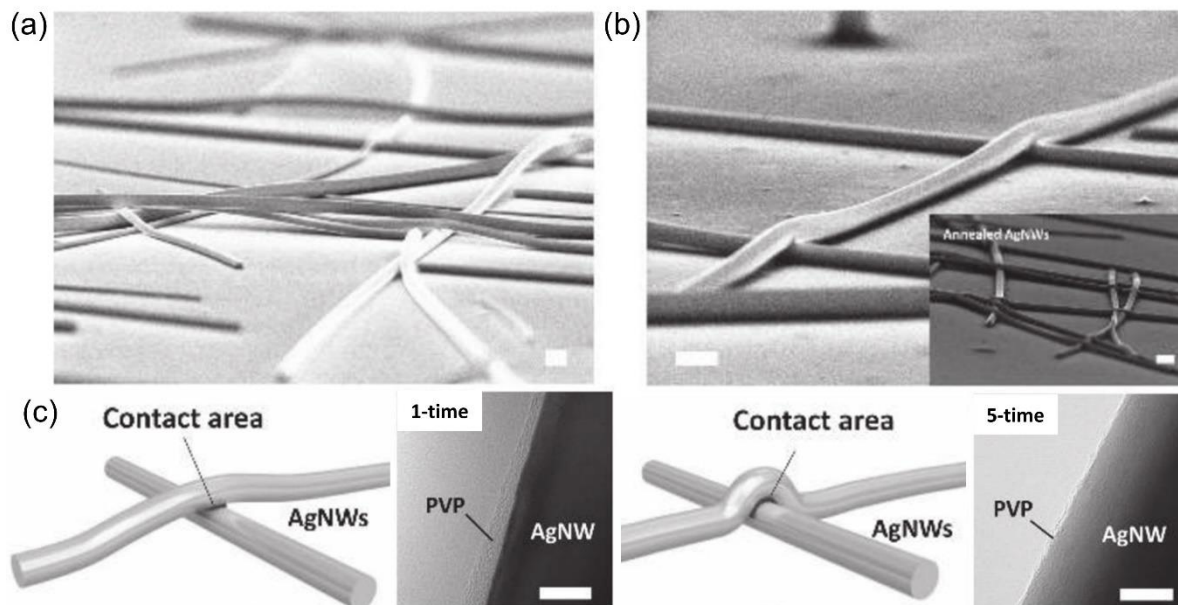


Figure 1.15 (a) SEM image of the drop-casted AgNWs. (b) SEM image of the sprayed AgNWs. Inset: annealed AgNWs at 230 $^{\circ}\text{C}$ for 20 min. (c) Schematics of drop-casted and sprayed AgNWs and TEM images of PVP layers after 1-time and 5-time solvent washing process [117].

The organic residue on the surface of the nanowire is generally removed by an organic reagent cleaning method. However, for CuNWs, in addition to organic residues, the oxide layer on the surface of the nanowires also increases the contact resistance. The organic acid cleaning method is used to remove surfactants and oxide layers from the CuNWs surface [120]. The conductivity of the CuNWs films obtained by the organic acid cleaning method is comparable to that of the films prepared by sintering in hydrogen atmospheres. Although this method is simple and fast, the damage to the CuNWs during the cleaning process cannot be avoided. Herein, the latest report of Yin et al. has proposed a technique similar to the pickling method, which is named as solvent dipped annealing method [121]. In this method, the obtained CuNWs film was immersed in glycerin and heated at a high temperature of 140 $^{\circ}\text{C}$. The thermal reduction reaction of glycerol removes oxides from the surface of CuNWs. Under high temperature heating conditions, the

nanowires are connected to each other to form a stable conductive pathway. This method has a low operating temperature and avoids the use of vacuum or reducing gases, which greatly reducing the production costs.

The surface roughness of CuNWs films also has a significant effect on its conductivity, which can easily cause short circuit during the device assembly process. In order to reduce the surface roughness of the CuNWs films, one method is to apply pressure to the obtained nanowire networks to reduce the roughness from 78 nm to 37 nm [41]. In addition, the CuNWs can be buried on the surface of the composite films by the transfer method to reduce the roughness of the nanowire networks. Pei et. al coat the surface of the nanowires with curable composite liquid layer, after the curing process, transfers the nanowires from the surface of the rigid substrate to the flexible composite film [43]. The nanowire films obtained by this method has a surface roughness of only 5 nm. After applying pressure on the CuNWs, Wiley et. al covered the surface of nanowire networks with a conductive PEDOT:PSS layer, which reduces the roughness of the films to 18 nm.

1.4 Purpose and scope of this study

The practical applications of CuNWs based conductors have been largely overshadowed due to their fast oxidation in ambient conditions. Therefore, the purpose of this study is to fabricate CuNWs based conductors with enhanced reliability, conductivity, and flexibility. This dissertation presents three methods to improve the performance of CuNWs based conductors, which including the formation of embedding structured CuNWs/substrates conductors, synthesis of core-shell structure that encapsulates CuNWs with an inert shell, and the combination of embedded structure and core-shell structure.

In chapter 1, a brief introduction to the definition, fabrication, and application of flexible conductors. The exploration of conductive materials used to form flexible electronic circuits, such as carbon nanomaterials, conductive polymers, and metallic nanomaterials. Based on the research background, the motivation and purpose of the present research are summarized.

In chapter 2, the highly conductive and stretchable conductor has been fabricated with enhanced reliability and robustness through fully embedding CuNWs into the surface layer of poly(dimethylsiloxane) (PDMS) and followed with a high-intensity pulsed light technique. The light energy absorbed by the film not only removes the oxides on the surface of nanowires but also enhances the inter-nanowire connection to achieve high conductivity. The oxidation resistance and stretchability of the fully embedded CuNWs/PDMS conductors were investigated in details. In addition, the potential applications of CuNWs/PDMS conductors were demonstrated by the fabrication of stretchable dipole antenna and conductive heater for wearable electronics.

In chapter 3, a facile adsorption and decomposition process is developed for galvanic replacement free and large-scale synthesis of highly stable Cu@Ag core-shell nanowires. Firstly, Ag-ammonia complex ($[\text{Ag}(\text{NH}_2\text{R})_2]^+$) as silver source adsorbs on CuNWs surface, and Cu@Ag-ammonia complex core-shell structure is formed. After that, Ag-ammonia complex is easily decomposed to pure Ag shell through a simple thermal annealing under air. By adjusting the concentration of Ag-ammonia, Cu@Ag core-shell nanowires with different thickness of silver shell can be easily obtained. The long-term stability, conductivity, and transparency of Cu@Ag nanowires based conductors were studied.

In chapter 4, transparent conductors with dense Cu@Ag alloy nanowires embedded in stretchable substrates are successfully fabricated by a high-intensity pulsed light (HIPL) technique within one step. The intense light energy not only induces rapid mutual dissolution between the Cu core and the Ag shell to form dense Cu@Ag alloy nanowires but also embeds the newly formed alloy nanowires into the stretchable substrates. The thermal stability and electro-mechanical stability of the conductors was evaluated under different conditions. Stretchable and transparent heaters have been fabricated based on the alloyed and embedded conductors to explore their application in the field of stretchable and wearable electronics.

In chapter 5, the summary of the dissertation and the prospect of the research is presented.

References

- [1] Huang, S. Y.; Liu, Y.; Zhao, Y.; Ren, Z. F.; Guo, C. F., Flexible Electronics: Stretchable Electrodes and Their Future. *Advanced Functional Materials* **2019**, *29*, 1805924.
- [2] Sun, Y. G.; Rogers, J. A., Inorganic Semiconductors for Flexible Electronics. *Advanced Materials* **2007**, *19*, 1897-1916.
- [3] Shi, C. Y.; Wang, J. J.; Sushko, M. R. A.; Qiu, W.; Yan, X. B.; Liu, X. Y., Silk Flexible Electronics: From Bombyx mori Silk Ag Nanoclusters Hybrid Materials to Mesoscopic Memristors and Synaptic Emulators. *Advanced Functional Materials* **2019**, 1904777.
- [4] Liu, L.; Feng, Y.; Liang, J.; Li, S. Q.; Tian, B.; Yao, W. J.; Wu, W., Structure-Designed Fabrication of All-printed Flexible in-Plane Solid-State Supercapacitors for Wearable Electronics. *J Power Sources* **2019**, *425*, 195-203.
- [5] You, R.; Liu, Y. Q.; Hao, Y. L.; Han, D. D.; Zhang, Y. L.; You, Z., Laser Fabrication of Graphene-Based Flexible Electronics. *Advanced Materials* **2019**, 1901981.
- [6] Wang, B. H.; Facchetti, A., Mechanically Flexible Conductors for Stretchable and Wearable E-Skin and E-Textile Devices. *Advanced Materials* **2019**, *31*, 1901408
- [7] Ji, D. Y.; Li, T.; Zou, Y.; Chu, M.; Zhou, K.; Liu, J. Y.; Tian, G. F.; Zhang, Z. Y.; Zhang, X.; Li, L. Q.; Wu, D. Z.; Dong, H. L.; Miao, Q.; Fuchs, H.; Hu, W. P., Copolymer Dielectrics with Balanced Chain-Packing Density and Surface Polarity for High-Performance Flexible Organic Electronics. *Nature Communications* **2018**, *9*, 2339.
- [8] Park, S.; Heo, S. W.; Lee, W.; Inoue, D.; Jiang, Z.; Yu, K.; Jinno, H.; Hashizume, D.; Sekino, M.; Yokota, T.; Fukuda, K.; Tajima, K.; Someya, T., Self-powered Ultra-Flexible Electronics via Nano-Grating-Patterned Organic Photovoltaics. *Nature* **2018**, *561*, 516-521.
- [9] Yu, Y.; Nyein, H. Y. Y.; Gao, W.; Javey, A., Flexible Electrochemical Bioelectronics: The Rise of In Situ Bioanalysis. *Advanced Materials* **2019**, 1902083.
- [10] Shafiee, A.; Ghadiri, E.; Salleh, M. M.; Yahaya, M.; Atala, A., Controlling the Surface Properties of an Inkjet-Printed Reactive Oxygen Species Scavenger for Flexible Bioelectronics Applications in Neural Resilience. *Ieee J Electron Devi* **2019**, *7*, 784-791.

- [11] Chang, H. Y.; Yogeesh, M. N.; Ghosh, R.; Rai, A.; Sanne, A.; Yang, S. X.; Lu, N. S.; Banerjee, S. K.; Akinwande, D., Large-Area Monolayer MoS₂ for Flexible Low-Power RF Nanoelectronics in the GHz Regime. *Advanced Materials* **2016**, *28*, 1818-1823.
- [12] Yogeesh, M. N.; Park, S.; Akinwande, D., Graphene Based GHz Flexible Nanoelectronics and Radio Receiver Systems. *Ieee Int Symp Circ S* **2015**, 2916-2919.
- [13] Kim, K.; Kim, B.; Lee, C. H., Printing Flexible and Hybrid Electronics for Human Skin and Eye-Interfaced Health Monitoring Systems. *Advanced Materials* **2019**, 1902051.
- [14] Zheng, S. H.; Wu, Z. S.; Zhou, F.; Wang, X.; Ma, J. M.; Liu, C.; He, Y. B.; Bao, X. H., All-Solid-State Planar Integrated Lithium Ion Micro-Batteries with Extraordinary Flexibility and High-Temperature Performance. *Nano Energy* **2018**, *51*, 613-620.
- [15] Asad, M.; Li, Q.; Lee, C. H.; Sachdev, M.; Wong, W. S., Integration of GaN Light-Emitting Diodes with a-Si:H Thin-Film Transistors for Flexible Displays. *Nanotechnology* **2019**, *30*, 324003.
- [16] Nguyen, C. T. Q.; Vu, H. N.; Nguyen, M. D., High-Performance Energy Storage and Breakdown Strength of Low-Temperature Laser-Deposited Relaxor PLZT Thin Films on Flexible Ti-Foils. *J Alloy Compd* **2019**, *802*, 422-429.
- [17] Kim, D. H.; Ghaffari, R.; Lu, N. S.; Rogers, J. A., Flexible and Stretchable Electronics for Biointegrated Devices. *Annu Rev Biomed Eng* **2012**, *14*, 113-128.
- [18] Hammock, M. L.; Chortos, A.; Tee, B. C. K.; Tok, J. B. H.; Bao, Z. A., 25th Anniversary Article: The Evolution of Electronic Skin (E-Skin): A Brief History, Design Considerations, and Recent Progress. *Advanced Materials* **2013**, *25*, 5997-6037.
- [19] Stoppa, M.; Chiolerio, A., Wearable Electronics and Smart Textiles: A Critical Review. *Sensors-Basel* **2014**, *14*, 11957-11992.
- [20] Zhang, X. Y.; Hu, Y. G.; Gu, H.; Zhu, P. L.; jiang, W.; Zhang, G.; Sun, R.; Wong, C. P., A Highly Sensitive and Cost-Effective Flexible Pressure Sensor with Micropillar Arrays Fabricated by Novel Metal-Assisted Chemical Etching for Wearable Electronics. *Adv Mater Technol* **2019**, 1900367.

- [21] Hong, Y. J.; Jeong, H.; Cho, K. W.; Lu, N.; Kim, D. H., Wearable and Implantable Devices for Cardiovascular Healthcare: from Monitoring to Therapy Based on Flexible and Stretchable Electronics. *Advanced Functional Materials* **2019**, *29*, 1808247.
- [22] de Oliveira, R. F.; Livio, P. A.; Montes-Garcia, V.; Ippolito, S.; Eredia, M.; Fanjul-Bolado, P.; Garcia, M. B. G.; Casalini, S.; Samori, P., Liquid-Gated Transistors Based on Reduced Graphene Oxide for Flexible and Wearable Electronics. *Advanced Functional Materials* **2019**, 1905375.
- [23] Dong, K.; Peng, X.; Wang, Z. L., Fiber/Fabric-Based Piezoelectric and Triboelectric Nanogenerators for Flexible/Stretchable and Wearable Electronics and Artificial Intelligence. *Advanced Materials* **2019**, 1902549.
- [24] Liao, Y.; Zhang, R.; Wang, H. X.; Ye, S. L.; Zhou, Y. H.; Ma, T. L.; Zhu, J. Q.; Pfefferle, L. D.; Qian, J., Highly Conductive Carbon-Based Aqueous Inks Toward Electroluminescent Devices, Printed Capacitive Sensors and Flexible Wearable Electronics. *Rsc Advances* **2019**, *9*, 15184-15189.
- [25] Yao, S. S.; Zhu, Y., Nanomaterial-Enabled Stretchable Conductors: Strategies, Materials and Devices. *Advanced Materials* **2015**, *27*, 1480-1511.
- [26] Park, S. I.; Xiong, Y. J.; Kim, R. H.; Elvikis, P.; Meitl, M.; Kim, D. H.; Wu, J.; Yoon, J.; Yu, C. J.; Liu, Z. J.; Huang, Y. G.; Hwang, K.; Ferreira, P.; Li, X. L.; Choquette, K.; Rogers, J. A., Printed Assemblies of Inorganic Light-Emitting Diodes for Deformable and Semitransparent Displays. *Science* **2009**, *325*, 977-981.
- [27] Son, D.; Lee, J.; Qiao, S.; Ghaffari, R.; Kim, J.; Lee, J. E.; Song, C.; Kim, S. J.; Lee, D. J.; Jun, S. W.; Yang, S.; Park, M.; Shin, J.; Do, K.; Lee, M.; Kang, K.; Hwang, C. S.; Lu, N. S.; Hyeon, T.; Kim, D. H., Multifunctional Wearable Devices for Diagnosis and Therapy of Movement Disorders. *Nature Nanotechnology* **2014**, *9*, 397-404.
- [28] Ko, H. C.; Stoykovich, M. P.; Song, J. Z.; Malyarchuk, V.; Choi, W. M.; Yu, C. J.; Geddes, J. B.; Xiao, J. L.; Wang, S. D.; Huang, Y. G.; Rogers, J. A., A Hemispherical Electronic Eye Camera Based on Compressible Silicon Optoelectronics. *Nature* **2008**, *454*, 748-753.

- [29] Xu, F.; Zhu, Y., Highly Conductive and Stretchable Silver Nanowire Conductors. *Advanced Materials* **2012**, *24*, 5117-5122.
- [30] Chun, K. Y.; Oh, Y.; Rho, J.; Ahn, J. H.; Kim, Y. J.; Choi, H. R.; Baik, S., Highly Conductive, Printable and Stretchable Composite Films of Carbon Nanotubes and Silver. *Nature Nanotechnology* **2010**, *5*, 853-857.
- [31] Xu, F.; Wang, X.; Zhu, Y. T.; Zhu, Y., Wavy Ribbons of Carbon Nanotubes for Stretchable Conductors. *Advanced Functional Materials* **2012**, *22*, 1279-1283.
- [32] Bowden, N.; Brittain, S.; Evans, A. G.; Hutchinson, J. W.; Whitesides, G. M., Spontaneous Formation of Ordered Structures in Thin Films of Metals Supported on An Elastomeric Polymer. *Nature* **1998**, *393*, 146-149.
- [33] Qin, Q. Q.; Zhu, Y., Static Friction between Silicon Nanowires and Elastomeric Substrates. *Acs Nano* **2011**, *5*, 7404-7410.
- [34] Zhu, Y.; Xu, F., Buckling of Aligned Carbon Nanotubes as Stretchable Conductors: A New Manufacturing Strategy. *Advanced Materials* **2012**, *24*, 1073-1077.
- [35] Durham, J. W.; Zhu, Y., Fabrication of Functional Nanowire Devices on Unconventional Substrates Using Strain-Release Assembly. *Acs Appl Mater Inter* **2013**, *5*, 256-261.
- [36] Shang, Y.; He, X.; Li, Y.; Zhang, L.; Li, Z.; Ji, C.; Shi, E.; Li, P.; Zhu, K.; Peng, Q.; Wang, C.; Zhang, X.; Wang, R.; Wei, J.; Wang, K.; Zhu, H.; Wu, D.; Cao, A., Super-Stretchable Spring-Like Carbon Nanotube Ropes. *Adv Mater* **2012**, *24*, 2896-900.
- [37] Jeong, C. K.; Lee, J.; Han, S.; Ryu, J.; Hwang, G. T.; Park, D. Y.; Park, J. H.; Lee, S. S.; Byun, M.; Ko, S. H.; Lee, K. J., A Hyper-Stretchable Elastic-Composite Energy Harvester. *Advanced Materials* **2015**, *27*, 2866-2875.
- [38] Tokuno, T.; Nogi, M.; Karakawa, M.; Jiu, J. T.; Nge, T. T.; Aso, Y.; Suganuma, K., Fabrication of Silver Nanowire Transparent Electrodes at Room Temperature. *Nano Research* **2011**, *4*, 1215-1222.
- [39] Han, S.; Hong, S.; Ham, J.; Yeo, J.; Lee, J.; Kang, B.; Lee, P.; Kwon, J.; Lee, S. S.; Yang, M. Y.; Ko, S. H., Fast Plasmonic Laser Nanowelding for a Cu-Nanowire Percolation Network

- for Flexible Transparent Conductors and Stretchable Electronics. *Advanced Materials* **2014**, *26*, 5808-5814.
- [40] Lee, J. Y.; Connor, S. T.; Cui, Y.; Peumans, P., Semitransparent Organic Photovoltaic Cells with Laminated Top Electrode. *Nano Letters* **2010**, *10*, 1276-1279.
- [41] Stewart, I. E.; Rathmell, A. R.; Yan, L.; Ye, S. R.; Flowers, P. F.; You, W.; Wiley, B. J., Solution-Processed Copper-Nickel Nanowire Anodes for Organic Solar Cells. *Nanoscale* **2014**, *6*, 5980-5988.
- [42] Gaynor, W.; Lee, J. Y.; Peumans, P., Fully Solution-Processed Inverted Polymer Solar Cells with Laminated Nanowire Electrodes. *Acs Nano* **2010**, *4*, 30-34.
- [43] Yu, Z. B.; Zhang, Q. W.; Li, L.; Chen, Q.; Niu, X. F.; Liu, J.; Pei, Q. B., Highly Flexible Silver Nanowire Electrodes for Shape-Memory Polymer Light-Emitting Diodes. *Advanced Materials* **2011**, *23*, 664-668.
- [44] Liang, J. J.; Li, L.; Tong, K.; Ren, Z.; Hu, W.; Niu, X. F.; Chen, Y. S.; Pei, Q. B., Silver Nanowire Percolation Network Soldered with Graphene Oxide at Room Temperature and Its Application for Fully Stretchable Polymer Light-Emitting Diodes. *Acs Nano* **2014**, *8*, 1590-1600.
- [45] Wei, Y.; Chen, S. L.; Li, F. C.; Lin, Y.; Zhang, Y.; Liu, L., Highly Stable and Sensitive Paper-Based Bending Sensor Using Silver Nanowires/Layered Double Hydroxides Hybrids. *Acs Appl Mater Inter* **2015**, *7*, 14182-14191.
- [46] Amjadi, M.; Pichitpajongkit, A.; Lee, S.; Ryu, S.; Park, I., Highly Stretchable and Sensitive Strain Sensor Based on Silver Nanowire-Elastomer Nanocomposite. *Acs Nano* **2014**, *8*, 5154-5163.
- [47] Choi, S.; Park, J.; Hyun, W.; Kim, J.; Kim, J.; Lee, Y. B.; Song, C.; Hwang, H. J.; Kim, J. H.; Hyeon, T.; Kim, D. H., Stretchable Heater Using Ligand-Exchanged Silver Nanowire Nanocomposite for Wearable Articular Thermotherapy. *Acs Nano* **2015**, *9*, 6626-6633.

- [48] Pyo, J. B.; Kim, B. S.; Park, H.; Kim, T. A.; Koo, C. M.; Lee, J.; Son, J. G.; Lee, S. S.; Park, J. H., Floating Compression of Ag Nanowire Networks for Effective Strain Release of Stretchable Transparent Electrodes. *Nanoscale* **2015**, *7*, 16434-16441.
- [49] Kholmanov, I. N.; Domingues, S. H.; Chou, H.; Wang, X. H.; Tan, C.; Kim, J. Y.; Li, H. F.; Piner, R.; Zarbin, A. J. G.; Ruoff, R. S., Reduced Graphene Oxide/Copper Nanowire Hybrid Films as High-Performance Transparent Electrodes. *Acs Nano* **2013**, *7*, 1811-1816.
- [50] Chao, J. F.; Meng, Y. Q.; Liu, J. B.; Zhang, Q. Q.; Wang, H., Review on the Synthesis and Antioxidation of Cu Nanowires for Transparent Conductive Electrodes. *Nano* **2019**, *14*, 1930005.
- [51] Xia, K. L.; Jian, M. Q.; Zhang, Y. Y., Advances in Wearable and Flexible Conductors Based on Nanocarbon Materials. *Acta Phys-Chim Sin* **2016**, *32*, 2427-2446.
- [52] Ho, X. N.; Wei, J., Films of Carbon Nanomaterials for Transparent Conductors. *Materials* **2013**, *6*, 2155-2181.
- [53] Zhang, D. H.; Ryu, K.; Liu, X. L.; Polikarpov, E.; Ly, J.; Tompson, M. E.; Zhou, C. W., Transparent, Conductive, and Flexible Carbon Nanotube Films and Their Application in Organic Light-Emitting Diodes. *Nano Letters* **2006**, *6*, 1880-1886.
- [54] Lipomi, D. J.; Vosgueritchian, M.; Tee, B. C. K.; Hellstrom, S. L.; Lee, J. A.; Fox, C. H.; Bao, Z. N., Skin-Like Pressure and Strain Sensors Based on Transparent Elastic Films of Carbon Nanotubes. *Nature Nanotechnology* **2011**, *6*, 788-792.
- [55] Siegal, M. P.; Overmyer, D. L.; Provencio, P. P., Precise Control of Multiwall Carbon Nanotube Diameters using Thermal Chemical Vapor Deposition. *Appl Phys Lett* **2002**, *80*, 2171-2173.
- [56] Chen, Y.; Shaw, D. T.; Guo, L. P., Field Emission of Different Oriented Carbon Nanotubes. *Appl Phys Lett* **2000**, *76*, 2469-2471.
- [57] Huang, S. M.; Cai, X. Y.; Liu, J., Growth of Millimeter-Long and Horizontally Aligned Single-Walled Carbon Nanotubes on Flat Substrates. *Journal of the American Chemical Society* **2003**, *125*, 5636-5637.

- [58] Kang, S. J.; Kocabas, C.; Kim, H. S.; Cao, Q.; Meitl, M. A.; Khang, D. Y.; Rogers, J. A., Printed Multilayer Superstructures of Aligned Single-Walled Carbon Nanotubes for Electronic Applications. *Nano Letters* **2007**, *7*, 3343-3348.
- [59] Shin, M. K.; Oh, J.; Lima, M.; Kozlov, M. E.; Kim, S. J.; Baughman, R. H., Elastomeric Conductive Composites Based on Carbon Nanotube Forests. *Advanced Materials* **2010**, *22*, 2663-2667.
- [60] Tsai, T. Y.; Lee, C. Y.; Tai, N. H.; Tuan, W. H., Transfer of Patterned Vertically Aligned Carbon Nanotubes onto Plastic Substrates for Flexible Electronics and Field Emission Devices. *Appl Phys Lett* **2009**, *95*, 013107.
- [61] Chandrashekar, B. N.; Deng, B.; Smitha, A. S.; Chen, Y. B.; Tan, C. W.; Zhang, H. X.; Peng, H. L.; Liu, Z. F., Roll-to-Roll Green Transfer of CVD Graphene onto Plastic for a Transparent and Flexible Triboelectric Nanogenerator. *Advanced Materials* **2015**, *27*, 5210-5216.
- [62] Rogala, M.; Wlasny, I.; Dabrowski, P.; Kowalczyk, P. J.; Busiakiewicz, A.; Kozlowski, W.; Lipinska, L.; Jagiello, J.; Aksienionek, M.; Strupinski, W.; Krajewska, A.; Sieradzki, Z.; Krucinska, I.; Puchalski, M.; Skrzetuska, E.; Klusek, Z., Graphene Oxide Overprints for Flexible and Transparent Electronics. *Appl Phys Lett* **2015**, *106*, 041901.
- [63] Rogala, M.; Kowalczyk, P. J.; Dabrowski, P.; Wlasny, I.; Kozlowski, W.; Busiakiewicz, A.; Pawlowski, S.; Dobinski, G.; Smolny, M.; Karaduman, I.; Lipinska, L.; Kozinski, R.; Librant, K.; Jagiello, J.; Grodecki, K.; Baranowski, J. M.; Szot, K.; Klusek, Z., The Role of Water in Resistive Switching in Graphene Oxide. *Appl Phys Lett* **2015**, *106*, 263104.
- [64] Tourillon, G.; Garnier, F., New Electrochemically Generated Organic Conducting Polymers. *J Electroanal Chem* **1982**, *135*, 173-178.
- [65] MacDiarmid, A. G., "Synthetic metals": A novel role for organic polymers (Nobel lecture). *Angew Chem Int Edit* **2001**, *40*, 2581-2590.

- [66] Tas, M.; Cin, Z. I.; Parmak, E. D. S.; Bedeloglu, A. C., Fabrication of Unilateral Conductive and Transparent Polymer Thin Films Decorated With Nanomaterials for Flexible Electrodes. *Polym Composite* **2018**, *39*, 1771-1778.
- [67] Chen, Y. T.; Carmichael, R. S.; Carmichael, T. B., Patterned, Flexible, and Stretchable Silver Nanowire/Polymer Composite Films as Transparent Conductive Electrodes. *Acs Appl Mater Inter* **2019**, *11*, 31210-31219.
- [68] Wang, G. M.; Swensen, J.; Moses, D.; Heeger, A. J., Increased Mobility from Regioregular Poly(3-hexylthiophene) Field-Effect Transistors. *J Appl Phys* **2003**, *93*, 6137-6141.
- [69] Heinze, J.; Frontana-Urbe, B. A.; Ludwigs, S., Electrochemistry of Conducting Polymers- Persistent Models and New Concepts. *Chem Rev* **2010**, *110*, 4724-4771.
- [70] McQuade, D. T.; Hegedus, A. H.; Swager, T. M., Signal Amplification of A "Turn-on" Sensor: Harvesting The Light Captured by A Conjugated Polymer. *Journal of the American Chemical Society* **2000**, *122*, 12389-12390.
- [71] Randriamahazaka, H., Electrodeposition Mechanisms and Electrochemical Behavior of Poly(3,4-ethylenedithiathiothiophene). *J Phys Chem C* **2007**, *111*, 4553-4560.
- [72] Balint, R.; Cassidy, N. J.; Cartmell, S. H., Conductive Polymers: Towards A Smart Biomaterial for Tissue Engineering. *Acta Biomater* **2014**, *10*, 2341-2353.
- [73] Shi, Y.; Peng, L. L.; Ding, Y.; Zhao, Y.; Yu, G. H., Nanostructured Conductive Polymers for Advanced Energy Storage. *Chem Soc Rev* **2015**, *44*, 6684-6696.
- [74] Kaur, G.; Adhikari, R.; Cass, P.; Bown, M.; Gunatillake, P., Electrically Conductive Polymers and Composites for Biomedical Applications. *Rsc Advances* **2015**, *5*, 37553-37567.
- [75] Cho, S. I.; Lee, S. B., Fast Electrochemistry of Conductive Polymer Nanotubes: Synthesis, Mechanism, and Application. *Accounts Chem Res* **2008**, *41*, 699-707.
- [76] Bettelheim, A.; White, B. A.; Raybuck, S. A.; Murray, R. W., Electrochemical Polymerization of Amino-Substituted, Pyrrole-Substituted, and Hydroxy-Substituted Tetraphenylporphyrins. *Inorganic Chemistry* **1987**, *26*, 1009-1017.

- [77] Li, G. R.; Feng, Z. P.; Zhong, J. H.; Wang, Z. L.; Tong, Y. X., Electrochemical Synthesis of Polyaniline Nanobelts with Predominant Electrochemical Performances. *Macromolecules* **2010**, *43*, 2178-2183.
- [78] Li, C.; Shi, G. Q., Synthesis and Electrochemical Applications of The Composites of Conducting Polymers and Chemically Converted Graphene. *Electrochim Acta* **2011**, *56*, 10737-10743.
- [79] Patois, T.; Sanchez, J. B.; Berger, F.; Rauch, J. Y.; Fievet, P.; Lakard, B., Ammonia Gas Sensors Based on Polypyrrole Films: Influence of Electrodeposition Parameters. *Sensor Actuat B-Chem* **2012**, *171*, 431-439.
- [80] Cong, H. P.; Ren, X. C.; Wang, P.; Yu, S. H., Flexible Graphene-Polyaniline Composite Paper for High-Performance Supercapacitor. *Energ Environ Sci* **2013**, *6*, 1185-1191.
- [81] Tai, Q. D.; Chen, B. L.; Guo, F.; Xu, S.; Hu, H.; Sebo, B.; Zhao, X. Z., In Situ Prepared Transparent Polyaniline Electrode and Its Application in Bifacial Dye-Sensitized Solar Cells. *Acs Nano* **2011**, *5*, 3795-3799.
- [82] Yang, L. C.; Wang, S. N.; Mao, J. J.; Deng, J. W.; Gao, Q. S.; Tang, Y.; Schmidt, O. G., Hierarchical MoS₂/Polyaniline Nanowires with Excellent Electrochemical Performance for Lithium-Ion Batteries. *Advanced Materials* **2013**, *25*, 1180-1184.
- [83] Sun, Y. G.; Mayers, B.; Herricks, T.; Xia, Y. N., Polyol Synthesis of Uniform Silver Nanowires: A Plausible Growth Mechanism and The Supporting Evidence. *Nano Letters* **2003**, *3*, 955-960.
- [84] Madaria, A. R.; Kumar, A.; Zhou, C. W., Large scale, Highly Conductive and Patterned Transparent Films of Silver Nanowires on Arbitrary Substrates and Their Application in Touch Screens. *Nanotechnology* **2011**, *22*, 245201.
- [85] Zhang, L. S.; Zhang, P. X.; Fang, Y., Magnetron Sputtering of Silver Nanowires Using Anodic Aluminum Oxide Template: A New Active Substrate of Surface Enhanced Raman Scattering and An Investigation of Its Enhanced Mechanism. *Anal Chim Acta* **2007**, *591*, 214-218.

- [86] Zhou, Y. J.; Hu, J. H., Spot Formation and Alignment of Silver Nanowires Using Ultrasonic Stage. *Proceedings of the 2012 Symposium on Piezoelectricity, Acoustic Waves and Device Applications (Spawda12)* **2012**, 49-52.
- [87] Caswell, K. K.; Bender, C. M.; Murphy, C. J., Seedless, Surfactantless Wet Chemical Synthesis of Silver Nanowires. *Nano Letters* **2003**, *3*, 667-669.
- [88] Coskun, S.; Aksoy, B.; Unalan, H. E., Polyol Synthesis of Silver Nanowires: An Extensive Parametric Study. *Cryst Growth Des* **2011**, *11*, 4963-4969.
- [89] Wang, J.; Jiu, J. T.; Araki, T.; Nogi, M.; Sugahara, T.; Nagao, S.; Koga, H.; He, P.; Suganuma, K., Silver Nanowire Electrodes: Conductivity Improvement Without Post-treatment and Application in Capacitive Pressure Sensors. *Nano-Micro Lett* **2015**, *7*, 51-58.
- [90] Kang, H.; Kang, I.; Han, J.; Kim, J. B.; Lee, D. Y.; Cho, S. M.; Cho, J. H., Flexible and Mechanically Robust Organic Light-Emitting Diodes Based on Photopatternable Silver Nanowire Electrodes. *J Phys Chem C* **2016**, *120*, 22012-22018.
- [91] Yang, L. Q.; Zhang, T.; Zhou, H. X.; Price, S. C.; Wiley, B. J.; You, W., Solution-Processed Flexible Polymer Solar Cells with Silver Nanowire Electrodes. *Acs Appl Mater Inter* **2011**, *3*, 4075-4084.
- [92] Gaynor, W.; Hofmann, S.; Christoforo, M. G.; Sachse, C.; Mehra, S.; Salleo, A.; McGehee, M. D.; Gather, M. C.; Lussem, B.; Muller-Meskamp, L.; Peumans, P.; Leo, K., Color in the Corners: ITO-Free White OLEDs with Angular Color Stability. *Advanced Materials* **2013**, *25*, 4006-4013.
- [93] Matyas, J.; Munster, L.; Olejnik, R.; Vlcek, K.; Slobodian, P.; Krcmar, P.; Urbanek, P.; Kuritka, I., Antenna of Silver Nanoparticles Mounted on a Flexible Polymer Substrate Constructed using Inkjet Print Technology. *Jpn J Appl Phys* **2016**, *55*, 02BB13.
- [94] Ding, J.; Liu, J.; Tian, Q. Y.; Wu, Z. H.; Yao, W. J.; Dai, Z. G.; Liu, L.; Wu, W., Preparing of Highly Conductive Patterns on Flexible Substrates by Screen Printing of Silver Nanoparticles with Different Size Distribution. *Nanoscale Res Lett* **2016**, *11*, 412.

- [95] Hyun, D. C.; Park, M.; Park, C.; Kim, B.; Xia, Y.; Hur, J. H.; Kim, J. M.; Park, J. J.; Jeong, U., Ordered Zigzag Stripes of Polymer Gel/Metal Nanoparticle Composites for Highly Stretchable Conductive Electrodes. *Advanced Materials* **2011**, *23*, 2946-2950.
- [96] Xu, H. Y.; Kan, C. X.; Wang, C. S.; Ni, Y.; Liu, J. S.; Xu, W.; Ke, J. H., Ultrafine Au Nanowires Synthesized via One-Step Wet Chemical Method. *Acta Phys-Chim Sin* **2015**, *31*, 1186-1190.
- [97] Gong, S.; Zhao, Y. M.; Shi, Q. Q.; Wang, Y.; Yap, L. W.; Cheng, W. L., Self-assembled Ultrathin Gold Nanowires as Highly Transparent, Conductive and Stretchable Supercapacitor. *Electroanal* **2016**, *28*, 1298-1304.
- [98] Wang, R. L.; Ruan, H. B., Synthesis of Copper Nanowires and Its Application to Flexible Transparent Electrode. *J Alloy Compd* **2016**, *656*, 936-943.
- [99] Zhang, Y.; Guo, J. N.; Xu, D.; Sun, Y.; Yan, F., Synthesis of Ultralong Copper Nanowires for High-Performance Flexible Transparent Conductive Electrodes: The Effects of Polyhydric Alcohols. *Langmuir* **2018**, *34*, 3884-3893.
- [100] Yao, Z.; Wang, C.; Li, Y.; Kim, N. Y., AAO-Assisted Synthesis of Highly Ordered, Large-Scale TiO₂ Nanowire Arrays via Sputtering and Atomic Layer Deposition. *Nanoscale Res Lett* **2015**, *10*, 166.
- [101] Wong, E. W.; Maynor, B. W.; Burns, L. D.; Lieber, C. M., Growth of Metal Carbide Nanotubes and Nanorods. *Chemistry of Materials* **1996**, *8*, 2041-2046.
- [102] Rathmell, A. R.; Bergin, S. M.; Hua, Y. L.; Li, Z. Y.; Wiley, B. J., The Growth Mechanism of Copper Nanowires and Their Properties in Flexible, Transparent Conducting Films. *Advanced Materials* **2010**, *22*, 3558-3563.
- [103] Mohl, M.; Pusztai, P.; Kukovecz, A.; Konya, Z.; Kukkola, J.; Kordas, K.; Vajtai, R.; Ajayan, P. M., Low-Temperature Large-Scale Synthesis and Electrical Testing of Ultralong Copper Nanowires. *Langmuir* **2010**, *26*, 16496-16502.

- [104] Jin, M. S.; He, G. N.; Zhang, H.; Zeng, J.; Xie, Z. X.; Xia, Y. N., Shape-Controlled Synthesis of Copper Nanocrystals in an Aqueous Solution with Glucose as a Reducing Agent and Hexadecylamine as a Capping Agent. *Angew Chem Int Edit* **2011**, *50*, 10560-10564.
- [105] Bhanushali, S.; Ghosh, P.; Ganesh, A.; Cheng, W. L., 1D Copper Nanostructures: Progress, Challenges and Opportunities. *Small* **2015**, *11*, 1232-1252.
- [106] Shen, X. Y.; Ho, C. M.; Wong, T. S., Minimal Size of Coffee Ring Structure. *J Phys Chem B* **2010**, *114*, 5269-5274.
- [107] Ahn, Y.; Jeong, Y.; Lee, Y., Improved Thermal Oxidation Stability of Solution-Processable Silver Nanowire Transparent Electrode by Reduced Graphene Oxide. *Acs Appl Mater Inter* **2012**, *4*, 6410-6414.
- [108] Lee, J.; Lee, P.; Lee, H.; Lee, D.; Lee, S. S.; Ko, S. H., Very Long Ag Nanowire Synthesis and Its Application in A Highly Transparent, Conductive and Flexible Metal Electrode Touch Panel. *Nanoscale* **2012**, *4*, 6408-6414.
- [109] Park, S. E.; Kim, S.; Lee, D. Y.; Kim, E.; Hwang, J., Fabrication of Silver Nanowire Transparent Electrodes using Electrohydrodynamic Spray Deposition for Flexible Organic Solar Cells. *Journal of Materials Chemistry A* **2013**, *1*, 14286-14293.
- [110] Ye, S. R.; Rathmell, A. R.; Chen, Z. F.; Stewart, I. E.; Wiley, B. J., Metal Nanowire Networks: The Next Generation of Transparent Conductors. *Advanced Materials* **2014**, *26*, 6670-6687.
- [111] Rathmell, A. R.; Wiley, B. J., The Synthesis and Coating of Long, Thin Copper Nanowires to Make Flexible, Transparent Conducting Films on Plastic Substrates. *Advanced Materials* **2011**, *23*, 4798-4803.
- [112] Won, Y.; Kim, A.; Yang, W.; Jeong, S.; Moon, J., A highly Stretchable, Helical Copper Nanowire Conductor Exhibiting a Stretchability of 700%. *Npg Asia Materials* **2014**, *6*, e123.
- [113] Hu, W. L.; Wang, R. R.; Lu, Y. F.; Pei, Q. B., An Elastomeric Transparent Composite Electrode Based on Copper Nanowires and Polyurethane. *Journal of Materials Chemistry C* **2014**, *2*, 1298-1305.

- [114] Hsu, P. C.; Wu, H.; Carney, T. J.; McDowell, M. T.; Yang, Y.; Garnett, E. C.; Li, M.; Hu, L. B.; Cui, Y., Passivation Coating on Electrospun Copper Nanofibers for Stable Transparent Electrodes. *Acs Nano* **2012**, *6* (6), 5150-5156.
- [115] Mehta, R.; Chugh, S.; Chen, Z. H., Enhanced Electrical and Thermal Conduction in Graphene-Encapsulated Copper Nanowires. *Nano Letters* **2015**, *15*, 2024-2030.
- [116] Stewart, I. E.; Ye, S. R.; Chen, Z. F.; Flowers, P. F.; Wiley, B. J., Synthesis of Cu-Ag, Cu-Au, and Cu-Pt Core-Shell Nanowires and Their Use in Transparent Conducting Films. *Chemistry of Materials* **2015**, *27*, 7788-7794.
- [117] Lee, J.; Lee, I.; Kim, T. S.; Lee, J. Y., Efficient Welding of Silver Nanowire Networks without Post-Processing. *Small* **2013**, *9*, 2887-2894.
- [118] Garnett, E. C.; Cai, W. S.; Cha, J. J.; Mahmood, F.; Connor, S. T.; Christoforo, M. G.; Cui, Y.; McGehee, M. D.; Brongersma, M. L., Self-limited plasmonic welding of silver nanowire junctions. *Nature Materials* **2012**, *11*, 241-249.
- [119] Jiu, J.; Nogi, M.; Sugahara, T.; Tokuno, T.; Araki, T.; Komoda, N.; Sugauma, K.; Uchida, H.; Shinozaki, K., Strongly Adhesive and Flexible Transparent Silver Nanowire Conductive Films Fabricated with a High-Intensity Pulsed Light Technique. *Journal of Materials Chemistry* **2012**, *22*, 23561-23567.
- [120] Mayousse, C.; Celle, C.; Carella, A.; Simonato, J. P., Synthesis and Purification of Long Copper Nanowires. Application to High Performance Flexible Transparent Electrodes with and without PEDOT:PSS. *Nano Research* **2014**, *7*, 315-324.
- [121] Yin, Z.; Song, S. K.; You, D. J.; Ko, Y.; Cho, S.; Yoo, J.; Park, S. Y.; Piao, Y.; Chang, S. T.; Kim, Y. S., Novel Synthesis, Coating, and Networking of Curved Copper Nanowires for Flexible Transparent Conductive Electrodes. *Small* **2015**, *11*, 4576-4583.

Chapter 2

Fabrication of fully embedded CuNWs/PDMS conductors

2.1 Introduction

Metallic nanowires have attracted considerable attention in designing stretchable conductors because they can be cost effectively processed by coating a nanowire solution on a substrate [1, 2]. In this case, silver has been so far the most explored metal for the fabrication of metallic nanowires [3, 4]. Recently, substitution of silver by copper would be of great interest mainly because the electrical conductivity of copper ($5.96 \times 10^7 \text{ S m}^{-1}$) is comparable to that of silver ($6.3 \times 10^7 \text{ S m}^{-1}$), while the cost is a hundred times less expensive than silver [5-7]. However, the poor stability of copper against oxidation in ambient conditions largely overshadows their practical applications [8-10]. Lately, several demonstrations have shown progress in improving the performance of CuNWs based conductor, including sheet resistance, flexibility, and stretchable properties [11, 12]. Encapsulation or embedding CuNWs into flexible substrates to achieve a composite structure is one of the approaches to improve the thermal stability of CuNWs. However, in previous reported CuNWs based conductors, CuNWs are deposited on or semi-embedded in the surface layer of substrates, which cannot avoid the oxidation. Additionally, CuNWs are easily delaminated from the substrates under repeated mechanical loading. Therefore, a fast and powerful method is urgently required to fabricate CuNWs based conductors with high conductivity, high stretchability, and high reliability simultaneously.

In this paper, a fully embedded conductor with CuNWs embedded in the surface layer of poly(dimethylsiloxane) (PDMS) was successfully achieved, which possess outstanding oxidation resistance as well as high conductivity. The cross-sectional and over view fabrication process is schematically illustrated in Figure 2.1. During the fabrication process, the curing conditions of PDMS and the accumulation of PDMS at CuNWs junctions lead to the sharp increase of resistance and then limit the application of CuNWs/PDMS conductor. Therefore, a high speed and room temperature operated high-intensity pulsed light technique was innovatively introduced to remove

the oxides on the surface of CuNWs and enhance the connection between CuNWs at the same time. The influence of light parameters on the conductivity of fully embedded CuNWs/PDMS conductors was systematically investigated. After that, the stretchability and oxidation resistance of such conductors were investigated in detail. After 1000 stretching/releasing cycles at 30% strain, the resistance of the fully embedded conductor increased less than 3 times compared with about 800 times of the semi-embedded conductor. In the latter stages, a stretchable conductive heater and a stretchable antenna are demonstrated by using the fully embedded CuNWs/PDMS conductors. The antenna could retain its sensitivity to specific radio frequencies even after 500 cycles of the stretching-releasing process.

2.2 Experimental

2.2.1 Synthesis of CuNWs

Anhydrous copper dichloride (CuCl_2 , 95%), glucose (98%), octadecylamine (ODA), chloroform and isopropanol were purchased from Wako Chemicals. All reagents were analytical grade and were used without further purification. The synthesis of CuNWs involves a Cu(II) salt, a surfactant and a reducing agent, using water as the solvent [13]. In a typical procedure, 0.4 mmol CuCl_2 , 0.4 mmol glucose and 2.4 mmol ODA were mixed in 30 mL of water at room temperature for 2 hours (h) under magnetic stirring until the solution gradually became a blue emulsion. Then the feedstock was transferred into a 50 mL capacity Teflon-lined autoclave and heated at 120 °C for 24 h. When the autoclave was cooled to room temperature naturally, the reddish product was collected by centrifugation, washed three times with water, chloroform and isopropanol (IPA), respectively. Finally, the CuNWs were dispersed in IPA to make CuNWs ink for further use.

2.2.2 Fabrication of fully embedded CuNWs conductors

Firstly, the as prepared CuNWs were diluted to the desired concentration about 20 mmol/L and then subjected to ultrasonic vibration to ensure a homogeneous distribution. Glass substrate was placed on a hot plate with a temperature of 40 °C, which could effectively negate the aggregation of CuNWs due to the rapid evaporation of IPA on the hot plate. Liquid PDMS was

prepared by mixing the “base” and the “curing agent” at a ratio of 10:1, followed by a vacuum centrifuge process. The fabrication process of fully embedded CuNWs/PDMS conductor is schematically illustrated in Figure 2.1. For fully embedded structure, the CuNWs ink was sprayed onto the glass substrates using a nozzle powered by an air compressor. After that, the liquid PDMS was cast onto the glass substrate which was coated with CuNWs film. Following that, all samples were thermally cured at 100 °C for 35 min and then peeled off from the glass substrate. This way, the CuNWs were fully embedded in the surface layer of PDMS. After that, the fully embedded CuNWs/PDMS films were treated with high-intensity pulsed light technique to obtain an enhanced conductive network. Finally, the CuNWs/PDMS conductors were carefully cut into thin strips ($5 \times 20 \text{ mm}^2$) for various evaluations. Semi-embedding structured CuNWs/PDMS conductors were fabricated with the traditional method. Firstly, the liquid PDMS was cast onto a pre-cleaned glass substrate and peeled off after the same curing process. Then, the CuNWs ink was sprayed onto the surface of the cured PDMS, which also placed on a hot plate with the same temperature. After that, the sample was treated with high-intensity pulsed light technique under the same parameters and cut into the same thin strips.

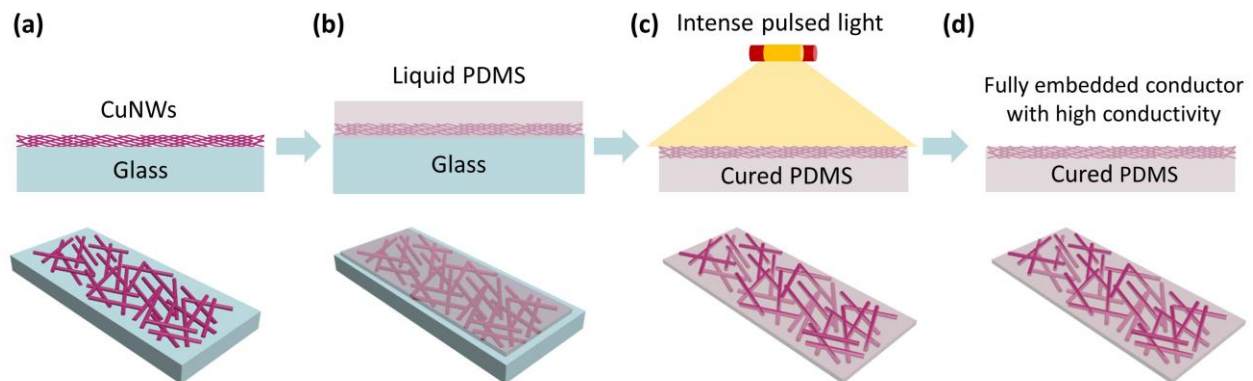


Figure 2.1 The cross-sectional and over view showing the fabrication process of fully embedded CuNWs/PDMS conductors.

2.2.3 Characterization

The morphologies of CuNWs, CuNWs/PDMS conductor were characterized by field-emission scanning electron microscopy (FESEM, Hitachi SU8020, Hitachi High Technologies)

and transmission electron microscopy (TEM, JEM-ARM200F, JEOL Ltd). The cross-section of CuNW was prepared by a focused ion beam (FIB, FB2100, Hitachi). The oxidation state of the sample was investigated by X-ray diffractometry (XRD, Rigaku Smart Lab, Rigaku). The electrical property of CuNWs/PDMS conductor was performed by attaching two ends of the sample onto a pair of grips in a dynamic mechanical analyzer (EZ Test, Shimadzu) with a speed of 60 mm/min. The resistance of printed electrodes during testing was recorded through a four-point probe method. The high-intensity pulsed light system used in this study was the Pulse Forge 3300 (Novacentrix, Austin, TX) that features a broadband emission range from 400 to 1500 nm. The water-cooled xenon lamp, located 10 mm from the substrate stage, can vary optical energy as a function of the electrical voltage and duration time. In this work, the duration time and the electrical voltage was changed to supply optical energies ranging from 1.36 to 2.44 J/cm². The environmental durability of the CuNWs/PDMS was evaluated at high temperatures of 85°C with 85% relative humidity (85 °C-85% RH). The return losses of the V-shaped dipole antennas were evaluated inside an electromagnetic shielding bag at 0.5–3.5 GHz, using a network analyzer (E5061A; Agilent Technologies, Inc., USA).

2.3 Results and discussion

2.3.1 Comparison of microstructure and electrical resistivity

Figure 2.2a shows SEM images of the synthesized CuNWs. The average diameter of the nanowires was around 70 nm, the average length of the nanowires was around 70 μm, as calculated from 50 nanowires randomly selected from the SEM images. As seen from SEM images, these nanowires were uniform and well-dispersed, no impurities (nanoparticles or other by-products) can be observed in the products. The magnified SEM image (Figure 2.2a inset) reveals that the obtained nanowires exhibited a pentagon cross-section. Figure 2.2b shows the surface of a single nanowire using the high-resolution TEM (HRTEM) images. The distance of lattice spaces is 0.21 nm, which could be indexed to the {111} planes of metal Cu, which is consistent with previous reports [14-18]. The cross section of the fully embedded conductor is shown in Figure 2.2c and d,

which further demonstrate the fully embedded structure. Figure 2.2e shows the SEM image of the top surface of the fully embedded conductor. The CuNWs are bonded to the cured PDMS, only scarce CuNWs are visible, all of the CuNWs being below the upper surface of PDMS. The SEM image of the semi-embedded conductor was shown in Figure 2.2f. By high-intensity pulsed light process, some parts of the CuNWs were buried into the surface layer of PDMS and form the semi-embedded conductor. For our method, the fully embedded structure is formed during the curing process of PDMS, the main function of high-intensity pulsed light is to remove the oxide layer and improve conductivity. But for conventional methods, high-intensity pulsed light technique is mainly used to form semi-embedded structures.

The resistivity of CuNWs films was examined before and after casting the PDMS. The resistivity of CuNWs film is about $35 \mu\Omega \cdot \text{cm}$ before the casting of PDMS. After casting PDMS, the sheet resistivity grows to $6319 \mu\Omega \cdot \text{cm}$ and some of the samples even lose conductivity. Due to the low viscosity and surface energy of liquid PDMS, when it is poured onto the CuNWs film, the PDMS penetrates into the CuNWs network and accumulates at the CuNWs junctions, thus increasing the effective resistance of the sample [19]. At the same time, the high curing temperature of PDMS also accelerate the oxidation of CuNWs and lead to an increase in resistance of CuNWs/PDMS conductors. In order to improve the conductivity of fully embedded conductor, the facile high-intensity pulsed light technique was introduced.

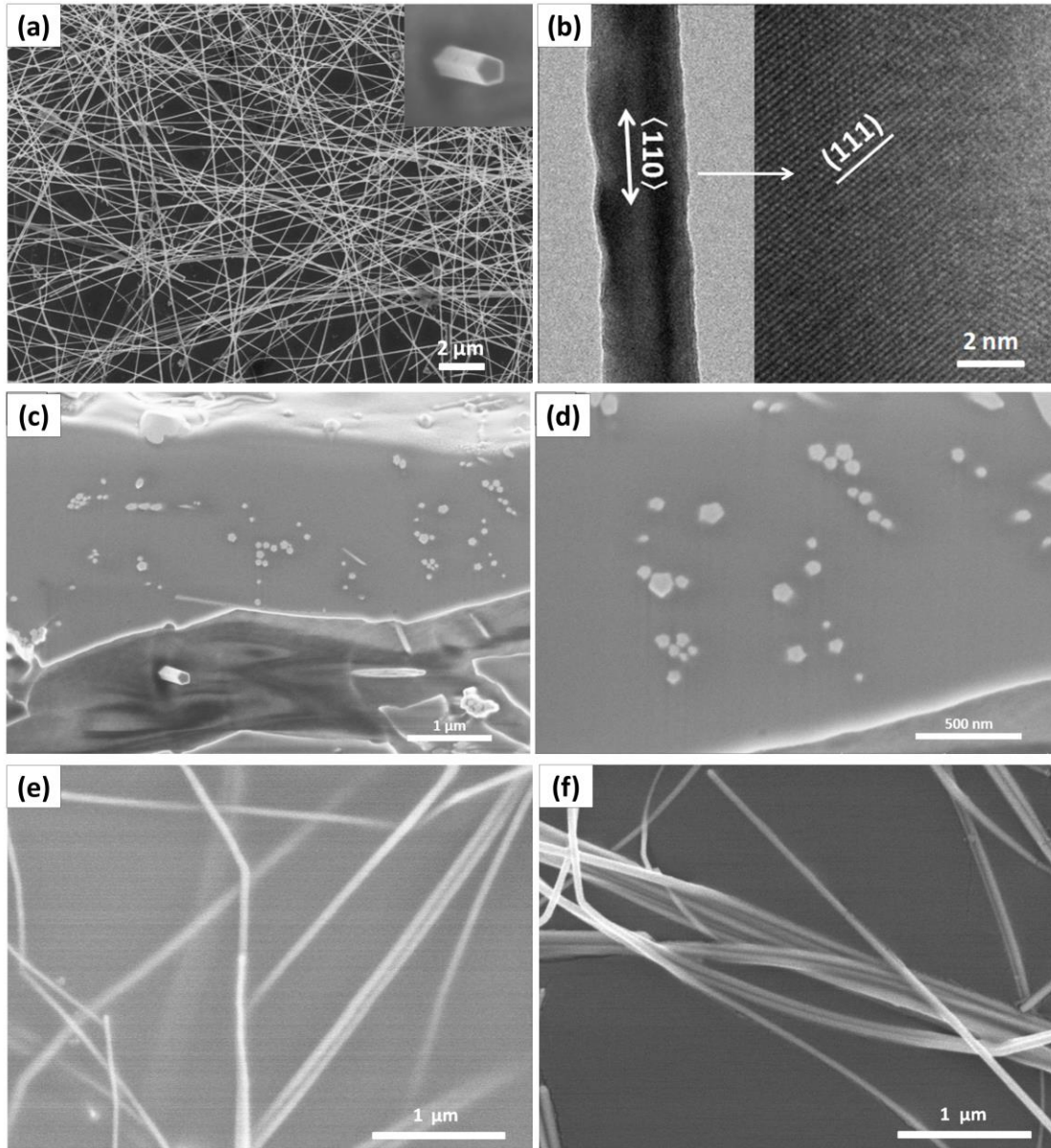


Figure 2.2 (a) SEM image of as prepared CuNWs, inset is the cross-section of a CuNW. (b) High-resolution TEM images of the CuNWs. (c) and (d) The SEM images of the cross section for fully embedded conductor. SEM image of (e) fully embedded and (f) semi-embedded conductor.

Figure 2.3a shows the resistivity evolution of fully embedded CuNWs/PDMS conductor after light treatment with different input energies of 1.36, 1.74, 2.15, and 2.44 J/cm² respectively. After the light treatment process, the resistivity of the sample is significantly reduced from several thousand to tens $\mu\Omega\cdot\text{cm}$. When the energy was as low as 1.36 J/cm², the resistivity of the fully embedded conductor after light treatment was around 94 $\mu\Omega\cdot\text{cm}$. The resistivity was dramatically

decreased to $31 \mu\Omega\cdot\text{cm}$ and $20 \mu\Omega\cdot\text{cm}$ when the energy was increased to 1.74 J/cm^2 and, 2.15 J/cm^2 , respectively. Unfortunately, increasing the energy to 2.44 J/cm^2 resulted in a higher resistivity around $40 \mu\Omega\cdot\text{cm}$. When the sample is treated with high light energy, the resistivity of the sintered electrodes begins to increase because the excessive energy during a short time may cause broke on the surface of CuNWs/PDMS conductor, and the CuNWs exposed to the surface of the PDMS was blown away and the transmittance of the sample had been increased. The stretching-releasing process of these four samples was also carried out as shown in Figure 3a. The resistivity of all samples increased slightly after cycling test, which mainly due to the composite structure of CuNWs and PDMS. It is worth noting that, the light treatment greatly enhanced the conductivity of the conductors, the light energy of 2.15 J/cm^2 showed the best improvement, which was fixed in the follow-up experiment.

To explore the phase changes of CuNWs during the high-intensity pulsed light process, we examined the XRD results of the fully embedded conductor before and after the light treatment, which were shown in Figure 2.3b. Before light treatment, we can see the peak at $2\theta = 36.4^\circ$, which corresponds to copper oxide (JCPDS 05-0667) [20]. This indicates that high conductivity cannot be directly achieved in CuNWs/PDMS film. A weak Cu_2O peak was also observed in the samples that were treated with a low light energy of about 1.36 and 1.74 J/cm^2 . With the increase of light energy, the Cu_2O phase diminishes, leaving only the Cu phase, three diffraction signals can be readily indexed at $2\theta = 43.5^\circ$, 50.7° , and 74.4° , which correspond to the (111), (200), and (220) crystal planes of face-centered-cubic copper (JCPDS 85-1326) respectively. There are no extra signals observed, indicating the high-purity of copper and no other crystallites were observed in the product after light treatment. The reduction degree of the CuNWs showed good consistent with the resistivity change of the conductors. The reduction of the Cu_2O phase to pure Cu during flashlight sintering may be related to the photochemical reaction and the thermal reaction process in the presence of organics on the surface of CuNWs. During the growth of CuNWs, the capping agent ODA was gradually adsorbed on the surface of the newly emerging copper crystals and grew with the crystals to be a nanolayer on the surface of nanowire. It is believed that residual ODA

may photodegrade to produce active H and N radicals under the irradiation of high intensity light, which then reacted with Cu_2O to remove the oxidation layer [21].

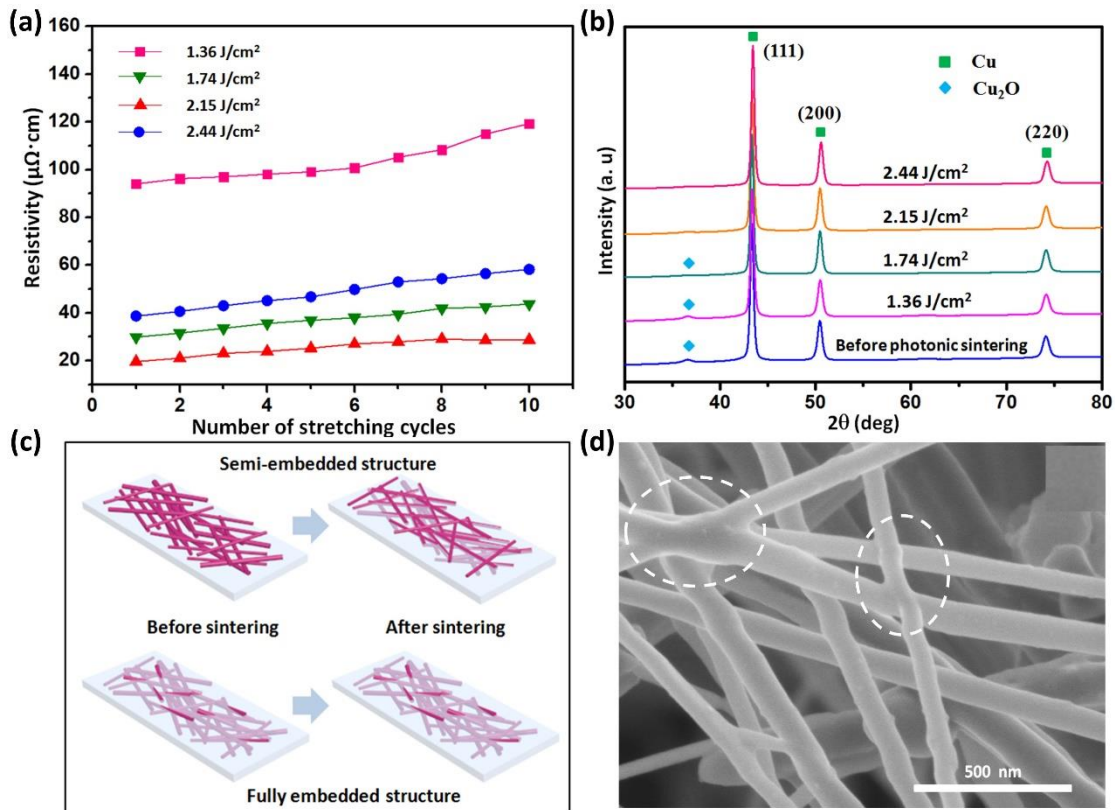


Figure 2.3 (a) Resistivity change of CuNWs/PDMS conductors during the stretching/releasing process. (b) XRD images of the CuNWs/PDMS conductor before and after high-intensity pulsed light treatment. (c) The surface microstructure changes of the fully embedded structure and semi-embedded structure after the light treatment. (d) SEM image of the CuNWs after the light treatment.

The SEM images of the fully embedded and semi-embedded conductors before and after the high-intensity pulsed light treatment were shown in Figure 2.4. The corresponding schematic diagram is shown in Figure 2.3c. It can be clearly seen that the morphology of the embedded structure before (Figure 2.4a) and after (Figure 2.4b) the light treatment has no obvious changes, which mainly due to that most of the CuNWs are already embedded in the upper surface layer of the PDMS. For semi-embedded structure, the CuNWs are evenly distributed on the surface of PDMS before the light treatment, and no embedding was observed (Figure 2.4c). After the light treatment, the CuNWs are partially embedded in the surface layer of PDMS (Figure 2.4d). The

high-intensity pulsed light technique is a fast and powerful method to anneal metal nanostructure in the air without protective atmosphere [21]. And the main approach of light treatment is the thermal conversion of the metal or metal precursor into its conductive counterparts [22]. When the CuNWs/PDMS conductor is exposed to strong light, it absorbs very high light energy within microseconds. The energy absorbed by the conductor is converted to thermal energy, which sinters the CuNWs to produce high conductivity. At the same time, because of the high thermal conductivity of the CuNWs, the heat from the light is easily and rapidly transmitted from the upper wires to the lower wires along the film thickness [13, 23]. Hence, the upper wires catch the thermal energy first and form many more dots, and conductivity has been significantly improved as shown in Figure 2.3d.

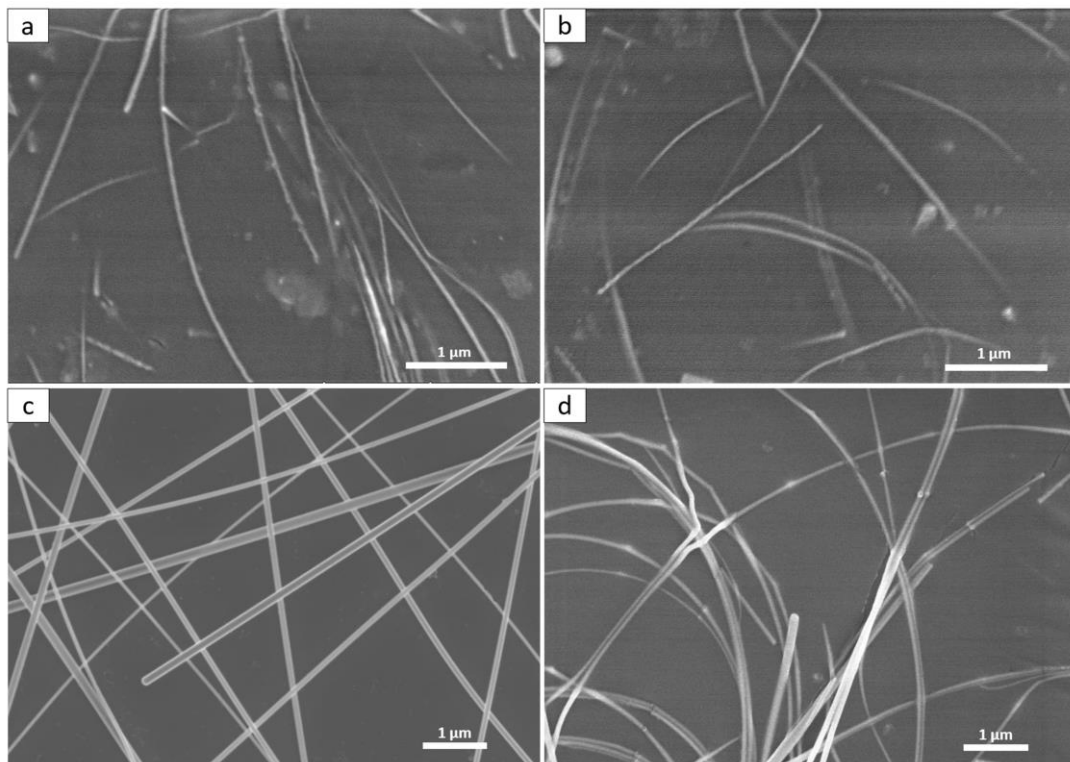


Figure 2.4 The SEM images of the embedded and semi-embedded conductors before and after the light treatment.

Based on these results, we can find that the high-intensity pulsed light plays an important role during the fabrication of fully embedded CuNWs/PDMS conductors. On the one hand, the oxide

layer on the surface of CuNWs is removed. On the other hand, the distance between nanowires was reduced, and welding is formed between the nanowires. Both of which have greatly improved the conductivity of the CuNWs/PDMS conductors and laid the foundation for subsequent applications.

2.3.2 Comparison of stretchability and stability

The stretchability of CuNWs/PDMS conductors after high-intensity pulsed light treatment was investigated. Figure 2.5a shows the resistance change of a CuNWs/PDMS conductor during the stretching process at a constant strain rate of 1 mm/min. The relative resistance of fully embedded conductor rose slowly at first. It increased to just 1.1 times when the strain was 20% and 2.5 times when the strain reached 50%. When the strain was further increased to 70% the resistance increased by about 8 times. At the same time, the resistance of semi-embedded conductor increased more than 20 times when the strain reached 70%. SEM image of the fully embedded conductor after stretching process was shown in Figure 2.5b. As seen from the SEM image, the surface of the conductor formed into wrinkled structures without breaking after the stretching process. For fully embedded conductor, due to the existence of the PDMS matrix, the intrinsically loose CuNWs network was mechanically robust. In addition, the CuNWs are buried deeper than semi-embedded structure, so that the sample could maintain high electrical conductivity during the stretching process. For semi-embedded conductor, only some of the CuNWs buried in the upper surface of PDMS, during the straining process, part of the contact spots among CuNWs became broken due to the sliding of nanowires under the stretching strain, and the concentration of CuNWs in certain areas was quickly reduced, all of which led to the large increase in resistance.

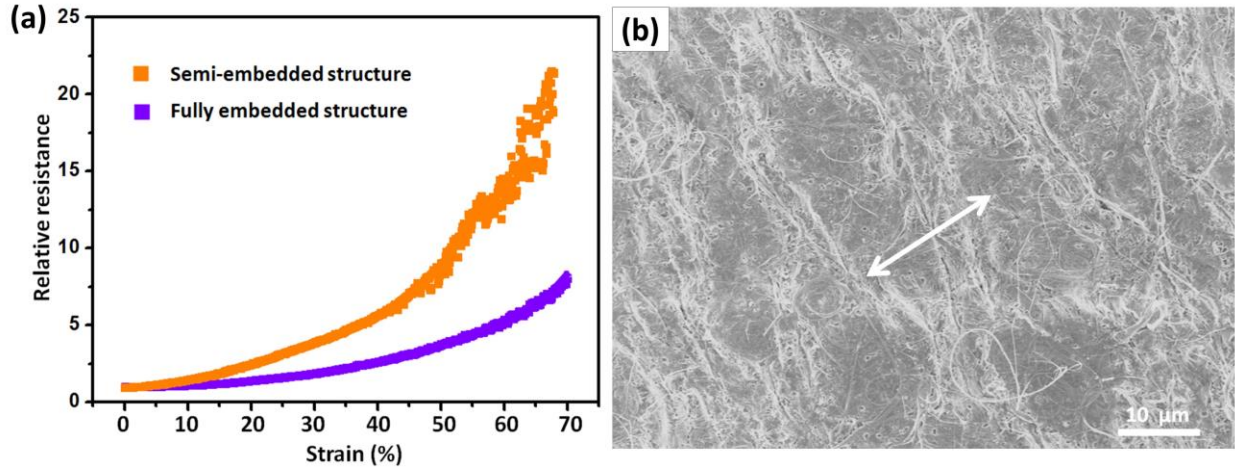


Figure 2.5 (a) Relative resistance (R/R_0) of fully embedded and semi-embedded CuNWs/PDMS conductors with strain up to 70% at a constant stretching speed of 1 mm/min. (b) SEM image of the CuNWs/PDMS conductor after stretching.

Dynamic stability is very important for a stretchable device. Therefore, the performance of the fabricated fully embedded and the semi-embedded conductor were investigated over multiple stretch-relaxation cycles. Figure 2.6a and b show the relative resistance of CuNWs/PDMS conductor measured during 1,000 cycles, at a constant strain rate of 60 mm/min, with peak strain at 10%, 20%, and 30% respectively. Figure 2.5a shows the resistance evolution of fully embedded conductor. The resistance increased to just 1.2 times upon being stretched to 10% strain. After repeatedly stretching/releasing under 20% strain, the resistance increased to 1.8 times. The resistance increased less than 3 times even after 1000 cycles under 30% strain, thus exhibiting an excellent stretching property compared with previous reports [24, 25]. For CuNWs/PDMS conductor with semi-embedded structure (Figure 2.6b), resistance increased to 1.9 times upon being stretched to 10% strain. When stretched to 20% strain, the resistance increased to 7.0 times of original value. Under a 30% strain, after 400 cycles, the resistance increased to 16.0 times and further increased near 800 times over 1,000 cycles. During the stretching process, the weak contact spots in semi-embedded structure were easily broken, especially under 30% strain, and only a few locations transferred the electron and resulting in the low resistance. At the same time, the CuNWs network in fully embedded structure maintained stable contact spots, resulting in stable

conductivity under a higher strain and improved dynamic stability. Combined with previous reports, it is clear that the superior dynamic stability of fully embedded conductor is mainly due to the outstanding stretchability of PDMS matrix, the strong adhesion between CuNWs and PDMS, and the buckled wavy shape of the CuNW/PDMS layer during the stretching process. These results clearly indicate that our fully embedded conductors represent an excellent advancement and can be successfully utilized in many stretchable devices.

The stability of our fully embedded CuNWs/PDMS conductors at high temperatures and high humidity is also required for its practical application. In order to confirm the anti-oxidation performance of CuNWs/PDMS conductors, we have compared the change of relative resistance for fully embedded and semi-embedded conductor with the temperature and relative humidity being 85 °C and 85% respectively. The results are shown in Figure 2.6c. For semi-embedded conductor, the relative resistance began to increase suddenly after just 1 hour and rapidly increased to about 36 times after 12 hours in high temperature and humidity. As a comparison, the relative resistance of fully embedded conductor remains almost stable, having only a slight increase of about 10 times after 12 hours. In addition, we have also compared the resistance evolution of two samples after 85 °C/85% RH test, with peak strain at 20%, during 1,000 cycles. Figure 2.6d shows the dynamic stability of the two sample after 3 hours under 85 °C/85% RH test. While under 20% strain, after 1000 cycles, the resistance increased about 6.0 times for embedding structure and over 24 times for non-embedding structure. For fully embedded conductor, PDMS substrate could effectively protect the CuNWs that were “underground” from the outer atmosphere. Therefore, it is easily understood they were stable as well. This result further indicates that the preferential oxidation of CuNWs can be significantly inhibited by the fully embedded structure.

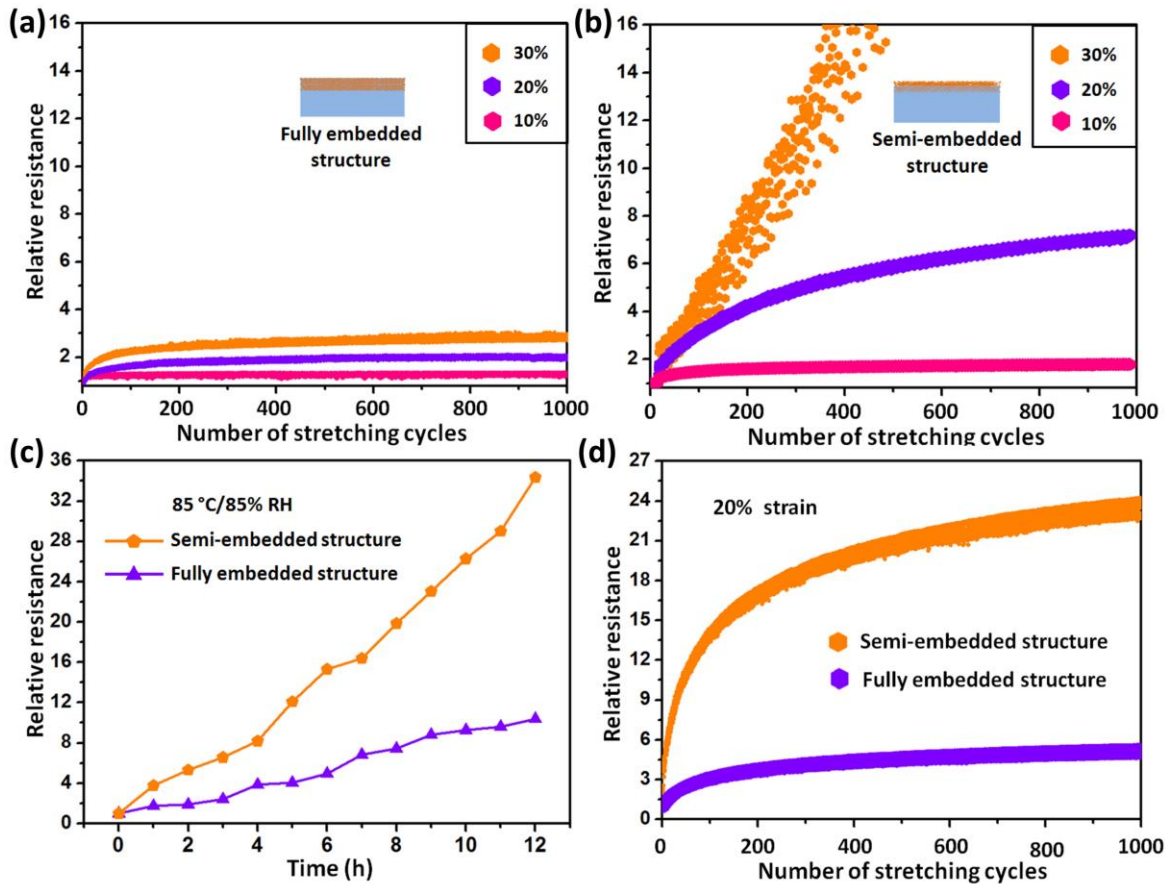


Figure 2.6 Performance comparison between semi-embedded and fully embedded CuNWs/PDMS structures. (a) and (b), relative resistance of the conductors during the stretching-releasing process with the peak value of 10%, 20%, 30% strain. (c) The change of relative resistance in harsh environment (85 °C/85% RH). (d) After 85 °C/85% RH test, the relative resistance of conductors during the stretching-releasing process with the peak value of 20% strain.

2.3.3 Applications of fully embedded CuNWs/PDMS conductors

The field of wireless communication devices requires technologies for the mass production of high-performance stretchable antennas [26, 27]. To demonstrate the applicability of our embedding structured CuNWs/PDMS conductors, V-shaped dipole CuNWs antenna patterns were successfully fabricated. The antenna patterns were 30 mm in length and 5 mm in width with an angle of about 30°, and the sizes of the PDMS substrates were 30.0 mm × 30.0 mm as shown in Figure 2.7a. Figure 2.7b shows the resonance frequency and the return loss of the CuNWs/PDMS

antennas before and after 500-cycles stretching test, the stretching strain is 20%. As seen, the return losses of CuNWs/PDMS antennas before stretching test is around 22.6 dB, after the stretching test it is 18.9 dB. There was no significant decrease in return loss of these two antennas, indicating that antenna sensitivity was maintained even after 500-cycles stretching test. Generally, the acceptable sensitivity for an antenna is that the return loss is less than 10 dB [28, 29]. Therefore, our results indicate that fully embedding structured CuNWs/PDMS antenna has high sensitivity and stability. The excellent stretching properties expand the application of embedding structured CuNWs/PDMS conductors into future wireless communication devices.

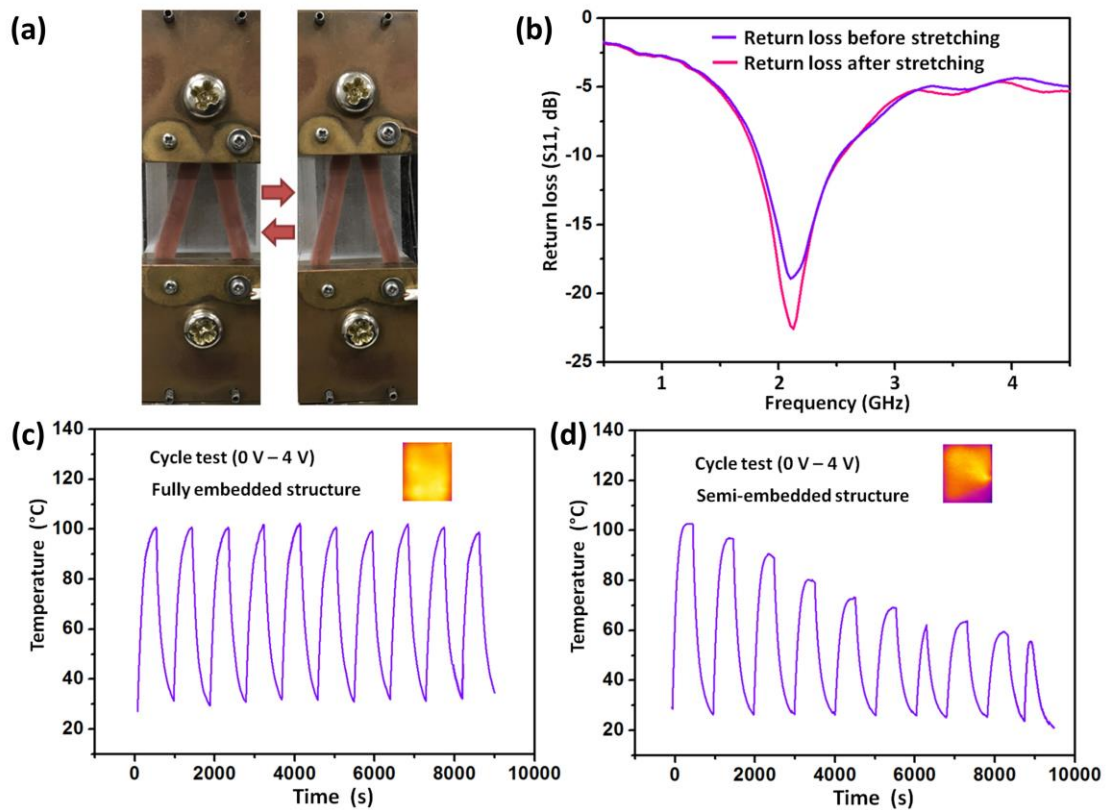


Figure 2.7 Applications of fabricated CuNWs/PDMS conductors for wearable electronics. (a) Optical images during the stretching process of CuNWs/PDMS antenna and (b) its return loss before and after the 500-cycles stretching test. The time-dependent average temperature of the (c) semi-embedded and (d) fully embedded conductors at on/off responses over 10 cycles under an applied voltage of 4 V. The insets present infrared images of the conductor during repeated heating tests.

A stretchable conductive heater was fabricated as another emerging application to demonstrate the stability of CuNWs/PDMS conductor. A constant voltage was applied at both ends of the CuNWs/PDMS conductor to induce electrically driven resistive Joule heating. Figure 2.7c and d show the time-dependent average temperature of the CuNWs/PDMS conductor at repeated applied voltages and temperature distribution infrared images. For fully embedded conductor, it was confirmed that there was no significant change in achievable temperature in repeated heating tests by inputting and turning off the voltage (4 V) for 10 times (Figure 2.7c), and uniform heating can be seen throughout the entire conductor during this process. At the same time, the temperature response of semi-embedded conductor was decreased with the increase of time, the temperature distribution is uneven after 5 times heating test (Figure 2.7d). The stable temperature response of fully embedded conductor indicates that our fully embedded conductor can be feasible to applications such as automobile window defrosters that require fast temperature switching and stability.

2.4 Conclusions

In summary, CuNWs-based highly reliable, conductive and stretchable conductors were fabricated by embedding CuNWs below the surface layer of PDMS and completed with a simple high-intensity pulsed light process. The influence of light parameters on the performance of conductors was investigated. The light energy absorbed by the film not only removes the oxides on the surface of nanowires but also enhance the connection between nanowires to produce high conductivity. Due to the wrap of the CuNWs in the PDMS matrix, the fully embedded conductor shows ultrahigh oxidation resistance, which remains stable in air at 85 °C and 85% RH. The electrical resistance of the conductor is maintained at low levels when the strain is more than 70%. The fully embedded conductor endured 1000 cycles of stretching-releasing at a rate of 60 mm/min, under 30% strain and showed a slight increase in resistance. Additionally, fully embedded conductor was used as a dipole antenna. The stretchable antenna retained its sensitivity to specific radio frequencies after 500 cycles of the stretching-releasing process. With their superior stability,

conductivity and stretchability, the fabricated fully embedded CuNWs/PDMS conductors possess broad applications in stretchable strain sensors, skin sensors, bendable displays and wearable electronics.

References

- [1] Won, Y.; Kim, A.; Lee, D.; Yang, W.; Woo, K.; Jeong, S.; Moon, J. Annealing-Free Fabrication of Highly Oxidation-Resistive Copper Nanowire Composite Conductors for Photovoltaics. *Open. Npg Asia Materials* **2014**, *6*, e105.
- [2] Cheng, Y.; Wang, S.; Wang, R.; Sun, J.; Gao, L. Copper Nanowire Based Transparent Conductive Films with High Stability and Superior Stretchability. *J. Mater. Chem. C* **2014**, *2*, 5309-5316.
- [3] Yang, Y.; Ding, S.; Araki, T.; Jiu, J.; Sugahara, T.; Wang, J.; Vanfleteren, J.; Sekitani, T.; Sugauma, K. Facile Fabrication of Stretchable Ag Nanowire/Polyurethane Electrodes using High Intensity Pulsed Light. *Nano Res.* **2016**, *9*, 401-414.
- [4] Yang, Y.; Xu, K.; Vervust, T.; Vanfleteren, J. Multifunctional and Miniaturized Flexible Sensor Patch: Design and Application for in Situ Monitoring of Epoxy Polymerization. *Sens. Actuators B* **2018**, *261*, 144-152.
- [5] Celle, C.; Cabos, A.; Fontecave, T.; Laguitton, B.; Benayad, A.; Guettaz, L.; Pelissier, N.; Nguyen, V. H.; Bellet, D.; Munozrojas, D. Oxidation of Copper Nanowire Based Transparent Electrodes in Ambient Conditions and Their Stabilization by Encapsulation: Application to Transparent Film Heaters. *Nanotechnology* **2018**, *29*, 085701.
- [6] Hatami, M. Production and Morphological Characterization of Low Resistance Polyimide/Silver Nanowire Nanocomposites: Potential Application in Nanoconductive Adhesives. *J Mater Sci: Mater Electron* **2017**, *28*, 3897-3908.
- [7] Rathmell, A. R.; Bergin, S. M.; Hua, Y. L., Li, Z. Y.; Wiley, B. J. The Growth Mechanism of Copper Nanowires and Their Properties in Flexible, Transparent Conducting Films. *Adv. Mater.* **2010**, *22*, 3558-3563.

- [8] Dou, L.; Cui, F.; Yu, Y.; Khanarian, G.; Eaton, S. W.; Yang, Q.; Resasco, J.; Schildknecht, C.; Schierle-Arndt, K.; Yang, P. Solution-Processed Copper/Reduced-Graphene-Oxide Core/Shell Nanowire Transparent Conductors. *Acs Nano* **2016**, *10*, 2600-2606.
- [9] Hsu, P. C.; Wu, H.; Carney, T. J.; McDowell, M. T.; Yang, Y.; Garnett, E. C.; Li, M.; Hu, L.; Cui, Y. Passivation Coating on Electrospun Copper Nanofibers for Stable Transparent Electrodes. *Acs Nano* **2012**, *6*, 5150-5156.
- [10] Zeng, D.; Chen, Y.; Lu, A., Li, M.; Guo, H.; Wang, J.; Peng, D. L. Injection Synthesis of Ni-Cu@Au-Cu Nanowires with Tunable Magnetic and Plasmonic Properties. *Chem. Commun* **2013**, *49*, 11545.
- [11] Guo, H.; Jin, J.; Chen, Y.; Liu, X.; Zeng, D.; Wang, L.; Peng, D. L. Controllable Synthesis of Cu-Ni Core-Shell Nanoparticles and Nanowires with Tunable Magnetic Properties. *Chem. Commun* **2016**, *52*, 6918.
- [12] Niu, Z.; Fan, C.; Yi, Y.; Becknell, N.; Sun, Y.; Khanarian, G.; Kim, D.; Dou, L.; Dehestani, A.; Schierlearndt, K.; Yang, P. Ultrathin Epitaxial Cu@Au Core-Shell Nanowires for Stable Transparent Conductors. *J. Am. Chem. Soc* **2017**, *139*, 7348-7354.
- [13] Ding, S.; Jiu, J.; Tian, Y.; Sugahara, T.; Nagao, S.; Suganuma, K. Fast Fabrication of Copper Nanowire Transparent Electrodes by a High Intensity Pulsed Light Sintering Technique in Air. *Phys. Chem. Chem. Phys* **2015**, *17*, 31110-31116.
- [14] Han, S.; Hong, S.; Ham, J.; Yeo, J.; Lee, J.; Kang, B.; Lee, P.; Kwon, J.; Lee, S. S.; Yang, M. Y. Flexible Electronics: Fast Plasmonic Laser Nanowelding for a Cu-Nanowire Percolation Network for Flexible Transparent Conductors and Stretchable Electronics. *Adv. Mater.* **2014**, *26*, 5808-5814.
- [15] Tang, Y.; Gong, S.; Chen, Y.; Yap, L. W.; Cheng, W. Manufacturable Conducting Rubber Ambers and Stretchable Conductors from Copper Nanowire Aerogel Monoliths. *Acs Nano* **2014**, *8*, 5707-5714.
- [16] Johnson, C. J.; Dujardin, E.; Davis, S. A.; Murphy, C. J.; Mann, S. Growth and Form of Gold Nanorods Prepared by Seed-Mediated, Surfactant-Directed Synthesis. *J. Mater. Chem*

2002, 12, 1765-1770.

- [17] Zhang, S. H.; Jiang, Z. Y.; Xie, Z. X.; Xu, X.; Huang, Rongbin.; Zheng, L. S. Growth of Silver Nanowires from Solutions: a Cyclic Penta-Twinned-Crystal Growth Mechanism. *J. Phys. Chem. B* **2005**, 109, 9416-9421.
- [18] Huang, X.; Zheng, N. One-Pot, High-Yield Synthesis of 5-Fold Twinned Pd Nanowires and Nanorods. *J. Am. Chem. Soc* **2009**, 131, 4602.
- [19] Xu, F.; Zhu, Y. Highly Conductive and Stretchable Silver Nanowire Conductors. *Adv. Mater.* **2012**, 24, 5117-5122.
- [20] Li, W.; Zhang, H.; Gao, Y.; Jiu, J.; Li, C. F.; Chen, C.; Hu, D.; Goya, Y.; Wang, Y.; Koga, H. Highly Reliable and Highly Conductive Submicron Cu Particle Patterns Fabricated by Low Temperature Heat-Welding and Subsequent Flash Light Sinter-Reinforcement. *J. Mater. Chem. C* **2016**, 5, 1155-1164.
- [21] Han, S.; Hong, S.; Yeo, J.; Kim, D.; Kang, B.; Yang, M. Y.; Ko, S. H. Nanowires: Nanorecycling: Monolithic Integration of Copper and Copper Oxide Nanowire Network Electrode Through Selective Reversible Photothermochemical Reduction. *Adv. Mater.* **2015**, 27, 6397-6403.
- [22] Jiu, J.; Nogi, M.; Sugahara, T.; Tokuno, T.; Araki, T.; Komoda, N.; Sugauma, K.; Uchida, H.; Shinozaki, K. Strongly Adhesive and Flexible Transparent Silver Nanowire Conductive Films Fabricated with a High-Intensity Pulsed Light Technique. *J. Mater. Chem* **2012**, 22, 23561-23567.
- [23] Kim, H. S.; Dhage, S. R.; Shim, D. E.; Hahn, H. T. Intense Pulsed Light Sintering of Copper Nanoink for Printed Electronics. *Appl Phys A*, **2009**, 97, 791.
- [24] Zhu, Y.; Qin, Q.; Xu, F.; Fan, F.; Ding, Y.; Zhang, T.; Wiley, B. J.; Wang, Z. L. Size Effects on Elasticity, Yielding, and Fracture of Silver Nanowires: In Situ Experiments *Phys Rev B*. **2012**, 85, 045443.
- [25] Jin, M.; He, G.; Zhang, H.; Zeng, J.; Xie, Z.; Xia, Y. Shape-Controlled Synthesis of Copper Nanocrystals in an Aqueous Solution with Glucose as a Reducing Agent and Hexadecylamine

as a Capping Agent. *Angew Chem Int Ed Engl*, **2011**, *123*, 10560-10564.

- [26] Inui, T.; Koga, H.; Nogi, M.; Komoda, N.; Suganuma, K. A Miniaturized Flexible Antenna Printed on a High Dielectric Constant Nanopaper Composite. *Adv. Mater.* **2015**, *27*, 1112-1116.
- [27] Kamyshny, A.; Magdassi, S. Conductive Nanomaterials for Printed Electronics. *Small*, **2014**, *10*, 3515.
- [28] Fujisaki, Y.; Koga, H.; Nakajima, Y.; Nakata, M.; Tsuji, H.; Yamamoto, T.; Kurita, T.; Nogi, M.; Shimidzu, N. Flexible Electronics: Transparent Nanopaper-Based Flexible Organic Thin-Film Transistor Array. *Adv Funct Mater* **2014**, *24*, 1656-1656.
- [29] Nogi, M.; Komoda, N.; Otsuka, K.; Suganuma, K. Foldable Nanopaper Antennas for Origami Electronics. *Nanoscale*, **2013**, *5*, 4395-43.

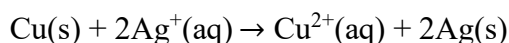
Chapter 3

Galvanic replacement free synthesis of Cu@Ag core-shell nanowires

3.1 Introduction

The obstacle hampering the real-world application of Copper nanowires (CuNWs) in stretchable conductive films is oxidation, which will produce copper oxide and decrease the conductivity and transparency of the conductors [1-4]. Herein, it is necessary to improve the oxidation stability of the CuNWs network. Several coating methods have been reported to protect the CuNWs against oxidation, like encapsulating the CuNWs in shells of organic materials [5], polymers [6, 7], metals [8, 9], or embedding the CuNWs in a flexible substrate [10]. In general, the applied layer should not only protect the CuNW from oxidation, but also maintain the high conductivity of the original nanowires [11-13]. Therefore, one of the best solutions is the coating of metals, which could provide oxidation protection and electrical contacts at the same time [14, 15]. Silver has the best intrinsic conductivity among all elements and it is more stable than copper when exposed to ambient environment [16-18]. Thus, the formation of Cu@Ag core-shell nanowires with a copper-core and silver-shell is considered to be one of the best solutions to improve the oxidation resistance of CuNWs.

Many researchers have devoted to the synthesis of Cu@Ag core-shell nanowires [19-22]. However, due to the difference in reduction potentials (E^0), the growth process of the silver ($\text{Ag}^+ \rightarrow \text{Ag}$, $E^0 = +0.7996 \text{ V}$) on the copper nanowires surface ($\text{Cu}^{2+} \rightarrow \text{Cu}$, $E^0 = +0.3419 \text{ V}$) always dominated by galvanic replacement reaction and easily results in hollow nanostructures [23-25]. Consequently, when AgNO_3 and CuNWs solution are mixed together, galvanic replacement reaction rapidly occurred between Cu atoms and Ag^+ ions, result in Cu^{2+} ions and Ag atoms [26-28]. The corresponding reaction equations are shown below:



Considerable efforts have been made to synthesis metallic core-shell nanowires by a galvanic replacement free process. Mirkin et al. reported that the introduction of a reducing agent (ascorbic

acid) and a capping agent (cetyltrimethylammonium bromide) could prevent most galvanic replacement reactions from occurring except for the corners of the Ag nanoprism [29]. Yin et al. introduce I^- ions to form complexes, thereby reducing the reduction potential of the Au salt. However, galvanic replacement still occurred during the synthesis of Ag@Au core-shell nanoplates and result in small voids on the surfaces of plates [30]. Niu et al. revealed that the E^0 and reduction rates could be reduced by the introduction of strong binding ligand (trioctylphosphine), and then prevent galvanic replacement reactions between Cu and Au precursor. It is found that all of these studies focused on the control of the reduction potential differences between the two involved metals, which requires expensive equipment to ensure stringent reaction conditions, thereby limit the large-scale production and increase the cost of preparation. Therefore, galvanic replacement free, large-scale and facile synthesis method is essential for obtaining the Cu@Ag core-shell nanowires as well as the widespread use of CuNWs in numerous wearable devices.

Herein, we show a large-scale and galvanic replacement free method to obtain Cu@Ag core-shell nanowires through a simple adsorption and decomposition process. Figure 3.1 shows the detail formation process. During the adsorption process, by adjusting the reaction conditions, the Ag-ammonia complex can uniformly cover on CuNWs surface, then form Cu@Ag-ammonia core-shell structure. In this process, since the Ag-ammonia complex ($[Ag(NH_2R)_2]^+$) and copper have similar reduction potentials, the replacement reaction between copper and silver can be completely avoided by using the Ag-ammonia complex as a silver source. After that, through a low temperature annealing process in air (140 °C for 5 minutes), Ag complex will decompose to pure silver, and well-defined Cu@Ag nanowires will be obtained. Different thicknesses of the Ag shell can be obtained by changing the amount of Ag complex. Cu@Ag nanowires based conductors exhibit similar conductivity as well as transparency with that made by CuNWs. In addition, due to the effectively protection of silver shell, the newly formed core-shell nanowires exhibit outstanding stability in harsh environment. The expected significance of this work is the development of a new galvanic replacement free pathway toward the synthesis of metallic core-

shell nanowires by a simple absorption and decomposition process, and achieve the large scale production.

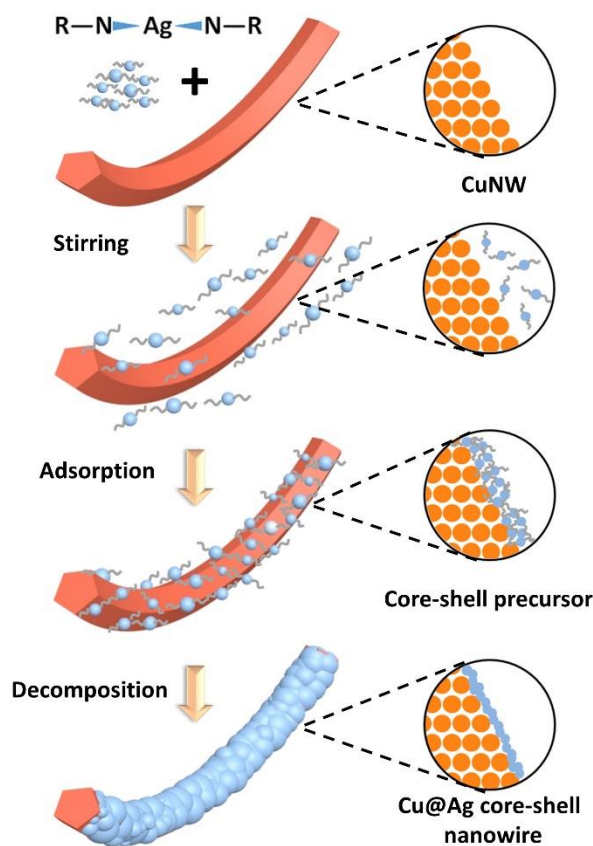


Figure 3.1 Schematic diagram of the galvanic replacement free formation of Cu@Ag core-shell nanowires.

3.2 Experiment section

3.2.1 Synthesis of CuNWs

Anhydrous copper dichloride ($CuCl_2$), octadecylamine ($C_{18}H_{39}N$, ODA), glucose ($C_6H_{12}O_6$), chloroform ($CHCl_3$), 2-ethylhexylamine ($C_8H_{19}N$), Ag-ammonia ($Ag(NH_3)_2OH$) and isopropanol (C_3H_8O , IPA) were purchased from Wako Chemicals Industries, Ltd. Ag (I) β -ketocarboxylate ($CH_3COCH(CH_3)COOAg$) was provided by Toppan Forms Co., Ltd. Glass substrate was purchased from Toray Industries, Inc. All reagents were analytical grade and used without further purification. CuNWs were prepared via a hydrothermal method. In a typical procedure, 0.4 mmol

CuCl₂, 0.4 mmol glucose and 2.4 mmol ODA were mixed in 30 mL of water at room temperature and stirred continuously for 2 hours until the solution gradually became a blue emulsion. Then the feedstock was transferred into a 50 mL capacity Teflon-lined autoclave and heated at 120 °C for 24 h. When the autoclave was cooled to room temperature naturally, the reddish product was collected and then washed three times with water, chloroform and isopropanol, respectively. Finally, the CuNWs were dispersed in IPA for further use.

3.2.2 Fabrication of Cu@Ag core-shell nanowire networks

Ag (I) β-ketocarboxylate was firstly added into 2-ethylhexylamine with a molar ratio of 1:2 to form Ag-ammonia complex solution. Then, Ag-ammonia complex ($[\text{Ag}(\text{NH}_2\text{CH}_2\text{CH}(\text{CH}_2\text{CH}_3)(\text{CH}_2)_3\text{CH}_3)_2]^+$) was uniformly distributed into CuNWs solution to make Cu@Ag-ammonia complex core-shell structure, which were stored in refrigerator for further use. The ratio of CuNWs and Ag-ammonia complex can be modified to tune the coverage and shell thickness of the resulting core-shell structure. After that, the Cu@Ag-ammonia core-shell structures were sprayed onto the PET substrates using a nozzle powered by an air compressor. The substrate was placed on a hot plate with a temperature of 40 °C, which could effectively avoid the aggregation of Cu@Ag-ammonia core-shell structure due to the rapid evaporation of solvent. Finally, the film was heated to a temperature of 140 °C for 5 min to fabricate the Cu@Ag core-shell nanowires conductors. The films were then used for tests in harsh environment and to fabricate transparent conductive heater. In addition, the Ag(NH₃)₂OH is used to mix with CuNWs to demonstrate that the adsorption process exists between CuNWs and $[\text{Ag}(\text{NH}_3)_2]^+$.

3.2.3 Characterization.

The crystalline nature and phase structures of the samples were characterized by powder X-ray diffraction (XRD, Rigaku Smart Lab, Rigaku). The morphologies, components and structures of the samples were observed by field-emission scanning electron microscopy (FE-SEM, Hitachi SU8020, Hitachi) and transmission electron microscopy (TEM, JEM-ARM200F, JEOL Ltd.), equipped with energy dispersive spectroscopy (EDS). The cross-section of the core-shell

nanowires was obtained by *gebrauchsanweisung* (Leica Ultracut UCT). The electrical resistivity of the sample was measured by four probe analyzer (LorestaGP T610, Mitsubishi Chemical Analytech Co. Ltd.). Optical transmittance of the conductor over the wavelength range of 300–800 nm was measured by a UV-visible near infrared spectrophotometer (V670, JASCO Corp.) using a sheet of pure PET as a reference. These measurements were performed at room temperature. The atomistic molecular dynamics simulations were performed in Material Studio 7.0. Environmental durability of the sample was evaluated by exploring them at high temperatures of 140 °C, and also at 85°C with 85 % relative humidity (85 °C, 85% RH). To evaluate the thermal stability in static occasions, two ends of the heaters were fixed tightly on a desk-top universal testing machine, and two electrically conductive clips were connected to the stretchable heaters to supply a constant voltage. The temperature evolutions on the surface of the heater under different applied voltages were recorded by using an infrared (IR) camera (R500EX, NIPPON AVIONICS, sensitivity: 0.025°C).

3.3 Results and discussion

3.3.1 Characterization of Cu@Ag core-shell nanowires

The SEM image of pure CuNWs is shown in Figure 3.2a. The average diameter of obtained nanowires are around 80 nm, which are uniform and have smooth surface. Figure 3.2b depicts the SEM image of the Cu@Ag-ammonia core-shell structure obtained from the mixed solution of CuNWs and Ag-ammonia complex. After mixed together, the entire surface of obtained CuNWs was covered by floccular structured Ag-ammonia complex. A core-shell precursor with CuNWs core and Ag-ammonia complex shell was obtained. Compared with CuNWs, the diameter of Cu@Ag-ammonia core-shell precursor has increased to 110~120 nm. After heated 5 min at 140 °C, the floccular structured Ag-ammonia complex decomposed into silver. As shown in Figure 3.2c, the uniform Cu@Ag core-shell nanowires were obtained with the diameter decreased to about 100 nm. The cross-section of Cu@Ag nanowires was prepared to obtain the structural information. As show in Figure 3.2d, the cross-section of the sample is almost circular, which is different from pentagon CuNWs. The elemental map shown in Figure 3.2e-g depicts the structure of the obtained

nanowires. A core-shell structure can be clearly observed, in which red copper nanowires are surrounded by green silver shells. The average thickness of silver shell is about 8 nm as seen from the results. The elemental map (Figure 3.2e) also reveals that the obtained CuNWs exhibit a pentagon cross section. The preparation of Cu@Ag core-shell nanowires indicates that our simple adsorption and decomposition method are effective to synthesize metallic core-shell structures.

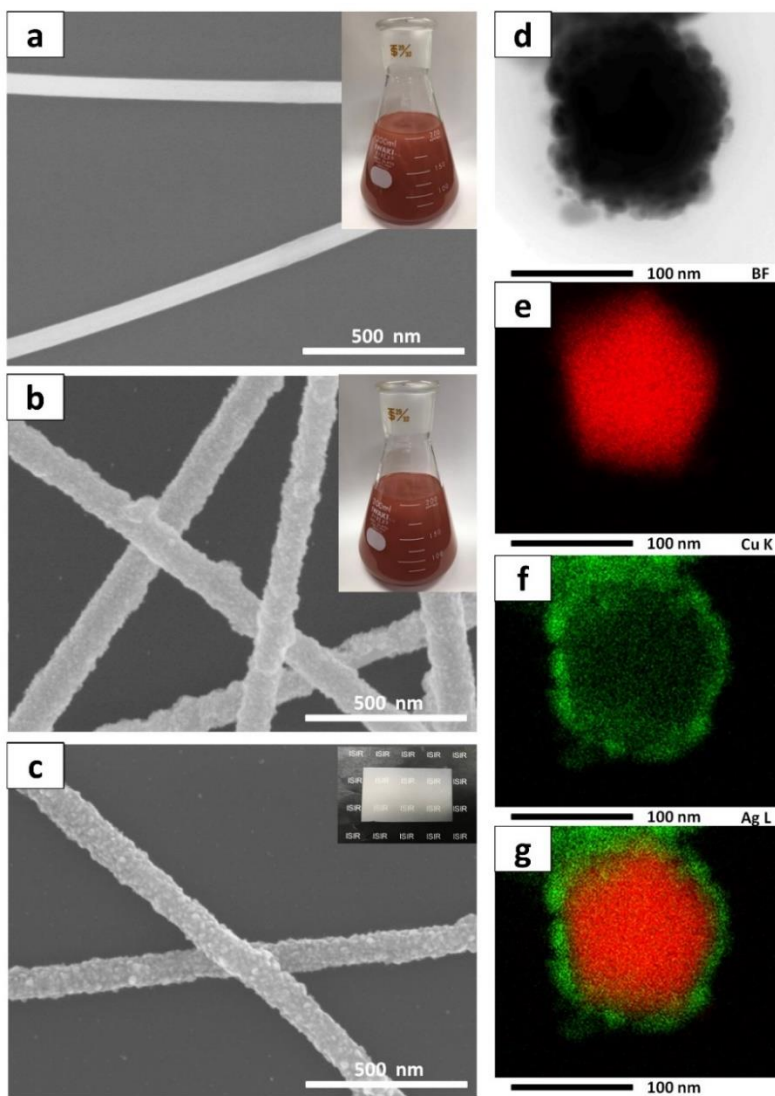


Figure 3.2 SEM images of (a) CuNWs, (b) Cu@Ag-ammonia core-shell structure and (c) Cu@Ag core-shell nanowires. TEM image of the cross-section for Cu@Ag core-shell nanowires (d), and the corresponding elemental mapping images (e-g). The samples all with 20 wt% of silver.

Cu@Ag core-shell nanowires with different thicknesses of silver shells can be obtained by

changing the amount of Ag complex in CuNWs solution. The SEM images of core-shell precursors with 5 wt%, 20 wt%, and 30 wt% of silver are given in Figure 3.3a-c. With a low Ag content of 5 wt%, the surface of CuNWs is partly coated with floccular structures (Figure 3.3a). When the content of Ag increases to 20 wt%, the entire surface of the CuNWs are covered by silver complex (Figure 3.3b). When an excessive amount of Ag complex (30 wt%) was added, the surface of nanowires become rougher, the diameter of the core-shell precursors was increased (Figure 3.3c). No obvious aggregation is formed during the formation of core-shell precursors, and the interfaces between nanowires are clear. After that, core-shell precursors were heated for 5 min at high temperature of 140 °C, and Cu@Ag core-shell nanowires with different silver shell thickness were formed. As shown in Figure 3.3d-f, with higher Ag content, the diameter of the nanowires gradually increased, and a large number of silver particles appeared. The size of Ag particle changed from 5 to 60 nm, and larger silver particles mainly occur in high silver concentration. In addition, after heating, although the surfaces of CuNWs became rough, but no impurities appeared during this period.

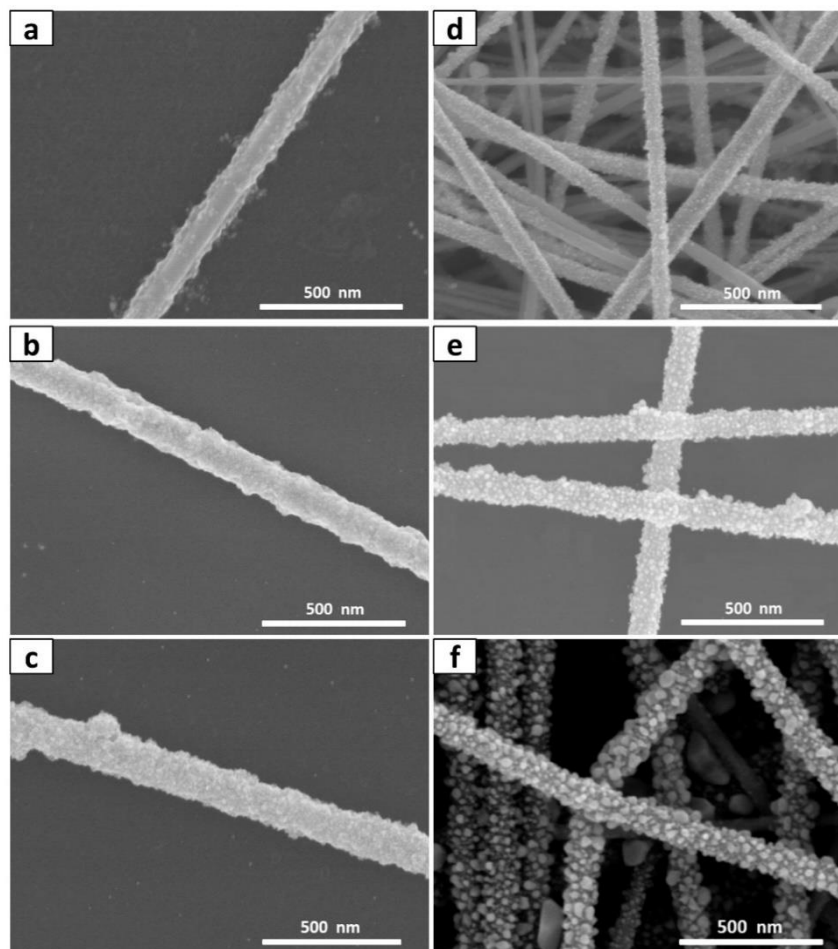


Figure 3.3 The SEM images of core-shell precursors with (a) 5 wt%, (b) 20 wt%, (c) 30 wt% of Ag and Cu@Ag core-shell nanowires with (d) 5 wt%, (e) 20 wt%, (f) 30 wt% of Ag.

The detailed time-dependent evolution of the morphology was evaluated in order to investigate the formation process of core-shell structure and its growth mechanism. Figure 3.4 shows the SEM images for pure CuNWs and Cu@Ag-ammonia core-shell structure that obtained from the CuNWs and Ag-ammonia complex mixed solution (Cu-20Ag). The surface of pure CuNWs is very smooth as seen from Figure 3.4a. When the Ag-ammonia complex is added and stirred for 1 min, floccular structured Ag-ammonia appear on the surface of CuNWs (Figure 3.4b). The floccular structure gradually increased and cover the most surface of CuNWs after 5 min (Figure 3.4c). When the reaction time is increased to 10 min, the floccular structure further increases and perfect core-shell nanowire with copper core and silver-complex shell (Figure 3.4d)

was formed. The Cu@Ag-ammonia core-shell precursors obtained from the solution that mixed for 5 min were heated for 5 min at the temperature of 140 °C, the cross-section of the corresponding nanowire was shown in Figure 3.4e, which was used to further explain the adsorption process. It can be clearly seen that there are many small particles scattered around the pentagon structure. The corresponding elemental map (Figure 3.4f-h) shows that, the nanoparticles are silver and, the pentagonal structure is copper, which further confirm the formation process of core-shell nanowires. We can conclude that at the beginning Ag-ammonia is distributed in solution. With the increase of stirring time, most of the complexes gradually adsorbed on CuNWs and core-shell structure was formed. Therefore, by the introduction of Ag-ammonia complex as silver source, Cu@Ag core-shell nanowires were obtained through a galvanic replacement free process.

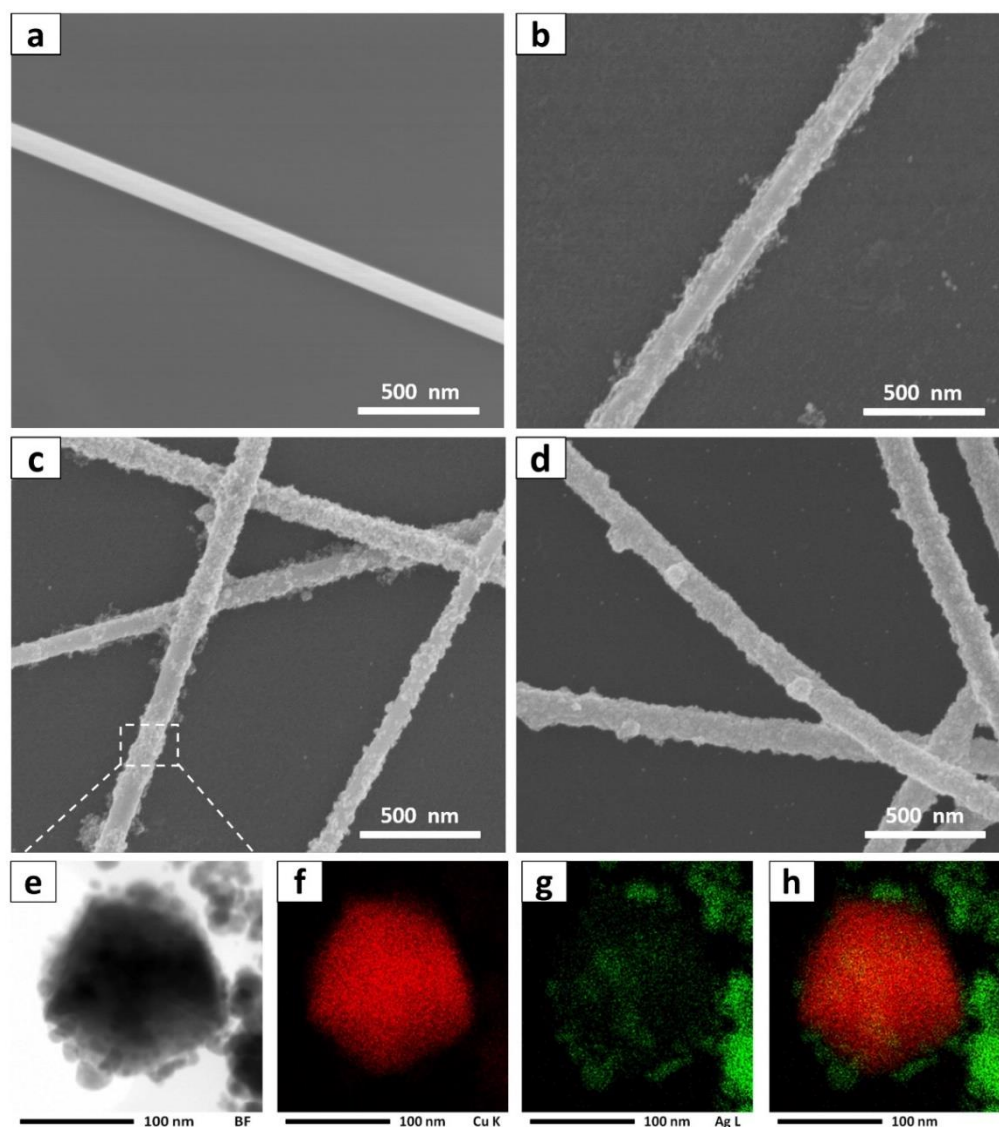


Figure 3.4 The growth process for the Cu@Ag-ammonia core-shell precursors. The SEM image of (a) pure CuNWs, the Cu@Ag-ammonia core-shell structure obtained with different stirring times: (b) 1 min, (c) 5 min and (d) 10 min. TEM image of the cross-section for (e) Cu@Ag nanowire, (f-h) the corresponding elemental mapping images, which obtained from the solution that mixed for 5 min. The silver is 20 wt% in complex inks.

3.3.2 Formation mechanism of core-shell structure

In order to analyze the adsorption process, atomistic molecular dynamics simulations are performed by Material Studio within a solution system including CuNWs, Ag-ammonia complex and IPA molecule. Figure 3.5a shows the adsorption process of

$[\text{Ag}(\text{NH}_2\text{CH}_2\text{CH}(\text{CH}_2\text{CH}_3)(\text{CH}_2)_3\text{CH}_3)_2]^+$ within 5 ps. It can be clearly seen that as the mixing time is extended, more Ag-ammonia is adsorbed onto the surface of CuNWs. At the same time, the evolution of energy over time in CuNWs and Ag-ammonia mixed solution are shown in Figure 3.5b and c. It can be clearly seen that when CuNWs and Ag-ammonia complex are mixed, the electrostatic energy and van der Waals energy in the solution are reduced by 3000 kcal/mol and 200 kcal/mol respectively, which is associated with the decrease of distance between CuNWs and Ag-ammonia complex.

Obviously, the electrostatic energy differences are greater than van der Waals energy differences, which indicates that the electrostatic energy is the dominant effect for adsorption process. Obviously, the change in electrostatic energy is larger than van der Waals energy, which indicates the dominant position of electrostatic energy in the adsorption process. In addition, total potential energy of the solution decreased at first and then remain stable after 10 ps, shows that the solution has reached a steady state after adsorption process. In practice, the adsorption process typically takes longer due to the large amounts of silver complex in the mixed solution. After that, in order to prove that the adsorption process could exist between CuNWs and other Ag-ammonia complex, we also simulate the adsorption process of $[\text{Ag}(\text{NH}_3)_2]^+$, as shown in Figure 3.5d. The same adsorption process can be observed with the increase of mixing time, which indicates that, the adsorption process can occur between CuNWs and other Ag-ammonia complex and form the core-shell precursors.

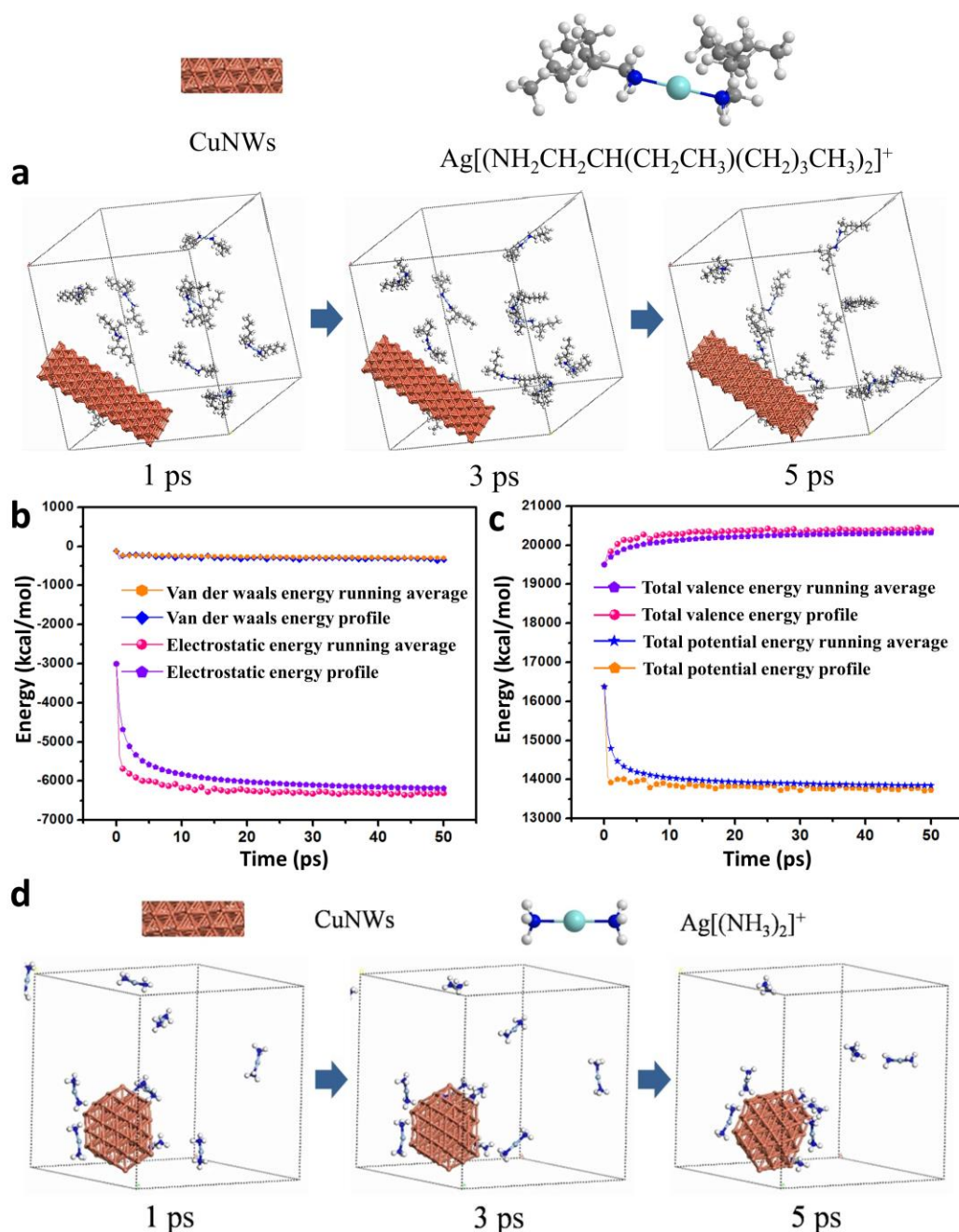


Figure 3.5 The adsorption process of (a) $\text{Ag}[(\text{NH}_2\text{CH}_2\text{CH}(\text{CH}_2\text{CH}_3)(\text{CH}_2)_3\text{CH}_3)_2]^+$ by atomistic molecular dynamics simulation. Time evolution of (b) electrostatic energy and van der Waals energy, (c) total valence energy and total potential energy of CuNWs and Ag-ammonia mixed solution. (d) The adsorption process of $\text{Ag}[(\text{NH}_3)_2]^+$ on the surface of CuNWs by atomistic molecular dynamics simulation.

The second step for the fabrication of Cu@Ag core-shell nanowires is thermal decomposition.

When Ag (I) β -ketocarboxylate and 2-ethylhexylamine are mixed together, an unstable Ag-ammonia complex ($[\text{Ag}(\text{NH}_2\text{CH}_2\text{CH}(\text{CH}_2\text{CH}_3)(\text{CH}_2)_3\text{CH}_3)_2]^+$) is formed. The appearance change of the mixed solution with time is shown in Figure 3.6. Initially, the Ag-ammonia complex ink was transparent without any color. The solution color changed from initial colorless to grayish after 20 minutes left at home temperature. The changes in color indicate the decomposition of Ag-ammonia complex ink [31-33]. XRD was introduced to demonstrate the complete decomposition of Ag-ammonia complex and other organic materials. Figure 3.7a shows the phase transition of Ag-ammonia complex under different annealing temperature. The diffraction signals at 34.1° , 39.1° , 43.3° , 48.9° , 53.9° , 60.9° all belong to the characteristic peaks of Ag_2NHCO_2 (JCPDS 28-1017). Therefore, we speculate that the Ag-ammonia complex decomposes into Ag_2NHCO_2 at room temperature. When increase the temperature to 60°C , the peaks of Ag (111), Ag (200), Ag (220), Ag (311) and Ag (222) appear. Further increase the temperature, the relative intensity of Ag peaks becomes much stronger while that of Ag_2NHCO_2 becomes weaker. When the temperature increase to 140°C , only the peaks of Ag can be seen, which means the complete decomposition of the Ag-ammonia complex. Cu@Ag-ammonia core-shell structure with different thickness of Ag-ammonia shell were treated at 140°C for 5 min, and the corresponding XRD patterns are shown in Figure 3.7b. With the increased amount of Ag-ammonia complex, the relative peak intensities of Ag were increased. There are no extra peaks observed, confirming the completely transformation of Cu@Ag-ammonia core-shell structure into Cu@Ag nanowires after heating, and no copper oxide is produced during this process. The XRD results illustrate that Cu@Ag core-shell nanowires can be easily obtained after a simple heating process without costly equipment and rigorous reaction conditions.

Combining the SEM results, dynamic simulation and XRD analysis results, we can conclude that the formation of Cu@Ag core-shell nanowire can be rationally expressed into three sequential steps: (1) When $\text{CH}_3\text{COCH}(\text{CH}_3)\text{COOAg}$ was added into $\text{CH}_3(\text{CH}_2)_3\text{CH}(\text{CH}_2\text{CH}_3)\text{CH}_2\text{NH}_2$ solution with a suitable molar ratio, floccular structured $[\text{Ag}(\text{NH}_2\text{CH}_2\text{CH}(\text{CH}_2\text{CH}_3)(\text{CH}_2)_3\text{CH}_3)_2]^+$ was formed after stirring. (2) Driven by electrostatic energy, the Ag-ammonia complex gradually

adsorbs onto CuNWs to form Cu@Ag-ammonia core-shell structure. (3) After heated at 140 °C for 5 min, Ag-ammonia complex shell decomposed to pure Ag shell, and Cu@Ag core-shell nanowires were obtained. Our method provides a new way to deposit Ag shell on CuNWs with a galvanic replacement free process.

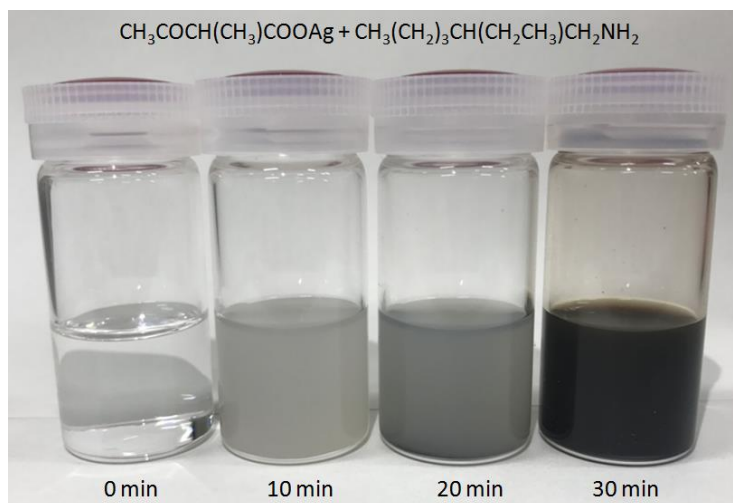


Figure 3.6 The appearance change of Ag (I) β -ketocarboxylate and 2-ethylhexylamine mixed solution at room temperature.

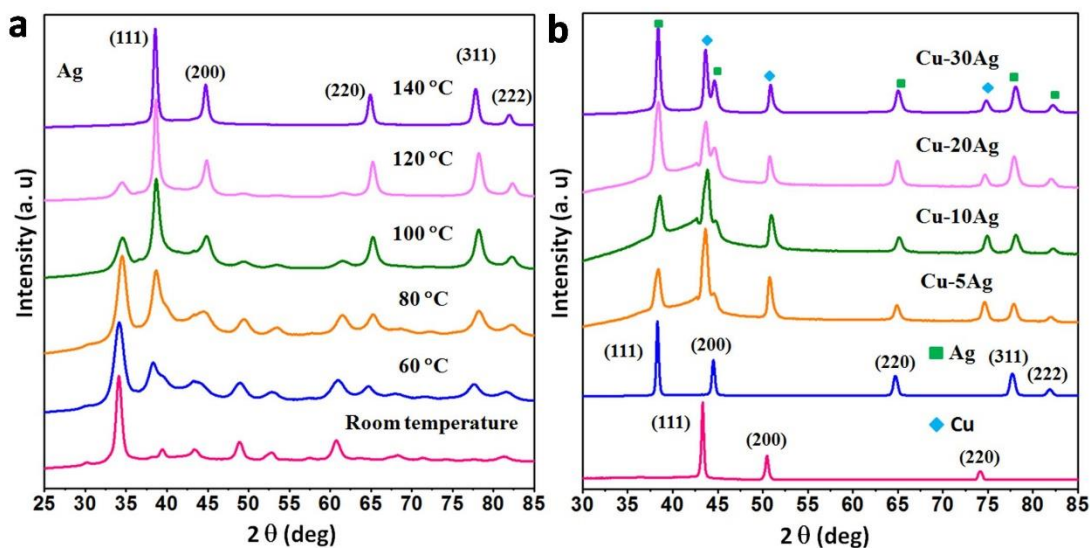


Figure 3.7 (a) XRD patterns of Ag-ammonia complex at different decomposition temperatures. (b) XRD patterns of the Cu@Ag core-shell nanowires with different amount of silver.

3.3.3 Stability and applications of core-shell nanowires based conductors

Figure 3.8a summarizes the relationship between sheet resistance and transmittance for

CuNWs conductor and Cu@Ag core-shell nanowire conductor with different thickness of silver shell. It is worth noting that, the Cu-5Ag nanowires exhibit similar properties to pure CuNWs, with no significant reduction in optical and electrical performance. Meanwhile, the transparency of Cu-20Ag and Cu-30Ag showed a slight decrease, which mainly due to the thicker Ag shell (10 nm or more).

The long-term stability is crucial for the practical application of the conductors. Therefore, we evaluated the ability of nanowires to maintain their original low resistance under high temperature and high humidity conditions (85 °C, 85% RH). The resistance evolution of the conductive ($T = 80\%$) made from CuNWs ($R_S = 32\ \Omega\ \text{sq}^{-1}$), Cu-5Ag ($R_S = 33\ \Omega\ \text{sq}^{-1}$), Cu-20Ag ($R_S = 31\ \Omega\ \text{sq}^{-1}$) and Cu-30Ag ($R_S = 37\ \Omega\ \text{sq}^{-1}$) core-shell nanowires in a harsh-environment was compared in Figure 3.8b. Not surprisingly, the unprotected CuNWs have the worst stability. The relative resistance (R/R_0 , R_0 is the original sheet resistance and R is the sheet resistance after oxidation) of CuNWs rapidly increases and almost no conductivity could be measured only after 10 h. Compared with CuNWs, the oxidation stability of the Cu-5%Ag nanowires has been improved. But after 100 h, the R/R_0 of the conductor increased more than 60 times, which mainly caused by incomplete coverage of the silver shell. Impressively, the R/R_0 for Cu-20Ag and Cu-30Ag only have a slight increase of 3.3 and 1.8 times even after 500 h, which also showed that the complete coverage of CuNWs surface can be realized when the amount of Ag is 20 wt %.

After that, we further evaluate the nanowires' stability toward high temperature. The evolution of relative resistance as a function of time for CuNWs and Cu@Ag core-shell nanowires conductors ($T = 80\%$) at 140 °C was shown in Figure 3.8c. The worst stability was observed in unprotected CuNWs, which almost lose the conductivity after 50 h. Although the stability of Cu-5%Ag nanowires was improved compared to pure CuNWs, its relative resistance increased nearly 70 times after 500 h. Cu-20%Ag and Cu-30%Ag nanowires conductors have the same level of conductivity, both of them undoubtedly exhibit improved thermal stability. The R/R_0 of Cu-20Ag and Cu-30Ag increased by 4 and 1.6 times, respectively after exposed to high temperature for 700 h. The presence of silver shells greatly improves the thermal stability of the Cu@Ag core-shell

nanowires.

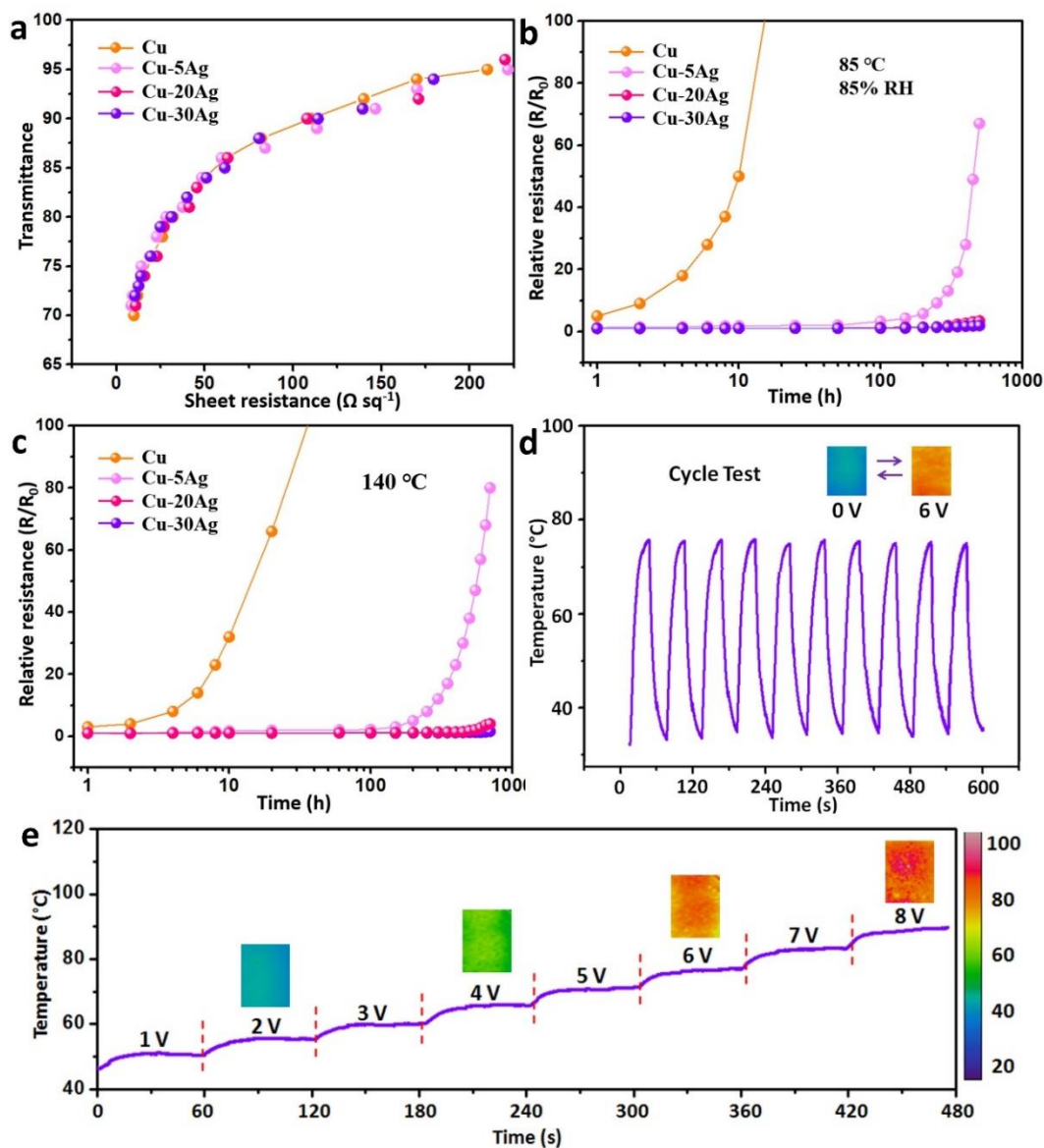


Figure 3.8 (a) Transmittance versus the sheet resistance of transparent conductors made from CuNWs, Cu-5Ag, Cu-20Ag and Cu-30Ag. Stability of transparent conductors ($T = 80\%$) in (b) standard harsh condition (85 °C, 85% RH) and (c) high temperature environment (140 °C). (d) On/off responses of transparent conductive heater (Cu-20Ag, $T = 80\%$) with the applied voltage of 6 V. (e) The temperature changes of the heater with the applied voltage changed from 1V to 8V, as well as the corresponding infrared images.

In order to demonstrate the performance of our Cu@Ag core-shell nanowires, a stretchable heater was fabricated. The two ends of the Cu-20Ag based heater ($T = 80\%$) were added with

voltage to obtain the Joule heat. As shown in Figure 3.8d, the temperature of the stretchable conductor remains stable after 10 cycles of opening and closing the high input voltage of 6 V. The variety of the temperature with input voltage for the Cu@Ag nanowires based heater is shown in Figure 6e. Due to the high thermal stability of the core-shell nanowire, a uniform temperature distribution was observed in the heaters that under different input energies. At the same time, when the input voltage is increased from 1 V to 8 V, the temperature of the heater rises rapidly and reaches stability, which showing a rapid temperature response.

3.4 Conclusions

In summary, to overcome the poor stability of CuNWs-based conductors, Cu@Ag core-shell nanowires with tunable thickness of silver shell could be obtained through a facile adsorption and decomposition process. The introduced Ag-ammonia complex can be adsorbed on the surface of CuNWs to form Cu@Ag-ammonia core-shell structure. After a low temperature heating process in air, silver complex was decomposed into pure silver shell. The use of Ag-ammonia complex as silver source could avoid the galvanic replacement that is encountered in traditional synthesis methods. The synthesis process and mechanism of adsorption and decomposition process are discussed in details. In addition, owing to the protection of silver shell, as-prepared Cu@Ag core-shell nanowires show excellent stability for at least 500 h at both high temperatures (140 °C) and standard harsh environment (85 °C, 85 % RH), which could be used in next-generation of stretchable transparent conductors.

References

- [1] Cheng, Y.; Wang, S.; Wang, R.; Sun, J.; Gao, L. Copper Nanowire Based Transparent Conductive Films with High Stability and Superior Stretchability. *J. Mater. Chem. C* **2014**, *2*, 5309-5316.
- [2] Zhu, Z.; Mankowski, T.; Balakrishnan, K.; Shikoh, A. S.; Touati, F.; Benammar, M. A.; Mansuripur, M.; Falco, C. M. Ultrahigh Aspect Ratio Copper-Nanowire-Based Hybrid

- Transparent Conductive Electrodes with PEDOT:PSS and Reduced Graphene Oxide Exhibiting Reduced Surface Roughness and Improved Stability. *ACS Appl. Mater. Interfaces* **2015**, *7*, 16223-16230.
- [3] Spain, E.; Mccooney, A.; Dolan, C.; Bagshaw, H.; Leddy, N.; Keyes, T. E.; Forster, R. J. Electrodeposited Gold-Copper Core-Shell Nanowires for High Sensitivity DNA Detection. *Analyst* **2014**, *139*, 5504-5508.
- [4] Guo, H.; Jin, J.; Chen, Y.; Liu, X.; Zeng, D.; Wang, L.; Peng, D. L. Controllable Synthesis of Cu-Ni Core-Shell Nanoparticles and Nanowires with Tunable Magnetic Properties. *Chem. Commun.* **2016**, *52*, 6918-6921.
- [5] Liu, Y.; Liu, Z.; Lu, N.; Preiss, E.; Poyraz, S.; Kim, M. J.; Zhang, X. Facile Synthesis of Polypyrrole Coated Copper Nanowires: A New Concept to Engineered Core-Shell Structures. *Chem. Commun.* **2012**, *48*, 2621-2623.
- [6] Kim, K. H.; Kim, J. Y.; Kim, K. B. Synthesis of Manganese Dioxide/Poly(3,4-Ethylenedioxythiophene) Core/Sheath Nanowires by Galvanic Displacement Reaction. *J. Electroceram.* **2012**, *29*, 149-154.
- [7] Im, H. G.; Jung, S. H.; Jin, J.; Lee, D.; Lee, J.; Lee, D.; Lee, J. Y.; Kim, I. D.; Bae, B. S. Flexible Transparent Conducting Hybrid Film Using a Surface-Embedded Copper Nanowire Network: A Highly Oxidation-Resistant Copper Nanowire Electrode for Flexible Optoelectronics. *Acs Nano* **2014**, *8*, 10973-10979.
- [8] Niu, Z.; Cui, F.; Yu, Y.; Becknell, N.; Sun, Y.; Khanarian, G.; Kin, D.; Dou L.; Dehestani, A.; Schierle-Arndt, K.; Yang, P. Ultrathin Epitaxial Cu@Au Core-Shell Nanowires for Stable Transparent Conductors. *J. Am. Chem. Soc.* **2017**, *139*, 7348-7354.
- [9] Guo, H.; Chen, Y.; Ping, H.; Jin, J.; Peng, D. L. Facile Synthesis of Cu and Cu@Cu-Ni Nanocubes and Nanowires in Hydrophobic Solution in The Presence of Nickel and Chloride Ions. *Nanoscale* **2013**, *5*, 2394-2402.
- [10] Ding, S.; Jiu, J.; Gao, Y.; Tian, Y.; Araki, T.; Sugahara, T.; Nagao, S.; Nogi, M.; Koga, H.; Suganuma, K.; Uchida, H. One-Step Fabrication of Stretchable Copper Nanowire Conductors

- by A Fast Photonic Sintering Technique and Its Application in Wearable Devices. *ACS Appl. Mater. Interfaces* **2016**, *8*, 6190-6199.
- [11] Yang, M.; Hood, Z. D.; Yang, X.; Chi, M.; Xia, Y. Facile Synthesis of Ag@Au Core-Sheath Nanowires with Greatly Improved Stability Against Oxidation. *Chem. Commun.* **2017**, *53*, 1965-1968.
- [12] Mckiernan, M.; Zeng, J.; Ferdous, S.; Verhaverbeke, S.; Leschkies, K. S.; Gouk, R.; Lazik, C.; Jin, M.; Briseno, A. L.; Xia, Y. Facile Synthesis of Bimetallic Ag/Ni Core/Sheath Nanowires and Their Magnetic and Electrical Properties. *Small* **2010**, *6*, 1927-1934.
- [13] Zhu, J. Surface Plasmon Resonance from Bimetallic Interface in Au–Ag Core–Shell Structure Nanowires. *Nanoscale Res. Lett.* **2009**, *4*, 977-981.
- [14] Yao, S.; Li, B.; Jing, M.; Tang, H.; Wu, X.; Hou, J.; Shen, X. Tunable Synthesis, Characterization and Magnetic Properties of Core–Shell Cu@M (M = Co or Ni) Nanowires. *J Nanosci Nanotechnol* **2017**, *17*, 661-665.
- [15] Chen, J.; Chen, J.; Li, Y.; Zhou, W.; Feng, X.; Huang, Q.; Zheng, J. G.; Liu, R.; Ma, Y.; Huang, W. Enhanced Oxidation-Resistant Cu-Ni Core-Shell Nanowires: Controllable One-Pot Synthesis and Solution Processing to Transparent Flexible Heaters. *Nanoscale*. **2015**, *7*, 16874-16879.
- [16] Yang, Y.; Ding, S.; Araki, T.; Jiu, J.; Sugahara, T.; Wang, J.; Vanfleteren, J.; Sekitani, T.; Suganuma, K. Facile Fabrication of Stretchable Ag Nanowire/Polyurethane Electrodes Using High Intensity Pulsed Light. *Nano Res.* **2016**, *9*, 401-414.
- [17] Hu, L.; Han, S. K.; Lee, J. Y.; Peumans, P.; Cui, Y. Scalable Coating and Properties of Transparent, Flexible, Silver Nanowire Electrodes. *Acs Nano* **2010**, *4*, 2955-2963.
- [18] Amjadi, M.; Pichitpajongkit, A.; Lee, S.; Ryu, S.; Park, I. Highly Stretchable and Sensitive Strain Sensor Based on Silver Nanowire-Elastomer Nanocomposite. *Acs Nano* **2014**, *8*, 5154-5163.
- [19] Hong, W.; Wang, J.; Wang, E. Dendritic Au/Pt and Au/PtCu Nanowires with Enhanced Electrocatalytic Activity for Methanol Electrooxidation. *Small* **2014**, *10*, 3262-3265.

- [20] Guo, H.; Jin, J.; Chen, Y.; Liu, X.; Zeng, D.; Wang, L.; Peng, D. L. Controllable Synthesis of Cu-Ni Core-Shell Nanoparticles and Nanowires with Tunable Magnetic Properties. *Chem. Commun.* **2016**, 52, 6918-6921.
- [21] Stewart, I. E.; Ye, S.; Chen, Z.; Flowers, P. F.; Wiley, B. J. Synthesis of Cu-Ag, Cu-Au, and Cu-Pt Core-Shell Nanowires and Their Use in Transparent Conducting Films. *Chem. Mater.* **2015**, 27, 7788-7794.
- [22] Zeng, D.; Chen, Y.; Lu, A.; Li, M.; Guo, H.; Wang, J.; Peng, D. L. Injection Synthesis of Ni-Cu@Au-Cu Nanowires with Tunable Magnetic and Plasmonic Properties. *Chem. Commun.* **2013**, 49, 11545-11547.
- [23] Xia, X.; Wang, Y.; Ruditskiy, A.; Xia, Y. ChemInform Abstract: 25th Anniversary Article: Galvanic Replacement: A Simple and Versatile Route to Hollow Nanostructures with Tunable and Well-Controlled Properties. *Adv. Mater.* **2013**, 25, 6313-6333.
- [24] Lu, X.; Chen, J.; Skrabalak, S. E.; Xia, Y. Galvanic Replacement Reaction: A Simple and Powerful Route to Hollow and Porous Metal Nanostructures. *Proc. Inst. Mec. Eng., Part N.* **2008**, 221, 1-16.
- [25] Au, L.; Lu, X.; Xia, Y. A Comparative Study of Galvanic Replacement Reactions Involving Ag Nanocubes and AuCl_2^- or AuCl_4^- . *Adv. Mater.* **2010**, 20, 2517-2522.
- [26] Ojani, R.; Raoof, J. B.; Hasheminejad, E. One-step Electroless Deposition of Pd/Pt Bimetallic Microstructures by Galvanic Replacement on Copper Substrate and Investigation of Its Performance for The Hydrogen Evolution Reaction. *Int. J. Hydrogen Energy* **2013**, 38, 92-99.
- [27] Rezaei, B.; Mokhtarianpour, M.; Ensafi, A. A. Fabricated of Bimetallic Pd/Pt Nanostructure Deposited on Copper Nanofoam Substrate by Galvanic Replacement as An Effective Electrocatalyst for Hydrogen Evolution Reaction. *Int. J. Hydrogen Energy* **2015**, 40, 6754-6762.
- [28] Yang, C.; Zhang, Q. B.; Abbott, A. P. Facile Fabrication of Nickel Nanostructures on A Copper-Based Template Via A Galvanic Replacement Reaction in A Deep Eutectic Solvent.

Electrochem. Commun. **2016**, *70*, 60-64.

- [29] Sanedrin, R. G.; Georganopoulou, D. G.; Park, S.; Mirkin, C. A. Seed-Mediated Growth of Bimetallic Prisms. *Adv. Mater.* **2010**, *17*, 1027-1031.
- [30] Yang, Y.; Liu, J.; Fu, Z. W.; Qin, D. Galvanic Replacement-Free Deposition of Au on Ag for Core-Shell Nanocubes with Enhanced Chemical Stability and SERS Activity. *J. Am. Chem. Soc.* **2014**, *136*, 8153-8156.
- [31] Li, W.; Hu, D.; Li, L.; Li, C. F.; Jiu, J.; Chen, C.; Ishina, T.; Sugahara, T.; Suganuma, K. Printable and Flexible Copper-Silver Alloy Electrodes with High Conductivity and Ultrahigh Oxidation Resistance. *ACS Appl. Mater. Interfaces* **2017**, *9*, 24711-24721.
- [32] Li, W.; Li, C. F.; Lang, F.; Jiu, J.; Ueshima, M.; Wang, H.; Liu, Z. Q.; Suganuma, K. Self-Catalyzed Copper-Silver Complex Inks for Low-Cost Fabrication of Highly Oxidation-Resistant and Conductive Copper-Silver Hybrid Tracks at A Low Temperature Below 100 °C. *Nanoscale* **2018**, *10*, 5254-5263.
- [33] Hatamura, M.; Yamaguchi, S.; Takane, S. Y.; Chen, Y.; Suganuma, K. Decarboxylation and Simultaneous Reduction of Silver(I) β -Ketocarboxylates with Three Types of Coordinations. *Dalton Trans.* **2015**, *44*, 1-15.

Chapter 4

Alloying and embedding of Cu-core/Ag-shell nanowires

4.1 Introduction

Considerable researches have been devoted to enhance the oxidation resistance whilst maintain the high electrical conductivity of CuNWs. Two main methods have recently been proposed to achieve CuNWs with high stability. One of the methods is to encapsulate or embed CuNWs into plastic substrates to achieve a composite structure [1-3]. For example, through in situ photo-polymerization, the CuNW network was transferred from a glass substrate to an elastic poly(acrylate) matrix and formed the partly embedded structure. No decrease in conductivity was observed in the corresponding composite electrode after 50 days under room condition (27 °C, 40% RH) [4]. In addition, by coating the liquid polyurethane (PU) precursor on the surface of CuNW networks, a CuNWs/PU composite electrode was successfully achieved, which can be reversibly stretched up to 60% strain without much loss of rubbery elasticity or electrical conductivity [5]. However, the complex and time-consuming transfer step greatly increase the fabrication cost.

The formation of a core-shell structure that encapsulates Cu with an inert shell is another approach [6-10]. For example, Cu@Au core-shell nanowires with enhanced resistance to heat (80 °C), humidity (80% relative humidity(RH)) and air for at least 700 h have been synthesized by a galvanic replacement free process [10]. In addition, a thin Ag shell was electroless deposited on CuNWs to confer oxidation resistance and conductivity. The resulting Cu@Ag core-shell nanowires were resistant to oxidation in high temperature (160 °C) and under humid conditions (85 °C, 85% RH) for 24 h [11]. However, such core-shell structures have some unavoidable disadvantages. For example, the loose and irregular accumulation of metal-shell is unable to completely obstruct the inward diffusion of O₂. The rapid reaction of Cu and O₂ tends to form an oxide layer between the Cu-core and metal-shell, resulting in high resistance [12-14]. Alloy nanowires with dense shell and strong interface between core and shell are expected to be the ideal solution to this problem [15-17].

In the present work, transparent (T) electrodes with dense Cu@Ag alloy (A) nanowires embedded (E) in the surface layer of stretchable substrates (TAE electrodes) were successfully fabricated by processing Cu@Ag core-shell nanowires/PU electrodes with a high-intensity pulsed light (HIPL) technique. The light energy absorbed by loose Cu@Ag core-shell nanowires drives the rapid diffusion between the Cu core and Ag shell, enabling the formation of dense Cu@Ag alloy nanowires. At the same time, the light improves the adhesion between wires and substrates, resulting in an embedded structure. The combination of dense alloy nanowires and embedded structures enable TAE electrodes to have ultra-high thermal stability, which maintain high conductivity at high temperature (140 °C) and high humidity (85 °C, 85% RH) up to 500 h. A stretchable and transparent heater was fabricated based on the TAE electrode, which exhibits uniform temperature distribution and high thermal stability due to the alloy nanowires and embedded structures.

4.2 Experiment section

4.2.1 Fabrication of TAE electrodes

Anhydrous copper dichloride (CuCl_2), octadecylamine ($\text{C}_{18}\text{H}_{39}\text{N}$, ODA), glucose ($\text{C}_6\text{H}_{12}\text{O}_6$), chloroform (CHCl_3), 2-ethylhexylamine ($\text{C}_8\text{H}_{19}\text{N}$) and isopropanol ($\text{C}_3\text{H}_8\text{O}$, IPA) were purchased from Wako Chemicals Industries, Ltd. Ag (I) β -ketocarboxylate ($\text{C}_5\text{O}_3\text{H}_7\text{Ag}$) was provided by Toppan Forms Co., Ltd. Polyurethane (PU) substrate was obtained from Takeda Sangyo Co., Ltd. All reagents were analytical grade and used without further purification.

Firstly, CuNWs were prepared via a hydrothermal method [18]. In a typical procedure, CuCl_2 , glucose, and ODA with a molar ratio of 1:1:6 were mixed in water and stirred continuously for 2 hours. Then the feedstock was transferred into a 50 mL capacity Teflon-lined autoclave and heated at 120 °C for 24 h. When the autoclave was cooled to room temperature, the product was collected by centrifugation, washed three times with water, chloroform, and isopropanol respectively. After that, the obtained CuNWs were dispersed in IPA.

Ag (I) β -ketocarboxylate was mixed with 2-ethylhexylamine solvent with a molar ratio of 1:2

to form Ag-amine complex solution. Then, the freshly prepared CuNWs and Ag-amine complex were mixed together with a molar ratio of 1: 8.3, which was sprayed onto the PU substrates using a nozzle powered by an air compressor to form the film. After that, the fabricated films were heated to a temperature of 140 °C for 5 min to form Cu@Ag core-shell nanowires with Ag content of 20 wt.% Cu, and then exposed to HIPL to form Cu@Ag alloy nanowires with embedded structures.

4.2.2 Characterization

The crystalline nature and phase structures of the samples were characterized by powder X-ray diffraction (XRD, Rigaku Smart Lab, Rigaku). The morphologies, components, and structures of the samples were observed by field-emission scanning electron microscopy (FE-SEM, Hitachi SU8020, Hitachi) that equipped with energy dispersive spectroscopy (EDS). The electrical resistivity of the sample was measured by four probe analyzer (LorestaGP T610, Mitsubishi Chemical Analytech Co. Ltd.). To evaluate the thermal stability in static occasions, two ends of the heaters were fixed tightly on a desk-top universal testing machine, and two electrically conductive clips were connected to the stretchable heaters to supply a constant voltage. The temperature evolutions on the surface of the heater under different applied voltages were recorded using an infrared (IR) camera (R500EX, NIPPON AVIONICS, sensitivity: 0.025°C). The photonic sintering system used in this study is the PulseForge 3300 (Novacentrix, Austin, TX) that features a broadband emission range from 200 to 1500 nm. The water-cooled xenon lamp, located 10 mm from the substrate stage, can vary the optical energy as a function of the electrical voltage and duration time. All of the measurements were performed at room temperature.

4.3 Result and discussion

4.3.1 Resistance and transparent evolution

Figure 4.1a schematically illustrates the fabrication process of TAE electrodes and highlights the structural changes during each step. As described in the previous work, uniform Cu@Ag-amine core-shell structures can be obtained by mixing CuNWs and Ag-amine complex and randomly being distributed on the surface of PU substrates through a spray coating process [18]. After a

simple heating treatment at 140 °C, Cu@Ag core-shell nanowires with a rough and loose surface are achieved on the surface of PU substrates. Finally, by processing Cu@Ag core-shell nanowires/PU electrodes with a controllable high-intensity pulsed light (HIPL) technique, TAE electrodes are obtained with denser and smoother Cu@Ag alloy nanowires embedded in the surface layer of PU substrates. Since the entire process is solution-processed in the air, TAE electrodes with a large size (15 cm × 15 cm) can be fabricated easily (Figure 4.1b and c). The TAE electrode can maintain high transmittance before and during the stretching process. In addition, the mechanical properties of TAE electrodes and pure PU substrates were measured (Figure 4.1d). The TAE electrodes exhibit similar stretchability to that of pure PU substrates, indicating that the fabrication process does not change the mechanical property of the original substrates, which facilitates their applications in next-generation stretchable and wearable electronic devices.

Cu@Ag core-shell nanowire/PU electrodes with transmittance of 78% (Group A) and 89% (Group B) were treated with light energies of 0.8, 1.6, 2.4, 3.2, 4.0, and 4.8 J/cm², respectively, to investigate the relationship between the sheet resistance (SR) and the input energy (Figure 4.2a). It is found that as the input energy increases, the SR of both samples decreases rapidly, and then becomes stable. For example, prior to light treatment, the SR of Group B is around 80 Ω/sq, which decreases to 35 Ω/sq with the light energy of 3.2 J/cm². Further increase the light energy to 4.0 J/cm² and 4.8 J/cm², the SR of the samples remains stable without further reduction. Thus, in order to obtain highly conductive TAE electrodes, the light energy of 3.2 J/cm² is enough in the study. In addition, the transmittance of the samples is kept almost unchanged during this process, which is very beneficial for achieving highly transparent electrodes. Besides, it is found that the transmittance of the samples become higher under a strain such as 30% because the relative density of nanowires on the substrate decreases during the stretching process (Figure 4.3a).

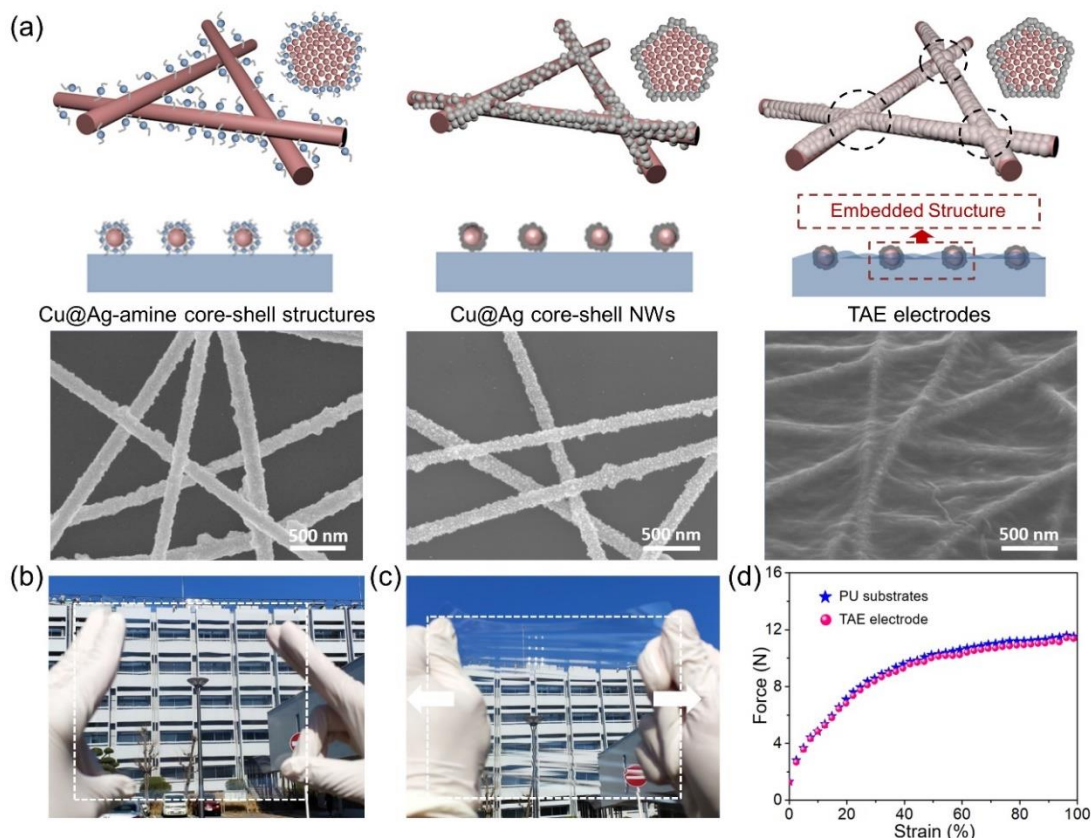


Figure 4.1 (a) Schematic of the fabrication process of TAE electrodes and corresponding SEM images of the products for each step: Cu@Ag-amine core-shell structures, Cu@Ag core-shell nanowires, and TAE electrodes. Optical images of the large-size TAE electrode before (b) and during (c) the stretching. (d) Typical force-strain curves of pure PU substrates and TAE electrodes.

The microstructures of Cu@Ag core-shell nanowires/PU electrodes ($T = 89\%$, Group B) under different input energies were investigated to support their SR evolution. As shown in Figure 4.2b, when treated with lower energy of 0.8 J/cm^2 , nanowires are randomly distributed on the surface of PU, and no obvious junctions exist between nanowires, which is consistent to the high resistance of $57 \text{ } \Omega/\text{sq}$. After treated with the higher energy of 2.4 J/cm^2 , the Cu@Ag nanowires are connected with each other and strong adhesion is formed between wires and the PU substrate (Figure 4.2c); therefore, the corresponding SR is reduced to $42 \text{ } \Omega/\text{sq}$. Further increasing the input energy to 3.2 J/cm^2 results in the minimum SR of $35 \text{ } \Omega/\text{sq}$. Also, under this situation, most of the nanowires are buried into the surface layer of the PU substrate, forming the embedded structure (Figure 4.2d). When Cu@Ag core-shell nanowire/PU electrodes are exposed to HIPL, the light

energy absorbed by nanowires transformed into thermal energy, which induces the welding between nanowires and produces high conductivity. At the same time, due to the high thermal conductivity of Cu@Ag nanowires, the heat instantaneously transmits to the PU substrate and softens the surface of the PU substrate, leading to the embedded structure [20, 21]. In addition, the evolution of surface roughness for Cu@Ag core-shell nanowires/PU electrodes ($T = 89\%$, Group B) under different light energy was measured (Figure 4.3b). The surface roughness of the original electrodes is around $0.89 \mu\text{m}$. With the increase of light energy from 0.8 , 2.4 to 3.2 J/cm^2 , the surface roughness is reduced to about 0.86 , 0.82 and $0.79 \mu\text{m}$, respectively. The evolution of the roughness indicates that the roughness of the patterns has been improved after HIPL process, which is consistent with the SEM results. Therefore, highly conductive and transparent Cu@Ag nanowire electrodes with embedded structures can be achieved easily.

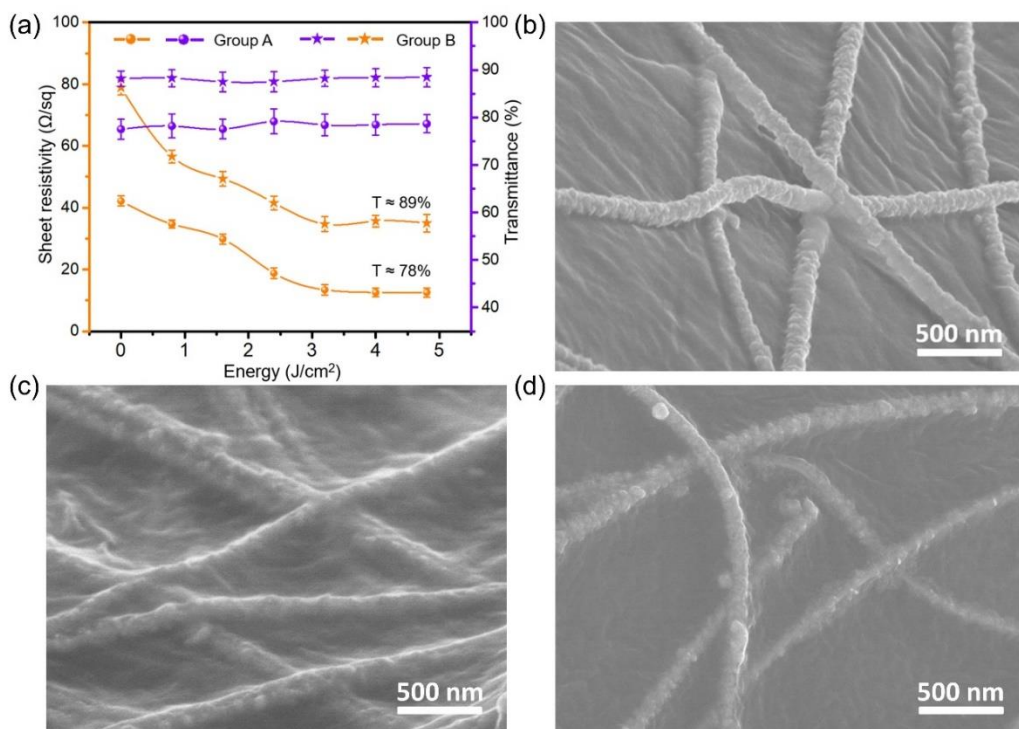


Figure 4.2 Resistance evolution and top-view images of Cu@Ag nanowires/PU electrodes as a function of supplied energies for HIPL process. (a) Resistance and transparent changes of Cu@Ag nanowires/PU electrodes treated with different light energy. SEM images of Cu@Ag networks on PU substrates treated with light energy of (b) 0.8 J/cm^2 , (c) 2.4 J/cm^2 , and (d) 3.2 J/cm^2 .

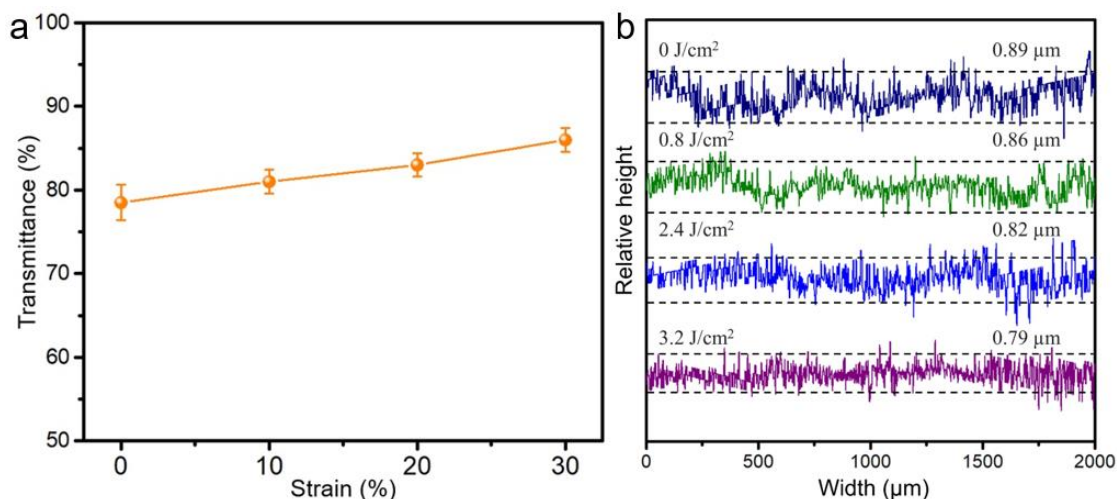


Figure 4.3 (a) The evolution of transmittance of the samples under different strain. (b) The surface roughness evolution of the Cu@Ag core-shell nanowires/PU electrodes ($T = 89\%$) that treated with the light energy of 0, 0.8, 2.4 to 3.2 J/cm².

4.3.2 Surface morphology and crystal structure evolution

The close-up SEM images in Figure 4.4a-c show the surface evolution of Cu@Ag core-shell nanowires with different input energies. The nanowires are placed on a silicon plate to avoid the formation of embedded structures on PU substrate. Prior to the HIPL treatment, the newly formed Ag nanoparticles cover the entire surface of the CuNWs. The Ag nanoparticles are relatively small and have clear boundaries with each other (Figure 4.4a). After treated with a low energy of 1.6 J/cm², the Ag nanoparticles are connected with each other and some large grains are formed as shown in Figure 4.4b. With the further increase of energy to 3.2 J/cm², the nanoparticles and CuNWs seem to be fused into an integral structure and the surface of the nanowires becomes denser and smoother (Figure 4.4c). The composition of the Cu@Ag nanowire that treated with light energy of 3.2 J/cm² was testified by energy dispersive spectroscopy (EDS) mapping. As shown in Figures 4.4d-f, Cu is mainly distributed in the center zone, while Ag is distributed at the edges, confirming the Cu@Ag core-shell structure.

The crystal structure of the Cu@Ag nanowires under different light energies was measured by X-ray diffraction (XRD) (Figure 4.4g). The corresponding lines for pure Cu and pure Ag are obtained from the JCPDS file number 85-1326 and 65-2871, respectively. All of the patterns

exhibit same diffraction peaks that can be indexed as (111), (200) and (220) planes of the face-centered cubic Cu and Ag crystal, which indicates that the obtained electrodes have high metallic purity without any oxides even though the whole experimental process is conducted in air. It is worth noting that, the diffraction peaks of the Cu@Ag nanowires exhibit a shift with the increase of input light energy. The peak of Ag (111) moves from the original 38.16° to the right 38.6° , while the Cu (111) peak of 43.34° shifts to the left of 43.05° (Figure 4.5a). Pure AgNW and CuNW electrodes were prepared and treated with light energy of 4.8 J/cm^2 for comparison. As shown in Figure 4.5b and c, no peak shift is observed. Therefore, these results suggest that the peak shifts are because of the formation of solid solution alloy nanowire rather than the residual stress in the electrodes [22, 23].

Since Cu and Ag have the same face-centered cubic structure and the relative atomic radius ratio between Ag and Cu is 11.1 pct, Cu@Ag alloy is a substitutional solid solution [24]. Herein, the interplanar spacing change of Ag (111) and Cu (111) were collected as shown in Figure 4.5d. It can be seen that the lattice of the Ag phase is compressed from 2.3493 \AA to 2.3128 \AA , while the lattice of the Cu phase is enlarged from 2.0862 \AA to 2.1008 \AA , which is due to the atomic radii difference between Cu (0.1278 nm) and Ag (0.1444 nm) [23]. The variation trend of the interplanar spacing further confirms the formation of Cu@Ag alloy nanowires. On the basis of average lattice constants obtained from the (111), (200), and (220) diffraction peaks of Ag and Cu phases, the solid solubilities of Cu into Ag and Ag into Cu were further estimated by Vegard's law (eq 1):

$$x = \frac{a - a_1}{a_2 - a_1} \times 100 \quad (1)$$

Where a is the lattice parameter of the alloy, a_1 is the lattice parameter of the solvent, a_2 is the lattice parameter of the solute, and x is the metastable solid solubility of the alloy. As shown in Figure 4.4h, with the increase of the light energy, the solubilities of Ag in Cu and Cu in Ag increase rapidly and finally reach saturation values of about 4.2 at. % and 12.2 at. %, respectively. The solubility shows that, during the HIPL process, Ag atoms randomly replace Cu atoms and vice versa, and alternate Ag- and Cu-rich domains are created. Always, the solid solubility limit of Ag in Cu or Cu in Ag is lower than 2.0 at. % at room temperature [14]. Cu@Ag alloy nanowires with

high solid solubility are obtained because the HIPL process produces extremely high heat in extremely short time, which drives the effective interdiffusion between Cu core and Ag shell and realizes the sintering of them [17]. Combining the above results, the HIPL process not only forms embedded structures but also produces dense Cu@Ag alloy nanowires with a high solid solubility.

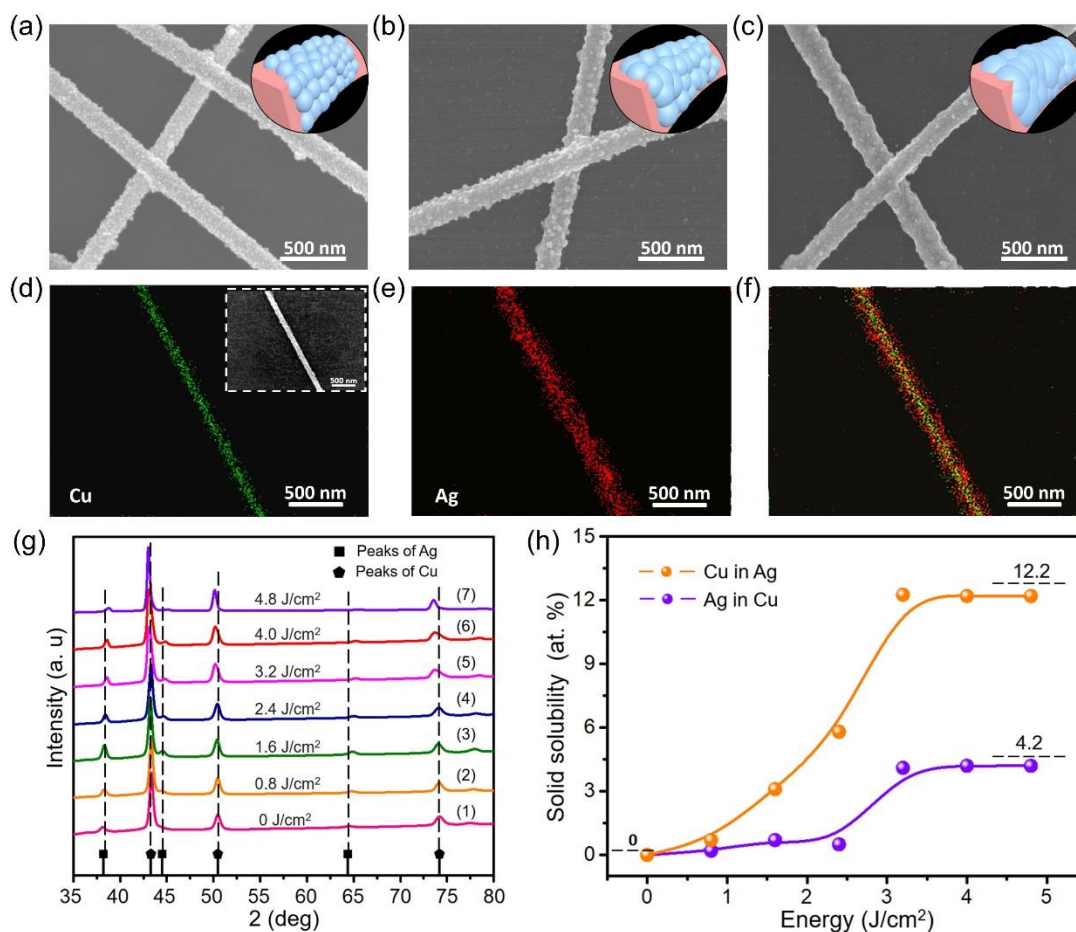


Figure 4.4 The evolutions of surface morphology and crystal structure of Cu@Ag nanowire electrodes treated with different light energies. SEM images of the surface transformation for Cu@Ag nanowires treated with energies of (a) 0 J/cm², (b) 1.6 J/cm², (c) 3.2 J/cm². (d-f) The EDS mapping images of Cu@Ag alloy nanowires. (g) XRD patterns of Cu@Ag nanowires after HIPL process with different energies. (h) The solid solubility changes of Cu in Ag and Ag in Cu.

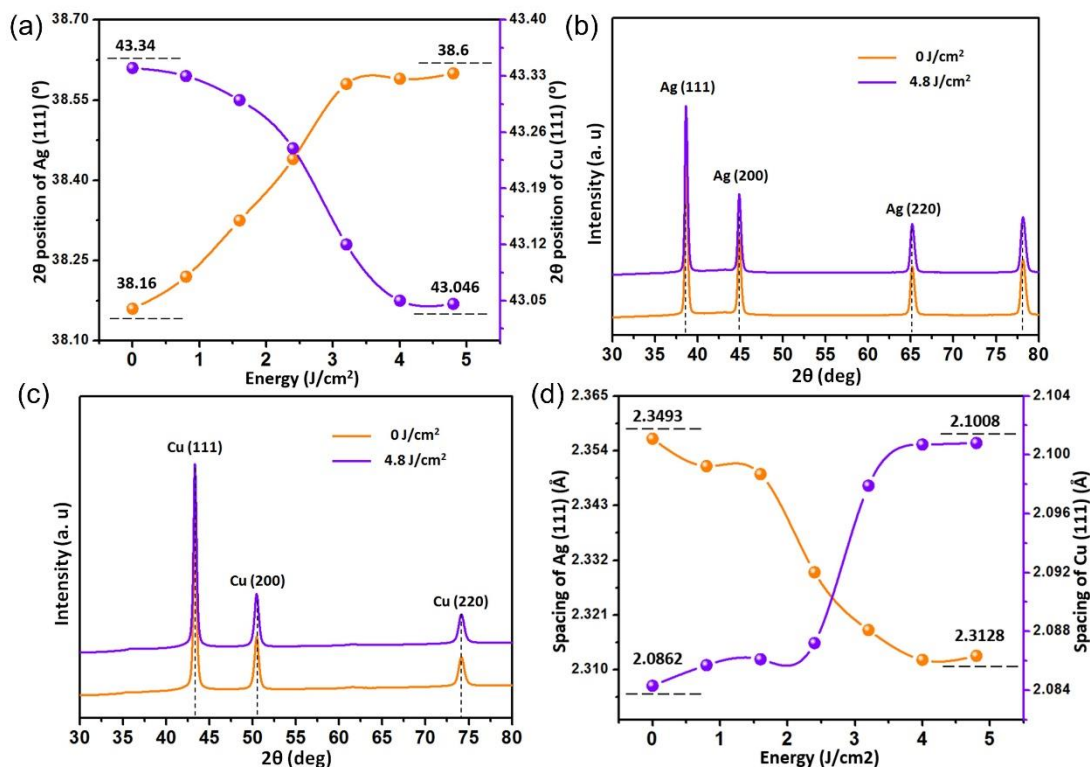


Figure 4.5 (a) The shift tendency of 2θ positions of Ag(111) and Cu(111) diffraction peaks as the input light energy increases. XRD patterns of (b) pure Ag electrode and (c) pure Cu electrode after HIPL process using the light energy of 4.1 J/cm^2 . (d) Spacing changes of Ag (111) and Cu (111) diffraction directions with different input energy.

4.3.3 Thermal stability and application of TAE electrodes

Remarkable stability under various environments and outstanding mechanical robustness against stretching are essential prerequisites for applications of TAE electrodes in wearable electronics. Figure 4.6a compares the thermal stability of TAE electrodes with CuNW electrodes, Cu@Ag core-shell NW electrodes, and representative electrodes from previous studies [25-27]. The relative resistance (R/R_0 , R_0 is the original resistance of electrodes and R is the resistance after the aging test) of the TAE electrodes exhibits more stable than CuNW electrodes, Cu@Ag core-shell NW electrodes and most previously reported electrodes, even though they are exposed to the more harsh condition (85°C , 85% RH). The high thermal stability of TAE electrodes is attributed to the combination of the dense alloy nanowire and the embedded structure, which hinders the inward diffusion of O_2 and greatly decreases the contact between Cu and O_2 . The corresponding

microstructure evolutions of CuNWs electrodes and TAE electrodes were observed (Figure 4.7). It can be clearly seen that, after ageing test for 10 h, the entire surface of the CuNWs become rough (Figure 4.7a). As the time increases to 50 h, the breakage of CuNWs is observed and some irregular particles appear (Figure 4.7b), which is likely because of the oxidation of Cu [28]. In contrast, the surface of TAE electrodes is kept almost unchanged (Figure 4.7c, d). In addition, the stability of the TAE electrodes at high temperature of 140 °C was further explored. As shown in Figure 4.6b, TAE electrodes show the highest stability again because of the combination effects of the alloy nanowire and the embedded structure.

Additionally, some mechanical tests were conducted to evaluate the electro-mechanical stability of the TAE electrodes. Figure 4.6c compares the R/R_0 variation of different electrodes under tensile strain up to 80%. It is found that the R/R_0 of electrodes fabricated from CuNWs and core-shell nanowires exhibit a rapid increase to about 25 at 80% strain, while that of TAE electrodes undergo a much smaller increase to only 6. The cyclic stretching-relaxation test at 30% strain was also conducted to evaluate the long-term stability of the fabricated electrodes (Figure 4.6d). The resistance of Cu@Ag core-shell nanowire electrodes is more stable than that of CuNW electrodes because the Ag particles produced from the decomposition of Ag-amine shell can enhance the connection between CuNWs. Compared with pure CuNW and Cu@Ag core-shell nanowire electrodes, a much smaller change in resistance of TAE electrodes is detected after 1000 cycles testing. The higher electro-mechanical stability of the TAE electrodes is mainly attributed to the robust Cu@Ag alloy nanowire network and the embedded structure. The superb thermal stability and high electro-mechanical stability of the TAE electrodes guarantee their application prospect in wearable electronics.

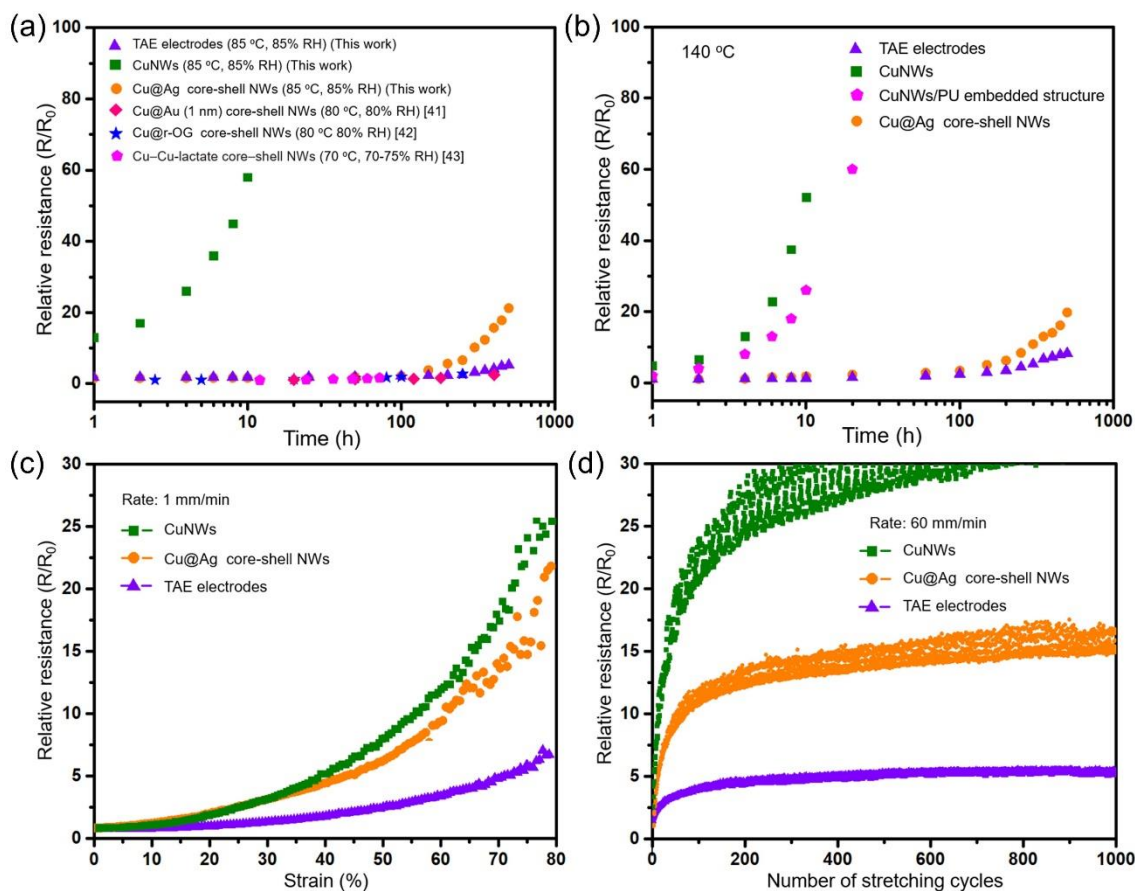


Figure 4.6 Thermal stability and electro-mechanical stability of TAE electrodes ($T = 85\%$, $SR = 23 \Omega/\text{sq}$). (a) Evolution of the R/R_0 of CuNW electrodes, Cu@Ag core-shell NW electrodes, TAE electrodes, and previously reported electrodes during the high temperature and high humidity aging test. (b) Evolution of the R/R_0 of the CuNW, Cu@Ag core-shell NW and TAE electrodes under high temperature of 140 °C. (c) Evolution of the R/R_0 of electrodes under a strain of up to 80%. (d) Evolution of the R/R_0 of electrodes during the cyclic test at 30% strain (12 s for one cycle).

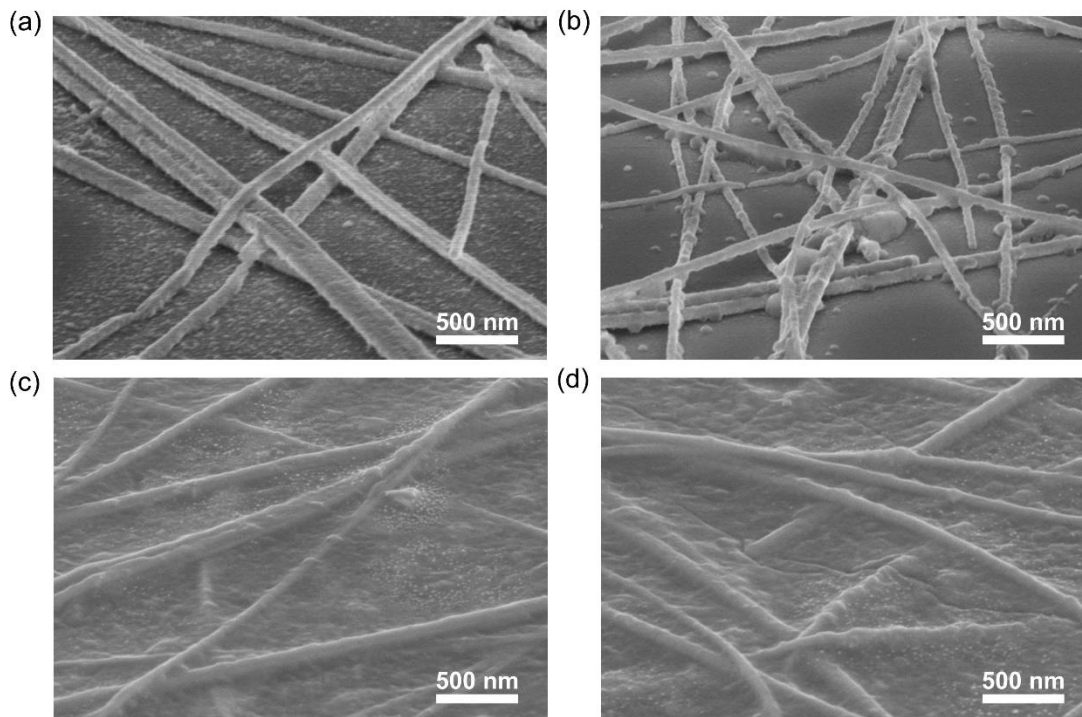


Figure 4.7 SEM images of the structure changes for (a, b) CuNW conductor and (c, d) AE conductor exposed at standard harsh environment (85 °C, 85% RH) for (a, c) 10 h and (b, d) 50 h.

As a proof-of-concept application of these ultra-stable TAE electrodes, a stretchable and invisible heater was fabricated. To evaluate the heating performance of the heater, its surface temperature at a certain input DC voltage was captured in real time with the aid of an infrared (IR) thermal camera. Figure 4.8a shows the temperature as a function of time with various DC voltages. By applying a constant DC voltage, the temperature of the heater is raised quickly due to the Joule heating of the Cu@Ag alloy network and reaches a plateau within 30 s. The saturation temperature is dependent on the applied voltage, which can be adjusted easily. A cyclic heating test was conducted by repeatedly applying input voltage of 5 V to the heater. As shown in Figure 4.8b, during the given period of 2400 s, 40 cycles with regular ascending and descending temperature are observed, indicating the repeatability of the heating performance and confirming the ultrahigh stability of TAE electrodes. To reveal the dependence of the heating performance on the initial sheet resistance, the time-dependent temperature curves of the TAE electrodes with different sheet resistance of 5.1, 10.7, and 15.2 Ω/sq were measured at different input voltage (2 V, 4 V, 6 V)

(Figure 4.8c). It is seen that the electrodes with lower sheet resistance yield higher surface temperatures because of the higher power supply at the same voltage. In addition, since wearable heaters will unavoidably suffer mechanical impacts during human body movements, it is absolutely essential to evaluate the heating performance of the heater under mechanical deformations. Figure 4.8d records the temperature variation of the heater that is heated to the saturation temperature of 76 °C and then gradually stretched up to the maximum strain of 60%. It is found that with the increase of tensile strain, the heater works stably with a slight temperature decrease because of the resistance increase of the heater. The heater can keep 90% and 82% heating performance at strain of 40% and 60% respectively. To sum up, the heater fabricated from low-cost TAE electrodes have outstanding Joule heating performance as well as high stability in both static and dynamic conditions, which is very promising in the field of thermal therapy.

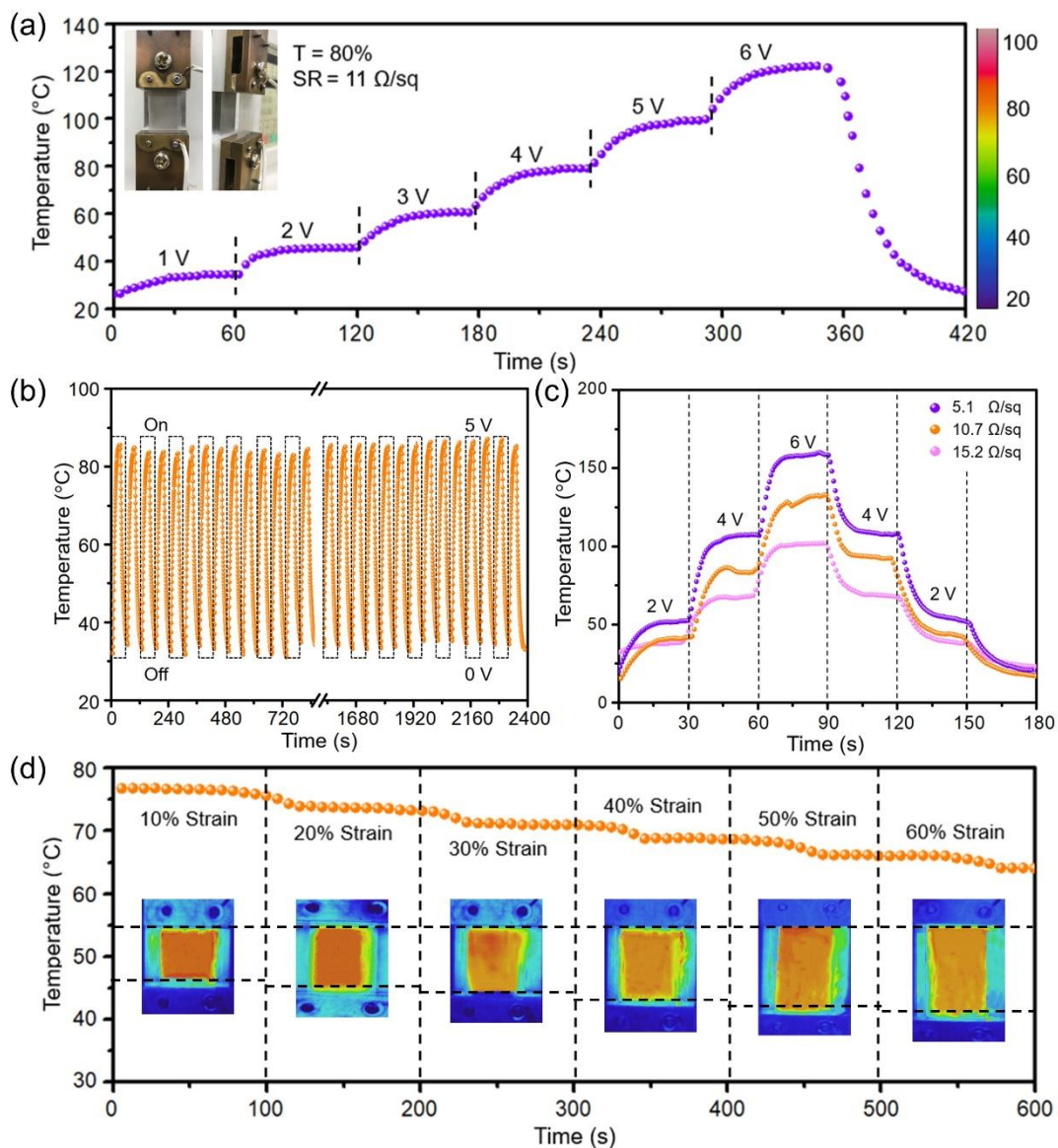


Figure 4.8 Characterization of stretchable transparent heaters based on TAE electrodes. (a) The temperature evolution of the heater for stepwise increases in voltage from 1 to 6 V. (b) The cyclic thermal stability test of the heater with the applied voltage of 5 V. (c) Temperature as a function of time for different applied voltages and for different initial SR. (d) Relative temperature change and the corresponding IR images of the heater ($T = 80\%$, $\text{SR} = 11 \Omega/\text{sq}$) as a function of applied tensile strain. The applied voltage is 4 V.

4.4 Conclusions

In conclusion, highly cost-effective, ultra-stable, transparent, and stretchable electrodes are successfully fabricated by alloying Cu-core/Ag-shell nanowires and embedding them in the

surface layer of substrates (TAE electrodes). The combination effects of dense alloy nanowires and embedded structures improve the thermal stability of TAE electrodes strikingly so that they have outstanding long-term stability without obvious changes in the resistance over 500 h in both high temperature (140 °C) and high humidity (85 °C, 85% RH), which is much better than previous reports. It also demonstrated that the TAE electrodes exhibit high electro-mechanical stability which can remain stable after 1000 stretching-relaxation cycles at 30% strain. A stretchable and transparent heater based on the TAE electrode is demonstrated with uniform temperature distribution as well as excellent reliability under both elevated temperatures and large strain. We believe that cost-effective TAE electrodes are very promising in the field of emerging wearable electronics because of their ultrahigh thermal stability as well as high stretchability.

References

- [1] Im, H. G.; Jung, S. H.; Jin, J.; Lee, D.; Lee, J.; Lee, D.; Lee, J. Y.; Kim, I. D.; Bae, B. S. Flexible Transparent Conducting Hybrid Film Using a Surface-Embedded Copper Nanowire Network: A Highly Oxidation-Resistant Copper Nanowire Electrode for Flexible Optoelectronics. *ACS Nano* **2014**, *8*, 10973-10979.
- [2] Ding, S.; Jiu, J.; Gao, Y.; Tian, Y.; Araki, T.; Sugahara, T.; Nagao, S.; Nogi, M.; Koga, H.; Suganuma, K.; Uchida, H. One-Step Fabrication of Stretchable Copper Nanowire Conductors by a Fast Photonic Sintering Technique and Its Application in Wearable Devices. *ACS Appl. Mater. Interfaces* **2016**, *8*, 6190-6199.
- [3] Yang, Y.; Ding, S.; Araki, T.; Jiu, J.; Sugahara, T.; Wang, J.; Vanfleteren, J.; Sekitani, T.; Suganuma, K. Facile Fabrication of Stretchable Ag Nanowire/Polyurethane Electrodes Using High Intensity Pulsed Light. *Nano Res.* **2016**, *9*, 401-414.
- [4] Cheng, Y.; Wang, S.; Wang, R.; Sun, J.; Gao, L. Copper Nanowire Based Transparent Conductive Films with High Stability and Superior Stretchability. *J. Mater. Chem. C* **2014**, *2*, 5309-5316.
- [5] Hu, W.; Wang, R.; Lu, Y.; Pei, Q. An Elastomeric Transparent Composite Electrode Based on

- Copper Nanowires and Polyurethane. *J. Mater. Chem. C* **2014**, *2*, 1298-1305.
- [6] Mehta, R.; Chugh, S.; Chen, Z. Enhanced Electrical and Thermal Conduction in Graphene-Encapsulated Copper Nanowires. *Nano Lett.* **2015**, *15*, 2024-2030.
- [7] Zeng, D.; Chen, Y.; Lu, A.; Li, M.; Guo, H.; Wang, J.; Peng, D.-L. Injection Synthesis of Ni–Cu@ Au–Cu Nanowires with Tunable Magnetic and Plasmonic Properties. *Chem. Commun.* **2013**, *49*, 11545-11547.
- [8] Guo, H.; Jin, J.; Chen, Y.; Liu, X.; Zeng, D.; Wang, L.; Peng, D.-L. Controllable Synthesis of Cu–Ni Core–Shell Nanoparticles and Nanowires with Tunable Magnetic Properties. *Chem. Commun.* **2016**, *52*, 6918-6921.
- [9] Ahn, Y.; Jeong, Y.; Lee, D.; Lee, Y. Copper Nanowire–Graphene Core–Shell Nanostructure for Highly Stable Transparent Conducting Electrodes. *ACS Nano* **2015**, *9*, 3125-3133.
- [10] Niu, Z.; Cui, F.; Yu, Y.; Becknell, N.; Sun, Y.; Khanarian, G.; Kin, D.; Dou L.; Dehestani, A.; Schierle-Arndt, K.; Yang, P. Ultrathin Epitaxial Cu@Au Core-Shell Nanowires for Stable Transparent Conductors. *J. Am. Chem. Soc.* **2017**, *139*, 7348-7354.
- [11] Stewart, I. E.; Ye, S.; Chen, Z.; Flowers, P. F.; Wiley, B. J. Synthesis of Cu–Ag, Cu–Au, and Cu–Pt Core–Shell Nanowires and Their Use in Transparent Conducting Films. *Chem. Mater.* **2015**, *27*, 7788-7794.
- [12] Tsai, C.-H.; Chen, S.-Y.; Song, J.-M.; Chen, I.-G.; Lee, H.-Y. Thermal Stability of Cu@Ag Core–Shell Nanoparticles. *Corros. Sci.* **2013**, *74*, 123-129.
- [13] Hai, H. T.; Takamura, H.; Koike, J. Oxidation Behavior of Cu–Ag Core–Shell Particles for Solar Cell Applications. *J. Alloys Compd.* **2013**, *564*, 71-77.
- [14] Li, J.; Li, Y.; Wang, Z.; Bian, H.; Hou, Y.; Wang, F.; Xu, G.; Liu, B.; Liu, Y. Ultrahigh Oxidation Resistance and High Electrical Conductivity in Copper-Silver Powder. *Sci Rep.* **2016**, *6*, 39650.
- [15] Shore, M. S.; Wang, J.; Johnston-Peck, A. C.; Oldenburg, A. L.; Tracy, J. B. Synthesis of Au (Core)/Ag (Shell) Nanoparticles and Their Conversion to AuAg alloy Nanoparticles. *Small* **2011**, *7*, 230-234.

- [16] Jian, L.; Mayer, J. W.; Colgan, E. G. Oxidation and Protection in Copper and Copper Alloy Thin Films. *J. Appl Phys.* **1991**, *70*, 2820-2827.
- [17] Li, W.; Hu, D.; Li, L.; Li, C. F.; Jiu, J.; Chen, C.; Ishina, T.; Sugahara, T.; Suganuma, K. Printable and Flexible Copper-Silver Alloy Electrodes with High Conductivity and Ultrahigh Oxidation Resistance. *Acs Appl Mater Inter* **2017**, *9*, 24711-24721.
- [18] Zhang, B.; Li, W.; Yang, Y.; Chen, C. T.; Li, C. F.; Suganuma, K. Fully Embedded CuNWs/PDMS Conductor with High Oxidation Resistance and High Conductivity for Stretchable Electronics. *J Mater Sci* **2019**, *54*, 6381-6392.
- [19] Zhang, B.; Li, W.; Jiu, J.; Yang, Y.; Jing, J.; Suganuma, K.; Li, C. F. Large-Scale and Galvanic Replacement Free Synthesis of Cu@Ag Core-Shell Nanowires for Flexible Electronics. *Inorg. Chem.* **2019**, *58*, 3374-3381.
- [20] Ding, S.; Jiu, J.; Tian, Y.; Sugahara, T.; Nagao, S.; Suganuma, K. Fast Fabrication of Copper Nanowire Transparent Electrodes by A High Intensity Pulsed Light Sintering Technique in Air. *Phys Chem Chem Phys.* **2015**, *17*, 31110-31116.
- [21] Jiu, J.; Nogi, M.; Sugahara, T.; Tokuno, T.; Araki, T.; Komoda, N.; Suganuma, K.; Uchida, H.; Shinozaki, K. Strongly Adhesive and Flexible Transparent Silver Nanowire Conductive Films Fabricated with A High-Intensity Pulsed Light Technique. *J. Mater. Chem.* **2012**, *22*, 23561-23567.
- [22] Ma, E. Alloys Created between Immiscible Elements. *Prog. Mater. Sci.* **2005**, *50*, 413-509.
- [23] Delogu, F.; Arca, E.; Mulas, G.; Manai, G.; Shvets, I. Numerical Investigation of The Stability of Ag-Cu Nanorods and Nanowires. *Phys. Rev. B* **2008**, *78*, 024103.
- [24] Lee, B.-J.; Shim, J.-H.; Baskes, M. J. Semiempirical Atomic Potentials for The Fcc Metals Cu, Ag, Au, Ni, Pd, Pt, Al, and Pb Based on First and Second Nearest-Neighbor Modified Embedded Atom Method. *Phys. Rev. B* **2003**, *68*, 144112.
- [25] Niu, Z. G.; Cui, F.; Yu, Y.; Becknell, N.; Sun, Y. C.; Khanarian, G.; Kim, D.; Dou, L.; Dehestani, A.; Schierle-Arndt, K.; Yang, P. D., Ultrathin Epitaxial Cu@Au Core-Shell Nanowires for Stable Transparent Conductors. *J Am Chem Soc* **2017**, *139*, 7348-7354.

- [26] Dou, L.; Cui, F.; Yu, Y.; Khanarian, G.; Eaton, S. W.; Yang, Q.; Resasco, J.; Schildknecht, C.; Schierle-Arndt, K.; Yang, P. D. Solution-Processed Copper/Reduced-Graphene-Oxide Core/Shell Nanowire Transparent Conductors. *Acs Nano* **2016**, *10*, 2600-2606.
- [27] Hwang, H.; Kim, A.; Zhong, Z.; Kwon, H. C.; Jeong, S.; Moon, J. Reducible-Shell-Derived Pure-Copper-Nanowire Network and Its Application to Transparent Conducting Electrodes. *Adv Funct Mater* **2016**, *26*, 6545-6554.
- [28] Xu, L.; Yang, Y.; Hu, Z.W.; Yu, S.H., Comparison Study on the Stability of Copper Nanowires and Their Oxidation Kinetics in Gas and Liquid. *ACS nano* **2016**, *10*, 3823-3834.

Chapter 5

Conclusions

In this dissertation, CuNWs based conductors have been successfully fabricated with outstanding stability, conductivity, and flexibility, which is benefit for the application of CuNWs in the field of wearable devices. Three methods have been proposed to address the oxidation problem of CuNWs, including a fully embedded structure, a core-shell structure, and the combination of core-shell structure and embedded structure.

In chapter 1, the emergence of flexible conductors, the approaches to enable flexibility and the application of flexible conductors have been described in detail. At present, the carbon nanomaterials, conductive polymers, and metallic nanomaterials are used as next-generation conductive materials to fabricate the flexible electronic circuits. Among them, CuNWs are appearances as the best choice in order to achieve cost-effective and high-performance flexible conductors. However, the poor stability of CuNWs in ambient conditions largely overshadowed their application. Therefore, three strategies are suggested to solve the oxidation problem of CuNWs and improve performance of CuNWs based conductors.

In chapter 2, the CuNWs-based highly reliable, conductive and stretchable conductors were fabricated by embedding CuNWs below the surface layer of PDMS and completed with a simple high-intensity pulsed light process. The influence of light parameters on the performance of conductors was investigated. The light energy absorbed by the film not only removes the oxides on the surface of nanowires but also enhance the connection between nanowires to produce high conductivity. Due to the wrap of the CuNWs in the PDMS matrix, the fully embedded conductor shows ultrahigh oxidation resistance, which remains stable in air at 85 °C and 85% RH. The electrical resistance of the conductor is maintained at low levels when the strain is more than 70%. The fully embedded conductor endured 1000 cycles of stretching-releasing at a rate of 60 mm/min, under 30% strain and showed a slight increase in resistance. Additionally, fully embedded conductor was used as a dipole antenna. The stretchable antenna retained its sensitivity to specific

radio frequencies after 500 cycles of the stretching-releasing process. With their superior stability, conductivity and stretchability, the fabricated fully embedded CuNWs/PDMS conductors possess broad applications in stretchable strain sensors, skin sensors, bendable displays and wearable electronics

In chapter 3, in order to overcome the poor stability of CuNWs-based conductors, Cu@Ag core-shell nanowires with tunable thickness of silver shell could be obtained through a facile adsorption and decomposition process. The introduced Ag-ammonia complex can be adsorbed on the surface of CuNWs to form Cu@Ag-ammonia core-shell structure. After a low temperature heating process in air, silver complex was decomposed into pure silver shell. The use of Ag-ammonia complex as silver source could avoid the galvanic replacement that is encountered in traditional synthesis methods. The synthesis process and mechanism of adsorption and decomposition process are discussed in details. In addition, owing to the protection of silver shell, as-prepared Cu@Ag core-shell nanowires show excellent stability for at least 500 h at both high temperatures (140 °C) and standard harsh environment (85 °C, 85 % RH), which could be used in next-generation of stretchable transparent conductors.

In chapter 4, highly cost-effective, ultra-stable, transparent, and stretchable electrodes are successfully fabricated by alloying Cu-core/Ag-shell nanowires and embedding them in the surface layer of substrates (TAE electrodes). The combination effects of dense alloy nanowires and embedded structures improve the thermal stability of TAE electrodes strikingly so that they have outstanding long-term stability without obvious changes in the resistance over 500 h in both high temperature (140 °C) and high humidity (85 °C, 85% RH), which is much better than previous reports. It also demonstrated that the TAE electrodes exhibit high electro-mechanical stability which can remain stable after 1000 stretching-relaxation cycles at 30% strain. A stretchable and transparent heater based on the TAE electrode is demonstrated with uniform temperature distribution as well as excellent reliability under both elevated temperatures and large strain. We believe that cost-effective TAE electrodes are very promising in the field of emerging wearable electronics because of their ultrahigh thermal stability as well as high stretchability.

List of publications

A. Papers

- [1] **Bowen Zhang**, Wanli Li, Masaya Nogi, Chuantong Chen, Yang Yang, Tohru Sugahara, Hirotaka Koga, and Katsuaki Suganuma. Alloying and embedding of Cu-core/Ag-shell nanowires for ultra-stable stretchable and transparent electrodes. *ACS Applied Materials & Interfaces*, 2019, 11, 18540-18547.
- [2] **Bowen Zhang**, Wanli Li, Jinting Jiu, Yang Yang, Jiangbo Jing, Katsuaki Suganuma, and Cai-Fu Li. Large-Scale and Galvanic replacement free synthesis of Cu@Ag core-shell nanowires for flexible electronics. *Inorganic Chemistry*, 2019, 58, 3374-3381.
- [3] **Bowen Zhang**, Wanli Li, Yang Yang, Chuantong Chen, Cai-Fu Li, and Katsuaki Suganuma. Fully embedded CuNWs/PDMS conductor with high oxidation resistance and high conductivity for stretchable electronics. *Journal of Materials Science*, 2019, 54, 6381-6392.
- [4] **Bowen Zhang**, Chuantong Chen, Wanli Li, Jeyun Yeoma, and Katsuaki Suganuma. Well-controlled decomposition of copper complex inks enabled by metal nanowire networks for highly compact, conductive, and flexible copper films. *Advanced Materials Interfaces*, 2019, 1901550.
- [5] Wanli Li, Yang Yang, **Bowen Zhang**, Lingying Li, Guiming Liu, Cai-Fu Li, Jinting Jiu, Katsuaki Suganuma. Three-dimensional stretchable and transparent conductors with controllable strain-distribution based on template-assisted transfer printing. *ACS Applied Materials & Interfaces*, 2019, 11, 2140-2148.
- [6] Wanli Li, Yang Yang, **Bowen Zhang**, Cai-Fu Li, Jinting Jiu, Katsuaki Suganuma. Highly densified Cu wirings fabricated from air-stable Cu complex ink with high conductivity, enhanced oxidation resistance, and flexibility. *Advanced Materials Interfaces*, 2018, 1800798.

B. proceeding and presentation

- [1] **Bowen Zhang**, Chuantong Chen, Wanli Li, Katsuaki Suganuma. Alloying and Embedding of Cu-Core/Ag-Shell Nanowires for Ultra-Stable Stretchable and Transparent electrodes. The 10th ICFPE (2019 International Conference on Flexible and Printed Electronics, 2019 ICFPE), Taipei, China, October 23-25, 2019.
- [2] **Bowen Zhang**, Chuantong Chen, Katsuaki Suganuma. Alloying and embedding of CuNWs-core/Ag-shell nanowires for ultra-stable stretchable and transparent electrodes. The 3rd A3 Foresight Symposium on Organic/Inorganic Nanohybrid Platforms for Precision Tumor Imaging and Therapy, Shanghai, China, October 9-11, 2019.
- [3] **Bowen Zhang**, Wanli Li, Cai-Fu Li, Chuantong Chen, Katsuaki Suganuma. Highly reliable and stretchable conductor prepared with copper nanowire and PDMS. The 9th ICFPE (2018 International Conference on Flexible and Printed Electronics, 2018 ICFPE), Changzhou, China, September 26-28, 2018.

Acknowledgements

I would like to express my sincere gratitude to my supervisor, Prof. Katsuaki Suganuma in the Institute of Scientific and Industrial Research (ISIR) at Osaka University, for his patience and unstinting support to my doctoral course. He provides us with an international, energetic, competitive, and enthusiastic research environment, which is the cornerstone for my three-year research work.

Besides my supervisor, I would like to thank the rest of my thesis committee: Prof. Masaya Nogi and Assoc. Prof. Hirotaka Koga, Assoc. Prof. Shijo Nagao, and Assoc. Prof. Sugahara for their invaluable advice and encouraging comments to my dissertation.

I would like to thank Dr. Chuantong Chen, Dr. Jinting Jiu, Dr. Wanli Li, Professor Zhi-Quan Liu, Assoc. Prof. Peng Xue, and Assoc. Prof. Cai-Fu Li, for their valuable advice and comments during my research.

I would also like to thank all the friends and colleagues at Suganuma Lab and Osaka University, Dr. Hao Zhang, Dr. Chun Pei, Dr. Zhenghong Wang, Dr. Seungjun Noh, Dr. Yue Gao, Mr. Chanyang Choe, Mr. Jeyun Yeom, Mr. Dong-Jin Kim, Ms. Haoran Ding, Mr. Zheng Zhang, Ms. Shanrong Zou, Ms. Fengpei Lang, Mr. Dawei Hu, Mr. Guiming Liu, Mr. Akio Shimoyama, Dr. Aripuru Reira, Mr. Koji Kimoto, Ms. Ming-Chun Hsieh, Ms. Noriko Kagami, Ms. Naomi Keenan, Ms. Seiyu Okuda, and Ms. Sachiko Moribe. Without their encouragement and support, it would not be possible to conduct this research.

Finally, I would like to thank the supporting and inspiring from my family member and Mr. Jiangbo Jing. I also want to thank myself for the persistence over the past years.